AN ANALYSIS OF SUB-BAND CODING TECHNIQUES FOR SPEECH COMMUNICATION

by

ARTHUR JAY BARABELL

SUBMITTED IN PARTIAL FULFILLMENT OF THE
REQUIREMENTS FOR THE DEGREES OF
BACHELOR OF SCIENCE
and
MASTER OF SCIENCE
at the
MASSACHUSETTS INSTITUTE OF TECHNOLOGY
October, 1981

Signature of Author: .....
Department of Electrical Engineering and
Computer Science
October 5, 1981

Certified by: .....
Thesis Supervisor (Academic)

Certified by: .....
Company Supervisor (VI-A Cooperating Company)

Accepted by: .....
Chairman, Departmental Committee on Graduate Students

An Analysis of Sub-band Coding Techniques

for Speech Communication

by

Arthur Jay Barabell

Submitted to the Department of Electrical Engineering and Computer Science on October 5, 1981, in partial fulfillment of the requirements for the degrees of Bachelor of Science and Master of Science.

ABSTRACT

Sub-band coding has been proposed as an efficient means of encoding signals for digital transmission. In this thesis, an analysis is presented of the various techniques used in the implementation of sub-band coders. An efficient scheme, due to Crochiere, for implementing pitch prediction in sub-band coders is presented, as well as a discussion on the design and analysis of such pitch prediction systems.

New designs for 9.6 kb/s and 16 kb/s sub-band coders are presented. These coders were simulated on a general purpose digital computer. The objective and subjective performance of the simulated coders is discussed, and comparisons are made with the performance of previous designs. Since these new sub-band coders are the first to incorporate pitch prediction, particular attention is paid to the improvement in performance due to the use of pitch prediction. Suggestions are made for obtaining further improvements in sub-band coder performance.

Thesis Supervisor: James H. McClellan

Title: Associate Professor of Electrical Engineering

Thesis Supervisor: Ronald E. Crochiere

Title: Member of Technical Staff, Bell Telephone Laboratories

ACKNOWLEDGEMENT

Many people have helped to make this thesis a worthwhile experience, and I would like to acknowledge their contribution.

The bulk of the thesis research was done at the Acoustics Research Department of Bell Laboratories, under the auspices of the MIT cooperative program in Electrical Engineering and Computer Science.

I would like to express my deepest appreciation to Dr. Ronald E. Crochiere, my thesis supervisor at Bell Labs, for all the advice and encouragement that he provided throughout the course of this project. I would also like to thank Dr. James L. Flanagan for not only making the facilities of his department available to me, but also for several suggestions which enhanced my understanding of speech processing. I would also like to acknowledge the contributions of James D. Johnston, who made numerous suggestions on the design of the systems simulated, and Carol A. McGonegal, who helped me cope with the computer system.

Several people at MIT also made valuable contributions to this thesis. Dr. Michael R. Portnoff read and commented on the thesis proposal, and his help was much appreciated. Professor James H. McClellan was kind enough to read the various drafts of this thesis document. His comments and suggestions have greatly enhanced the clarity of the presentation.

Finally, I would like to thank Mrs. Delphine Radcliffe for the super job she did in typing the manuscript.

TABLE OF CONTENTS

TABLE OF CONTENTS (continued)

LIST OF FIGURES

CHAPTER 1

INTRODUCTION

1.1 Introduction

The advantages of digital coding of signals are well known and widely discussed in the literature. Some of these advantages include robustness, efficient signal regeneration, the possibility of combining transmission and switching functions, and easy encryption. However, in achieving these benefits, one must pay a price - digital signals, such as PCM signals, have greater transmission bandwidth and storage requirements than their analog counterparts. Thus, there has been a great amount of research interest in the efficient coding of digital signals. A substantial portion of this continuing effort is devoted to the coding of digital speech signals [1].

The speech coding systems which have been devised fall into several categories. At one end of the spectrum [sic] are waveform coders. Waveform coders attempt to reproduce the signal waveform, traditionally taking advantage of only a few properties of the signal being encoded (i.e. finite bandwidth, finite dynamic range, some correlation between successive samples, etc.). Thus, these schemes may be used for a large variety of signals - speech, music, and video - to cite a few examples. These algorithms are capable of yielding coded signals which are robust with respect to transmission and storage errors. Furthermore, the original signal may be reproduced with virtually any fidelity required by increasing the number of bits used to encode each sample. However, these algorithms are not very efficient - they require rather high bit rates (e.g. 56 kb/s for log PCM) to reproduce toll quality speech [1].

At the opposite end of the speech coder spectrum [sic] are vocoders, which attempt to analyze the original speech signal, and transmit the parameters of a speech production model for future regeneration. The fidelity of the reproduced signal to the original is very much dependent upon the accuracy of the model. In addition, vocoded speech signals are very error sensitive, due to their low redundancy. Even under error-free conditions, vocoded speech sounds rather unnatural, due to the failure of even current state-of-the-art models to fully characterize the human speech mechanism. However, vocoders are capable of yielding intelligible speech at bit rates as low as 500 b/s (for formant vocoders).

From the brief discussion above, one can see that neither waveform coders nor vocoders would entirely satisfy the requirements of a digital speech transmission system for use over standard telephone lines; fairly high quality speech at 4.8 kb/s to 16 kb/s in a transmission environment which is not error-free. Thus, much recent research has been focussed on coding schemes which exploit speech and hearing models, without making the algorithm totally dependent on these models.

The redundancy in speech due to the vocal tract filtering action can be removed in the time domain by exploiting the resulting correlations between successive speech samples. Alternatively, this redundancy can be removed in the frequency domain by exploiting the quasi-stationary, nonuniform nature of the short-time spectral envelope of speech signals.

The redundancy in speech due to the quasi-periodic nature of voiced speech can be removed in the time domain by exploiting the correlation between speech segments one or more pitch periods apart. Alternatively, this redundancy can be removed in the frequency domain

by exploiting the spectral fine structure associated with the harmonics of the pitch frequency.

Sub-band coding [2-5] efficiently exploits the redundancies in speech due to the vocal tract filtering process. In addition, sub-band coding exploits models for auditory perception.

A generic sub-band coder is shown in Fig. 1.1. In this figure, s(n) is the discrete time representation of a bandlimited signal which has been sampled at the Nyquist rate. This discrete time signal is split into a number of sub-band signals, typically four to eight, by the bank of band-pass filters. Each sub-band signal is translated down to dc and then re-sampled at the Nyquist rate for that sub-band.* It is these base-band signals which are separately encoded, multiplexed, and then transmitted. At the receiver, the bit stream is demultiplexed and decoded. The sub-band signals are reconstructed at the original, higher sampling rate, band-pass translated to the proper frequency, and then added, to produce a facsimile of the original speech signal.

By allowing the quantizers' step-sizes to adapt independently according to the signal level in each sub-band, the coder takes advantage of the quasi-stationarity and nonuniformity of the short-time spectral envelope of speech. Since quantizing noise produced in each sub-band is localized to that sub-band, signals in one sub-band will not be masked by the quantizing noise produced by another sub-band. The total number of bits available may be allocated to each band according to perceptual criteria. Dynamic bit allocation schemes have been proposed [5] which

---

* Although it is useful to think of these steps as being physically separate, in practice one combines their implementation to achieve the same results with fewer operations.

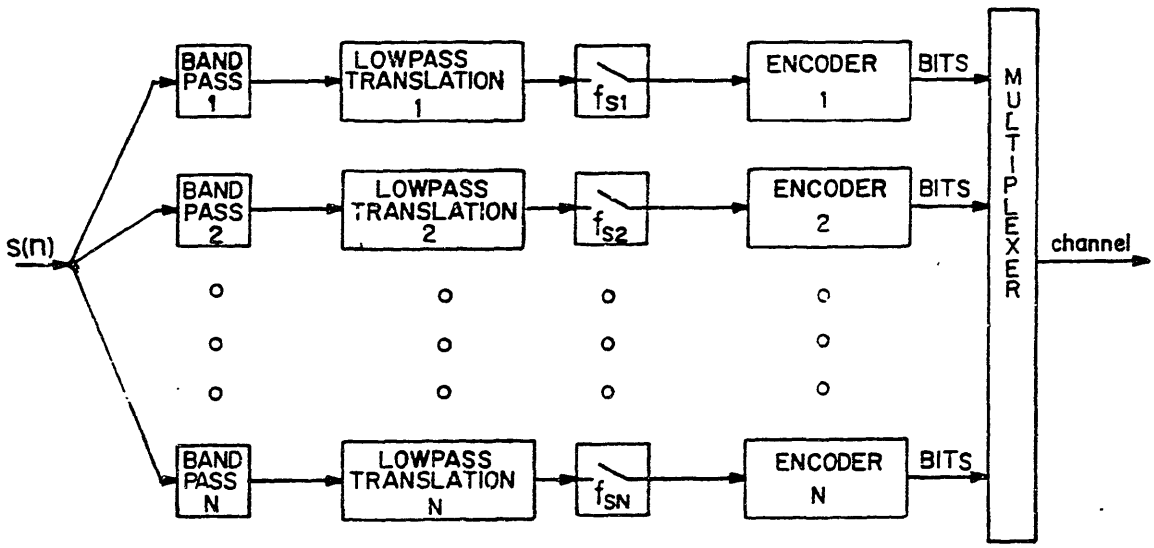

Fig. 1.1(a) Transmitter section of a generic sub-band coder.

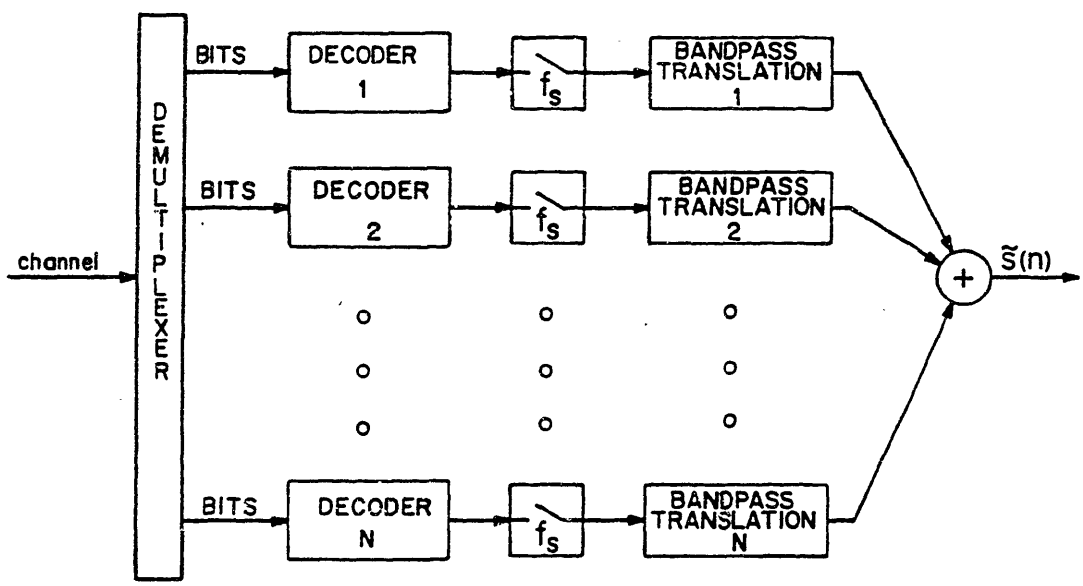

Fig. 1.1(b) Receiver section of a generic sub-band coder.

periodically update the bit allocation according to the spectral content of the signal being coded.

1.2 The Scope of this Thesis

The sub-band coders proposed by Crochiere et al. [2, 3] and Esteban and Galand [4, 5] have demonstrated the ability to produce toll quality speech using 24 kb/s systems and communications quality speech using 9.6 kb/s systems [1, 6]. The new 9.6 kb/s and 16 kb/s sub-band coders designed and simulated on a general purpose digital computer as part of this thesis project make use of a combination of techniques previously demonstrated by the researchers cited above. In addition, the proposed coders exploit the quasi-periodic nature of voiced speech using an efficient pitch prediction technique proposed by Crochiere [7]. An important goal of this thesis is to evaluate the improvement in performance due to the use of pitch prediction, since these are the first sub-band coders to make use of such systems. The thesis is organized as follows:

Chapter 2 is concerned with methods for the division of the original, full band speech signal into several baseband sub-band signals. The discussion includes considerations on the choice of sub-band locations and widths, a presentation of efficient systems for the conversion of the full band signal into several sub-bands, a treatment of the design of filters for use by these systems, and a comparison of the computational costs of implementing these techniques.

Chapter 3 is concerned with the use of pitch prediction in sub-band coding. The chapter begins with a brief discussion of time domain methods for predictive coding, and then focusses on the specific example of pitch predictive coding. This discussion is followed by a presentation

of an efficient technique (due to Crochiere [7]) for the implementation of pitch prediction in sub-band coders. The description of this technique is followed by a discussion on the practical design of such systems, and some constraints on their performance. Some of these constraints are due to the particular prediction and sub-band coding systems implemented, while other constraints are due to the properties of voiced speech signals. The chapter concludes with a consideration of the computational costs of adding pitch prediction to a given sub-band coding system.

Chapter 4 presents a discussion on quantization techniques and bit allocation issues in sub-band coders. Since the quantization techniques are widely discussed in the literature [1, 8-11], this discussion is relatively brief.

The first part of Chapter 5 is devoted to a presentation of the final design configurations for the 9.6 kb/s and 16 kb/s sub-band coders which were simulated. The second part is devoted to the consideration of the simulation results. This consideration focusses on two topics: the improvement in coder performance due to the utilization of pitch predictive encoding, and comparisons on the subjective performance of the proposed coders and the earlier coders of Crochiere [3].

Chapter 6 concludes the thesis with a summary of the major results and some suggestions for the improvement of the proposed sub-band coders.

CHAPTER 2

BAND-SPLITTING AND FREQUENCY TRANSLATION METHODS

2.1 Introduction

This chapter begins with a brief discussion on the selection of sub-band widths and locations. Following this discussion is a presentation of a general method of bandsplitting and frequency translation, commonly referred to as integer-band sampling [2, 3]. Also presented in this chapter is an important sub-class of this method, which incorporates the so-called "Quadrature Mirror Filters" (QMF's) [4, 5, 12]. Filter design considerations for these methods are presented. The chapter concludes with a comparison of the computational costs of implementing integer-band sampling with either conventional filters or QMF's.

2.2. Selection of Sub-band Widths and Locations

In choosing the locations and widths of the sub-bands, one may be guided by the concept of an articulation index (AI) [13, 14]. The AI specifies the division of the frequency scale into twenty nonuniform contiguous bands, where each "articulation band" contributes equally to the average total intelligibility of speech. Thus, the sub-bands of the system are allocated so that each sub-band contains an equal number of "articulation bands", then each sub-band will make an equal contribution to the intelligibility of the system. As will soon be demonstrated, the method chosen for band -splitting may restrict the ability of the designer to meet this requirement. Fortunately, however, little loss in performance is perceived if this equal contribution to intelligibility constraint is approximated [2, 3].

2.3 Integer Band Sampling

There are various techniques available for the translation and re-sampling of the sub-band signals. Several of these schemes are discussed in Reference [2]. Figures 2.1 and 2.2 illustrate the implementation of a sub-band coder based on integer band sampling. The speech band is partitioned into N sub-bands by band-pass filters BP_1 to BP_N. The speech signal s(n) is assumed to be a discrete-time signal The pass-band of BP_i has lower and upper limits of $\frac{m_i}{D_i}\pi$ and $\frac{(m_i + 1)}{D_i}\pi$, respectively, where m_i and D_i are integers, and $m_i + 1 \leq D_i$. Thus, when filter output $s_i(n)$ is down-sampled by the factor D_i, practically no information is lost due to aliasing (assuming, of course, that the band-pass filter is good enough, as will be discussed later in this section). This process of band-pass filtering followed by a sampling rate reduction is commonly referred to in the literature as band-pass decimation [15].

The sub-band signals $r_1(n)$ through $r_N(n)$ are encoded and then multiplexed for transmission over a single channel. At the receiver, the channel signal is demultiplexed and decoded. The sampling rate of each sub-band signal $\tilde{r}_i(n)$ is increased back to the original rate by inserting zeros and the resulting signal $w_i(n)$ is interpolated by filtering with another band-pass filter, identical to BP_i. This filter needs to have a gain of D_i to compensate for the signal energy which was lost in the decimation process. The process of increasing a signal's sampling rate, followed by band-pass filtering is known as band-pass interpolation [15]. The filter outputs $\tilde{s}_1(n)$ to $\tilde{s}_N(n)$ are then summed together to form a facsimile of the original speech signal.

Integer band sampling is preferable over other techniques for frequency translation and resampling because it eliminates the need for modulators. This technique can be made to be even more efficient if the

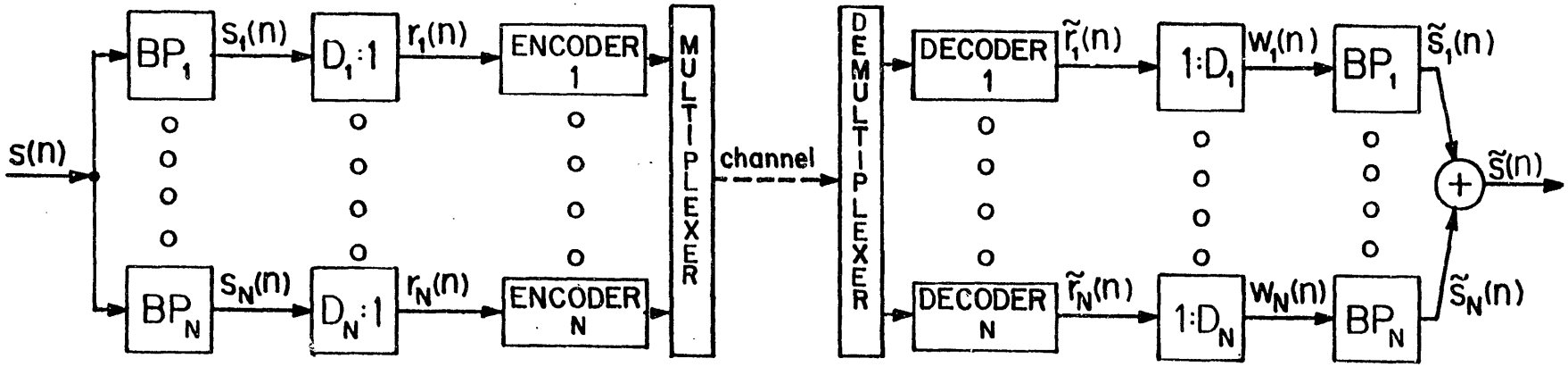

Fig. 2.1(a) Implementation of sub-band coder based on integer band sampling.

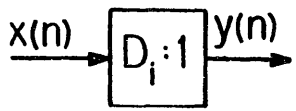

$$y(n) = x(D_i n)$$

Fig. 2.1(b)

Decrease in sampling rate by a factor D_i.

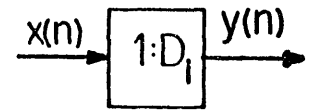

$$y(n) = \begin{cases} x(\frac{n}{D_i}) , n = 0, \pm D_i, \pm 2D_i, \ldots \\ 0 \quad , \text{otherwise} \end{cases}$$

Fig. 2.1(c)

Increase in sampling rate by a factor D_i.

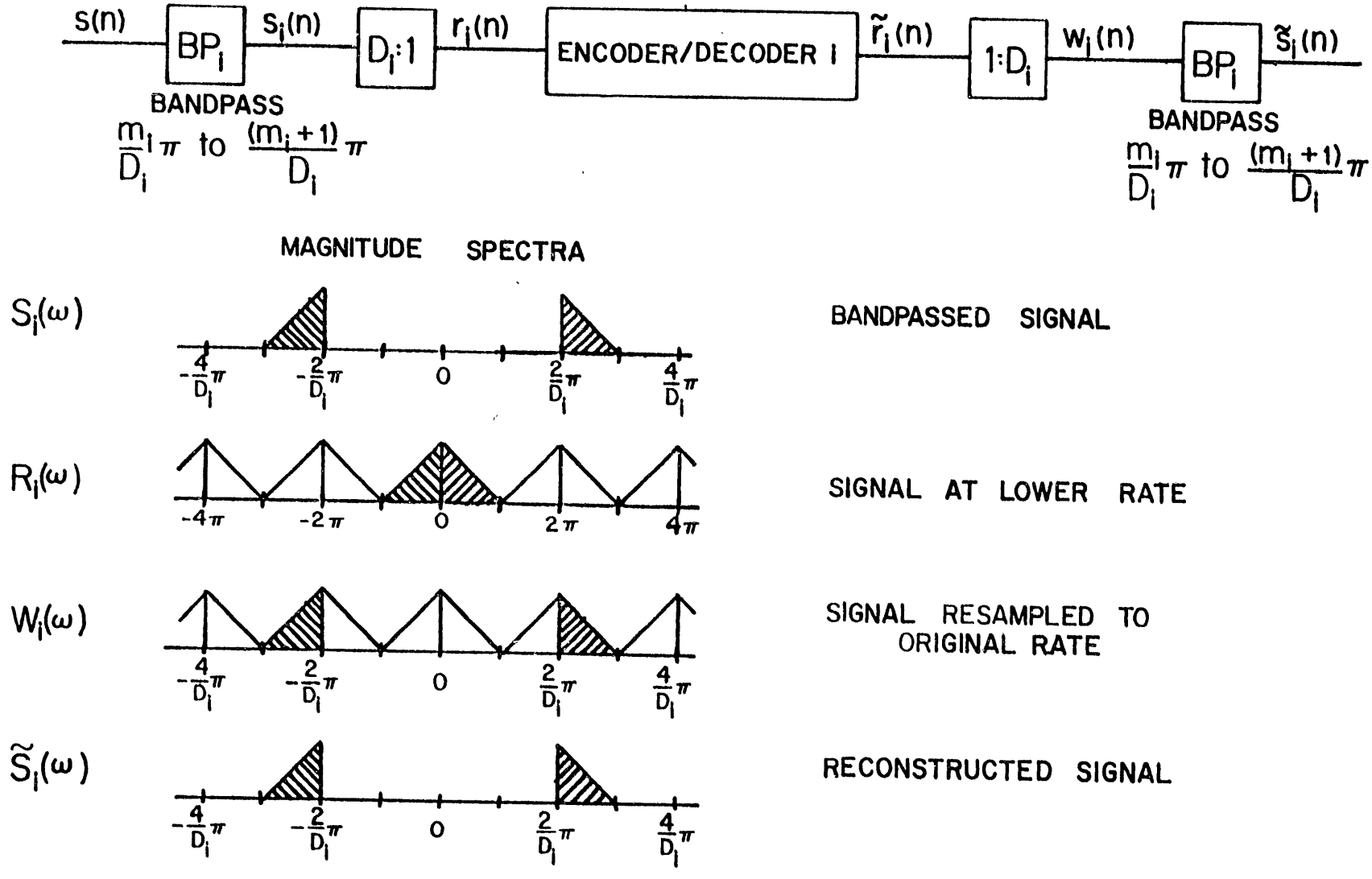

Fig. 2.2 A frequency domain interpretation of integer band sampling.

band-pass filters are implemented using nonrecursive (i. e. Finite Impulse Response (FIR)) designs. When using a nonrecursive filter in the band-pass decimator, only one out of every D_i filter output samples need be computed; these are the only samples that will remain after the decrease in sampling rate. In contrast, when recursive filters are employed in band-pass decimators, every filter output point must be computed, since the desired filter output points depend on all the past filter outputs. At the band-pass interpolator, $D_i - 1$ out of every D_i input samples to the filter is zero; hence these samples do not affect the computation [15] when nonrecursive filters are used.

When using integer-band sampling, it will not be possible to select the sub-band widths and locations to exactly satisfy the equal AI contribution criterion. This restriction is due to the requirement that sub-bands lie between $\frac{m_i}{D_i}\frac{f_s}{2}$ and $\frac{m_i + 1}{D_i}\frac{f_s}{2}$, where f_s is the original full-band sampling rate, m_i and D_i are integers, and $m_i < D_i$. In practice, the slight relaxation of the equal AI contribution criterion has only a slight degrading effect on the sub-band coder performance [3].

In designing the band-pass filters BP_1 through BP_N, one must take into account several considerations. As shown in Fig. 2.3, during the decimation process in the transmitter, signal frequencies outside the sub-band are aliased into the sub-band. For this aliasing effect to go unperceived, the stop band attenuation of the band-pass filters must be considerable; in practice, on the order of 45 dB [3]. Due to the filter's finite transition region, the filter pass-band must have a slightly narrower frequency range than the sub-band width, in order to minimize aliasing effects at the edges of the sub-band. Filter attenuations of 12 dB at the sub-band edges will leave the aliasing effects unperceived,

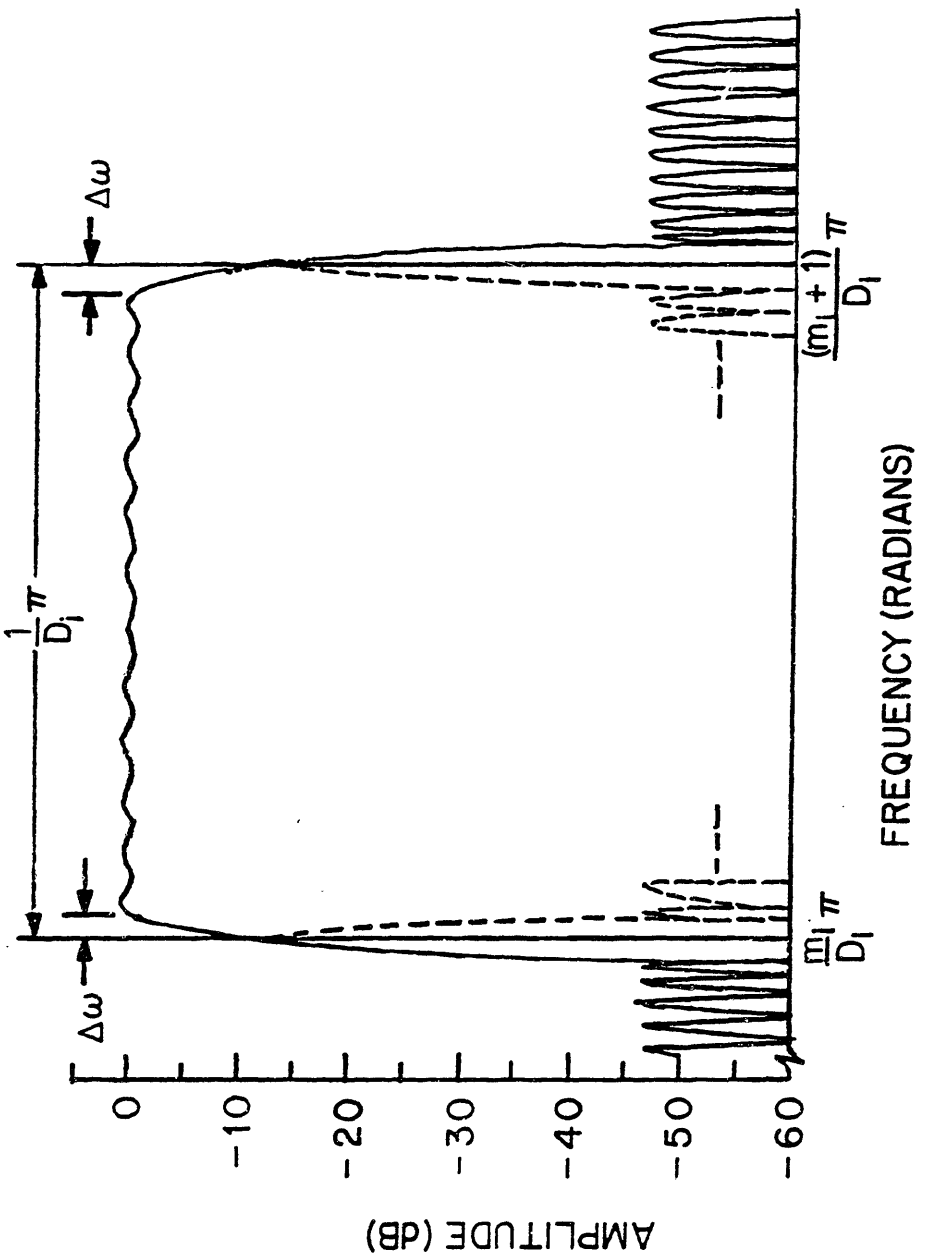

Fig. 2.3 Parameters of the bandpass filters.

as they are being confined to a very narrow frequency region [3]. When 175 - 200 tap FIR filters are used, it is possible to obtain the above requirements with a pass-band ripple of $\pm$ 0.5 dB and a $\Delta\omega$ of 0.01 π radians, which corresponds to 50 - 60 Hz when sampling rates of 9.6 to 10.67 kHz are used, as in Reference [3]. If the different sub-bands are contiguous, the resultant gaps in the overall system frequency response will cause the coder to have a reverberant quality. To minimize this reverberance, it is possible to overlap the sub-bands slightly, and obtain a smoother frequency response. However, this will increase the channel bandwidth requirement, which for a fixed bit-rate means reducing the number of bits available for quantization, resulting in an increase in quantization noise. For the five-band, 16 kb/s coder of Reference [3], the lower sub-bands are overlapped slightly, while the upper sub-bands are contiguous. For the four-band, 9.6 kb/s coders of Reference [3], the lower sub-bands are contiguous, while the upper sub-bands have gaps between them in order to conserve transmission bandwidth. The subjective quality of these systems will be discussed in Chapter 5.

2.4 Integer Band Sampling Incorporating Quadrature Mirror Filters

As discussed in the previous section, the necessity of minimizing aliasing effects forces the designer to compromise between computation load (which depends on the band-pass filter order), reverberance, and noise level. In some cases, however, it is possible to utilize "Quadrature Mirror Filters" (QMF's) [4, 5, 12], which provide for the cancellation of aliasing terms. Thus, sub-band edges need not be attenuated, and the sub-bands can be contiguous without creating gaps in the overall frequency response. In addition, the requirements on the

filter transition region are relaxed, permitting the use of lower order filters.

To illustrate the use of QMF's, consider the system in Fig. 2.4 in which the speech band is split into two equal-width sub-bands for coding purposes. If the frequency spectrum at each stage of the coder is expressed in terms of the original spectrum, one obtains the following:

$$S_1(\omega) = H_1(\omega)\, S(\omega) \tag{2.1a}$$

$$S_2(\omega) = H_2(\omega)\, S(\omega) \tag{2.1b}$$

$$R_1(\omega) = \tfrac{1}{2}\left\{S_1\left(\frac{\omega}{2}\right) + S_1\left(\frac{\omega + 2\pi}{2}\right)\right\} \tag{2.2a}$$

$$R_2(\omega) = \tfrac{1}{2}\left\{S_2\left(\frac{\omega}{2}\right) + S_2\left(\frac{\omega + 2\pi}{2}\right)\right\} \tag{2.2b}$$

To simplify the analysis, assume (for the moment) that the coder-decoder systems used in each band are identity systems, i.e.,

$$\tilde{R}_1(\omega) = R_1(\omega) \tag{2.3a}$$

$$\tilde{R}_2(\omega) = R_2(\omega) \tag{2.3b}$$

$$W_1(\omega) = \tilde{R}_1(2\omega) = R_1(2\omega) \tag{2.4a}$$

$$W_2(\omega) = \tilde{R}_2(2\omega) = R_2(2\omega) \tag{2.4b}$$

Using this assumption, one obtains:

$$\tilde{S}(\omega) = K_1(\omega)W_1(\omega) + K_2(\omega)W_2(\omega) \tag{2.5a}$$

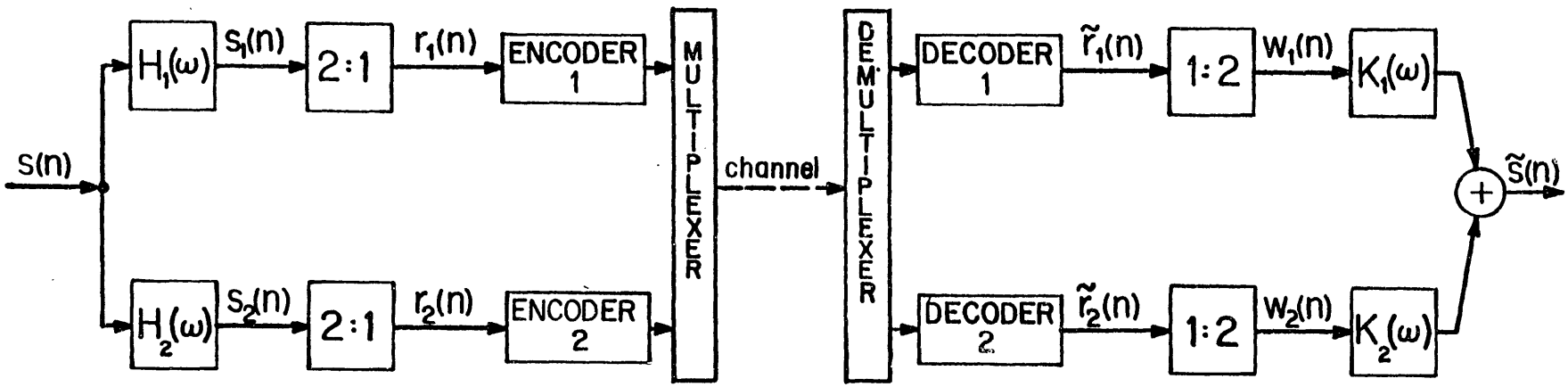

Fig. 2.4(a) A two-band sub-band coder.

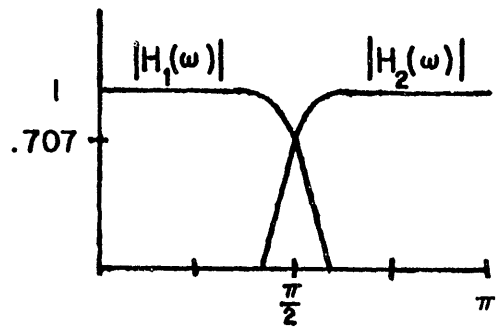

Fig. 2.4(b) Frequency response of typical quadrature mirror filters.

$$= \tfrac{1}{2} K_1(\omega) \left\{ H_1(\omega) S(\omega) + H_1(\omega + \pi) S(\omega + \pi) \right\}$$

$$+ \tfrac{1}{2} K_2(\omega) \left\{ H_2(\omega) S(\omega) + H_2(\omega + \pi) S(\omega + \pi) \right\} \qquad (2.5b)$$

$$= \tfrac{1}{2} S(\omega) \left\{ H_1(\omega) K_1(\omega) + H_2(\omega) K_2(\omega) \right\}$$

$$+ \tfrac{1}{2} S(\omega + \pi) \left\{ H_1(\omega + \pi) K_1(\omega) + H_2(\omega + \pi) K_2(\omega) \right\} \qquad (2.5c)$$

The first term in Equation (2.5c) is the desired signal, while the second represents the unwanted, aliased, image. To minimize the amount of work to be done in designing filters, it is reasonable to pick $K_1(\omega)$ and $K_2(\omega)$ so that:

$$|K_1(\omega)| = 2 |H_1(\omega)| \qquad (2.6a)^*$$

and

$$|K_2(\omega)| = 2 |H_2(\omega)| \qquad (2.6b)$$

A specific choice is:

$$K_1(\omega) = 2 H_1(\omega) \qquad (2.7a)$$

and

$$K_2(\omega) = -2 H_2(\omega) \qquad (2.7b)^{**}$$

Thus, the expression for the system output becomes:

---

* The gain of 2 is necessary to compensate for the energy lost in producing the aliased image.

** Although the minus sign might seem a bit peculiar, it is nonetheless necessary. The same condition which provides for cancellation of the aliasing term would also cause the signal term to disappear as well if one set $K_2(\omega) = 2 H_2(\omega)$.

$$\tilde{S}(\omega) = S(\omega)\left\{H_1^2(\omega) - H_2^2(\omega)\right\}$$

$$+ S(\omega+\pi)\left\{H_1(\omega+\pi)H_1(\omega) - H_2(\omega+\pi)H_2(\omega)\right\} \qquad (2.8)$$

The aliasing term will be eliminated if:

$$H_1(\omega+\pi)H_1(\omega) = H_2(\omega+\pi)H_2(\omega) = 0 \qquad (2.9)^*$$

This condition is satisfied if:

$$H_2(\omega) = \pm H_1(\omega+\pi) \qquad (2.10)$$

If $h_1(n)$ and $H_2(n)$ are the impulse responses associated with $H_1(\omega)$ and $H_2(\omega)$, respectively, then this condition is equivalent to:

$$h_2(n) = \pm (-1)^n h_1(n) \qquad (2.11)$$

Assuming the above condition is satisfied, then the system transfer function, $G(\omega)$, is given by:

$$G(\omega) = \frac{\tilde{S}(\omega)}{S(\omega)} = H_1^2(\omega) - H_1^2(\omega+\pi) \qquad (2.12)$$

For reasons which will become clear later in this chapter, H_1 will be assumed to be implemented as a real valued symmetric FIR filter (i.e. $h_1(n) = h_1(N-1-n)$, where N is the filter length). In this case, it is well known that [16-18]:

$$H_1(\omega) = \pm |H_1(\omega)| e^{-j\omega(N-1)/2} \qquad (2.13)$$

Combining Equations (2.12) and (2.13):

---

* If H_1 and H_2 were ideal filters, with perfect stop-band attenuation, then $H_1(\omega)H_1(\omega+\pi) = 0$ and $H_2(\omega)H_2(\omega+\pi) = 0$, and the aliasing term is always eliminated (as expected).

$$G(\omega) = e^{-j\omega(N-1)} \left\{ |H_1(\omega)|^2 - e^{-j\pi(N-1)} |H_1(\omega+\pi)|^2 \right\} \qquad (2.14)$$

Since $h_1(n)$ is real valued,

$$|H_1(\omega)| = |H_1(-\omega)| \qquad (2.15)$$

So at $\omega = \pi/2$, the transfer function becomes

$$G(\tfrac{\pi}{2}) = e^{-j\frac{\pi}{2}(N-1)} |H_1(\tfrac{\pi}{2})|^2 \left\{ 1 - e^{-j\pi(N-1)} \right\} \qquad (2.16)$$

Clearly, if N is odd, the transfer function will equal zero at $\omega = \pi/2$, regardless of the specific filter design. Thus, only even order filters will be considered, in which case the transfer function is of the form:

$$G(\omega) = e^{-j\omega(N-1)} \left\{ |H_1(\omega)|^2 + |H_1(\omega+\pi)|^2 \right\} \qquad (2.17)$$

For the most faithful reproduction of the signal, the expression in brackets should be as close to unity as possible. The linear phase term implies that the output is a delayed version of the input, a necessary consequence of the utilization of only causal systems.

At this point, it is useful to pause, remind oneself of the context in which this system is being used, and address some pertinent questions:

- To obtain the advantages of sub-band coding, it is necessary that the two sub-bands (of the system of Fig. 2.4) be well isolated, i.e. the "leakage" between bands, as indicated by the shaded region in Fig. 2.4b, should be fairly small. Given this consideration, is it possible to design a useful H_1 so that the magnitude of the system response is identically equal to one? If not, how does one design H_1 to obtain reasonable sub-band isolation and fairly flat system response?
- In the above anaylsis, it was assumed that the coder/decoder

systems used in each band are identity systems. How do the results change when this assumption is altered? Specifically, what happens when the encoder-decoder systems are also sub-band coders? (If a sub-band coder system employing QMF's is to be implemented with more than two bands, it will be necessary to "nest" band-splitting networks.) Also, what happens when one considers quantization effects?

With these considerations in mind, the analysis can proceed in an orderly and useful fashion.

From Equation (2.12):

$$G(\omega) = H_1^2(\omega) - H_1^2(\omega + \pi)$$

$$= \{H_1(\omega) - H_1(\omega + \pi)\}\ \{H_1(\omega) + H_1(\omega + \pi)\} \qquad (2.18)$$

In the time domain, this is equivalent to:

$$g(n) = \{h_1(n)\ [1 - (-1)^n]\} * \{h_1(n)\ [1 + (-1)^n]\} \qquad (2.19)$$

where * denotes convolution.

In order that $|G(\omega)| \equiv 1$, g(n) must consist of a single sample. Now define

$$h_o(n) = \tfrac{1}{2} h_1(n)\,[1 - (-1)^n] = \begin{cases} h_1(n) & n \text{ odd} \\ 0 & n \text{ even} \end{cases} \qquad (2.20a)$$

$$h_E(n) = \tfrac{1}{2} h_1(n)\,[1 + (-1)^n] = \begin{cases} 0 & n \text{ odd} \\ h_1(n) & n \text{ even} \end{cases} \qquad (2.20b)$$

Since $h_1(n)$ is a symmetric filter of length N,

$$h_o(n) = h_E(N - 1 - n) \qquad (2.21)$$

So:

$$g(n) = 2h_E(n) * 2h_o(n) = 4 \sum_{k=0}^{N-1} h_E(k)\, h_o(n-k)$$

$$= 4 \sum_{k=0}^{N-1} h_E(k)\, h_E(N - 1 - (n-k)) \qquad (2.22)$$

and

$$g(N-1) = 4 \sum_{k=0}^{N-1} h_E^2(k) \qquad (2.23)$$

But $h_E(0) = h_1(0) = h_1(N-1) \neq 0$ (since $h_1(n)$ is of length N), so $g(N-1) \neq 0$, thus implying:

$$g(n) = 0 \quad \text{for} \quad n \neq N-1 \qquad (2.24)$$

Using Equations (2.22) and (2.24), one obtains:

$$g(1) = h_E(0)\, h_E(N-2) = h_1(0)\, h_1(1) = 0$$

$$\Rightarrow h_1(1) = 0$$

Repeated application of Equations (2.22) and (2.24) yields:

$$h_1(n) = \begin{cases} \frac{1}{2} & n = 0 \text{ or } N-1 \\ 0 & \text{otherwise} \end{cases} \qquad (2.25)$$

and so:

$$H_1(\omega) = \tfrac{1}{2}(1 + e^{-j\omega(N-1)}) = e^{-j\omega(N-1)/2} \cos \omega \left(\frac{N-1}{2}\right) \qquad (2.26)$$

Clearly, such a filter is not suitable for the needs of a sub-band system, and so it will be necessary to formulate a compromise design.

Hanning filters [16, 17] have several properties that make them suitable for use in the sub-band system under consideration [19]. The stop-band attenuation of a Hanning filter increases with increasing distance from the cutoff frequency. Since the long-term average spectrum of speech drops off with increasing frequency, such filters

would provide for better isolation of the low-energy, high frequency sub-bands from the high-energy, low frequency sub-bands than filters with equiripple stop-band regions. However, since the power spectral density of speech signals does not exhibit a large change over small changes in frequency, the wide transition region of Hanning filters (vis-à-vis other filter designs) is not a significant drawback. In addition, Hanning filters have an extremely flat pass-band response, so when they are used in two-band QMF systems, the resulting overall frequency response, as given by Equation (2.17), is quite flat, with the maximum amount of the ripple occurring in the crossover region between the low-pass and high-pass filters. As the filter order is increased, this crossover region becomes narrower, and the ripple is confined to a narrower region. Empirical results show that when properly-designed Hanning filters are used, the maximum ripple amplitude of the system response given by Equation (2.17) is about $\pm$ 0.2 dB, regardless of filter length. Figure 2.5 illustrates a 16-tap low-pass Hanning filter, and the resulting two-band system response.

Let us now turn our attention to the effects of encoder-decoder systems shown in Fig. 2.4. Suppose that in the analysis of the system of Fig. 2.4 a more general expression for $\tilde{R}_1(\omega)$ and $\tilde{R}_2(\omega)$ was used, i.e.,

$$\tilde{R}_1(\omega) = G_1(\omega)R_1(\omega) \qquad (2.27a)^*$$

and

$$\tilde{R}_2(\omega) = G_2(\omega)R_2(\omega) \qquad (2.27b)$$

---

* Since the encoder-decoder systems could be nonlinear, $G_1(\omega)$ and $G_2(\omega)$ may depend on $R_1(\omega)$ and $R_2(\omega)$, respectively, as well as the encoder-decoder systems.

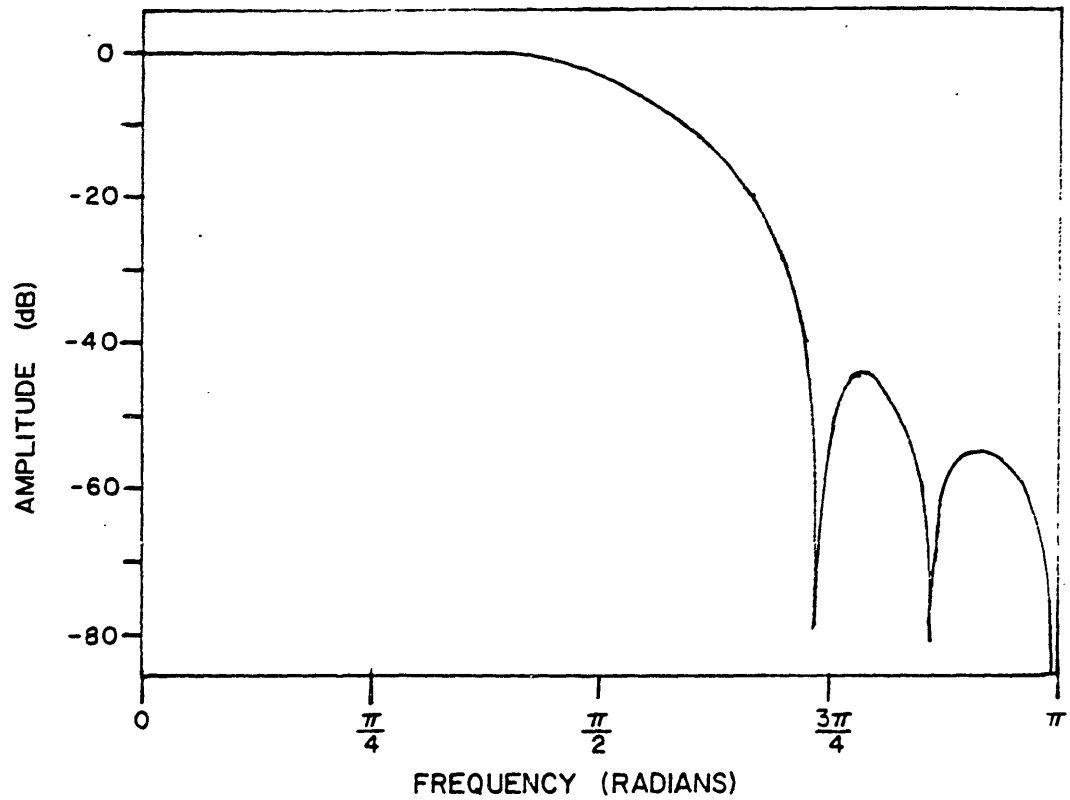

Fig. 2.5(a) Frequency response of a 16-tap low-pass Hanning filter designed for use in a two-band QMF-based sub-band coder.

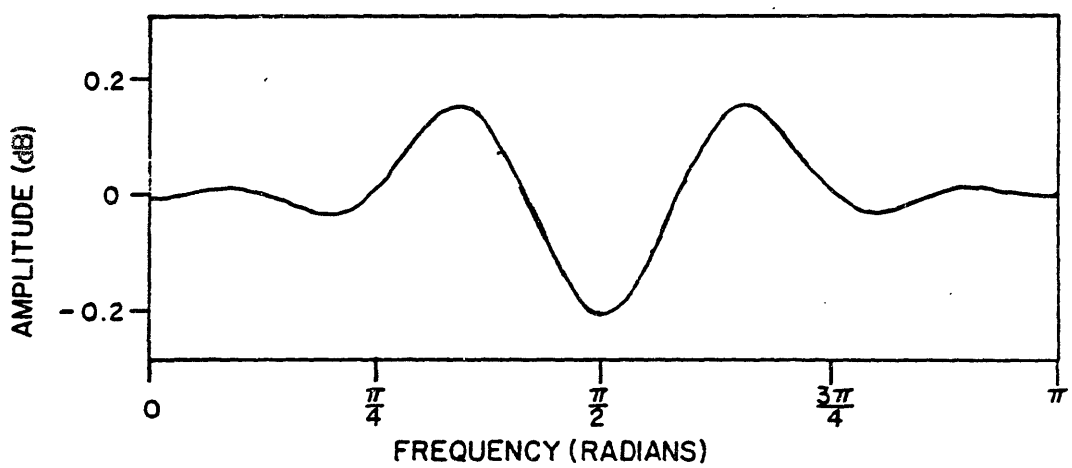

Fig. 2.5(b) Overall frequency response of the two-band QMF-based sub-band coder of Fig. 2.4(a) implemented with the filter of Fig. 2.5(a). (Note the difference in amplitude scale between Figs. 2.5(a) and 2.5(b).)

So now:

$$W_1(\omega) = \tilde{R}_1(2\omega) = G_1(2\omega)\, R_1(2\omega) \qquad (2.28a)$$

$$W_2(\omega) = \tilde{R}_2(2\omega) = G_2(2\omega)\, R_2(2\omega) \qquad (2.28b)$$

Assume that the same set of filters is being used as before, i.e.,

$$K_1(\omega) = 2\, H_1(\omega)$$

$$K_2(\omega) = 2\, H_2(\omega)$$

$$H_2(\omega) = H_1(\omega + \pi)$$

So:

$$\tilde{S}(\omega) = 2\, H_1(\omega)\, W_1(\omega) - 2\, H_2(\omega)\, W_2(\omega) \qquad (2.29)$$

$$= H_1(\omega)G_1(2\omega)\, \{H_1(\omega)S(\omega) + H_1(\omega + \pi)S(\omega + \pi)\}$$

$$- H_2(\omega)G_2(2\omega)\, \{H_2(\omega)S(\omega) + H_2(\omega + \pi)S(\omega + \pi)\}$$

$$= S(\omega)\, \{H_1^2(\omega)G_1(2\omega) - H_2^2(\omega)G_2(2\omega)\}$$

$$+ S(\omega + \pi)\, \{H_1(\omega)H_1(\omega + \pi)G_1(2\omega) - H_2(\omega)H_2(\omega + \pi)G_2(2\omega)\}$$

$$= S(\omega)\, \{H_1^2(\omega)G_1(2\omega) - H_1^2(\omega + \pi)G_2(2\omega)\}$$

$$+ S(\omega + \pi)H_1(\omega)H_1(\omega + \pi)\, \{G_1(2\omega) - G_2(2\omega)\} \qquad (2.30)$$

From Equation (2.30), one can observe that the amount of aliasing cancellation will depend on how closely $G_1(2\omega)$ and $G_2(2\omega)$ are matched. If the encoder/decoder systems are identical QMF sub-band systems (without quantization), then there will be no aliasing, and

$$\tilde{S}(\omega) = S(\omega)G(\omega)G_1(2\omega) \qquad (2.31)$$

where $G(\omega)$ is given by Equation (2.12).

Now suppose one is interested in obtaining a three-band sub-band system, by starting with the system of Fig. 2.4, and replacing the first encoder-decoder system with a two-band QMF system implemented with appropriately designed N tap Hanning filters, so that:

$$G_1(2\omega) = e^{-j2\omega(N-1)} |G_1(2\omega)| \approx e^{-j2\omega(N-1)}$$

For the aliasing term of Equation (2.30) to be minimized, the second encoder-decoder system should be replaced by an all-pass network whose response, $G_2(\omega)$, closely matches $G_1(\omega)$. In fact, as shown by Equations (2.18) and (2.19), $G_2(\omega)$ can be set identically equally to $G_1(\omega)$, thus guaranteeing complete aliasing cancellation, by picking:

$$g_2(n) = \left\{h(n)[1 + (-1)^n]\right\} * \left\{h(n)[1 - (-1)^n]\right\} \qquad (2.32)$$

where $h(n)$ is the prototype Hanning low-pass filter used to generate the two lower bands. The obvious drawback to this approach is that the highest frequency sub-band essentially requires as much computation to generate as the two lower frequency sub-bands. A far simpler alternative is to use a delay of N - 1 samples. In this case, the magnitude of the aliased image will be given by:

$$|S(\omega + \pi)| \, |H_1(\omega)H_1(\omega + \pi)| \, |1 - |G_2(2\omega)||$$

If H_1 is a Hanning low-pass filter, then the factor $|H_1(\omega)H_1(\omega + \pi)|$ will be quite small, except for the region near $\omega = \pi/2$. However, this is precisely the frequency region where $|G_2(2\omega)|$ is closest to unity. (See, for example, Fig. 2.5b.) Thus, the aliased image will still be

attenuated quite adequately.*

Now suppose the encoder-decoder sub-systems are quantizers. In this case,

$$G_1(2\omega) = 1 + \Delta G_1(2\omega)$$

$$G_2(2\omega) = 1 + \Delta G_2(2\omega)$$

and the magnitude of the aliased image is given by:

$$|S(\omega+\pi)|\,|H_1(\omega)H_1(\omega+\pi)|\,|\Delta G_1(2\omega) - \Delta G_2(2\omega)|$$

$$\leq |S(\omega+\pi)|\,|H_1(\omega)H_1(\omega+\pi)|\,\{|\Delta G_1(2\omega)| + |\Delta G_2(2\omega)|\}$$

where the upper bound is obtained using the triangle inequality [20]. Once again, if H_1 is a Hanning low-pass filter, then the factor $|H_1(\omega)H_1(\omega+\pi)|$ will be quite small, except for the region near $\omega = \pi/2$ (at $\omega = \pi/2$, $|H_1(\pi/2)H_1(3\pi/2)| \approx 1/2$). In this region, the aliased image will be produced at a level comparable to the quantizing noise level.

Thus far, it has been demonstrated that the use of QMF's in a two-band system provides for a significant reduction in aliasing terms, even when more complex schemes are used to code each sub-band signal. Thus, to employ them in a multi-band configuration, two-band systems can be "nested" in a tree structure. This tree structure may be either symmetric or asymmetric, in order to obtain sub-bands with equal or unequal widths, respectively. Figures 2.6 and 2.7 show four-band and five-band systems, respectively, illustrating these methods.

---

*If the prototype low-pass filter had been implemented using an IIR filter, then this simple alternative would not have been available. This illustrates one of the advantages of using symmetric FIR filters to implement the QMF's.

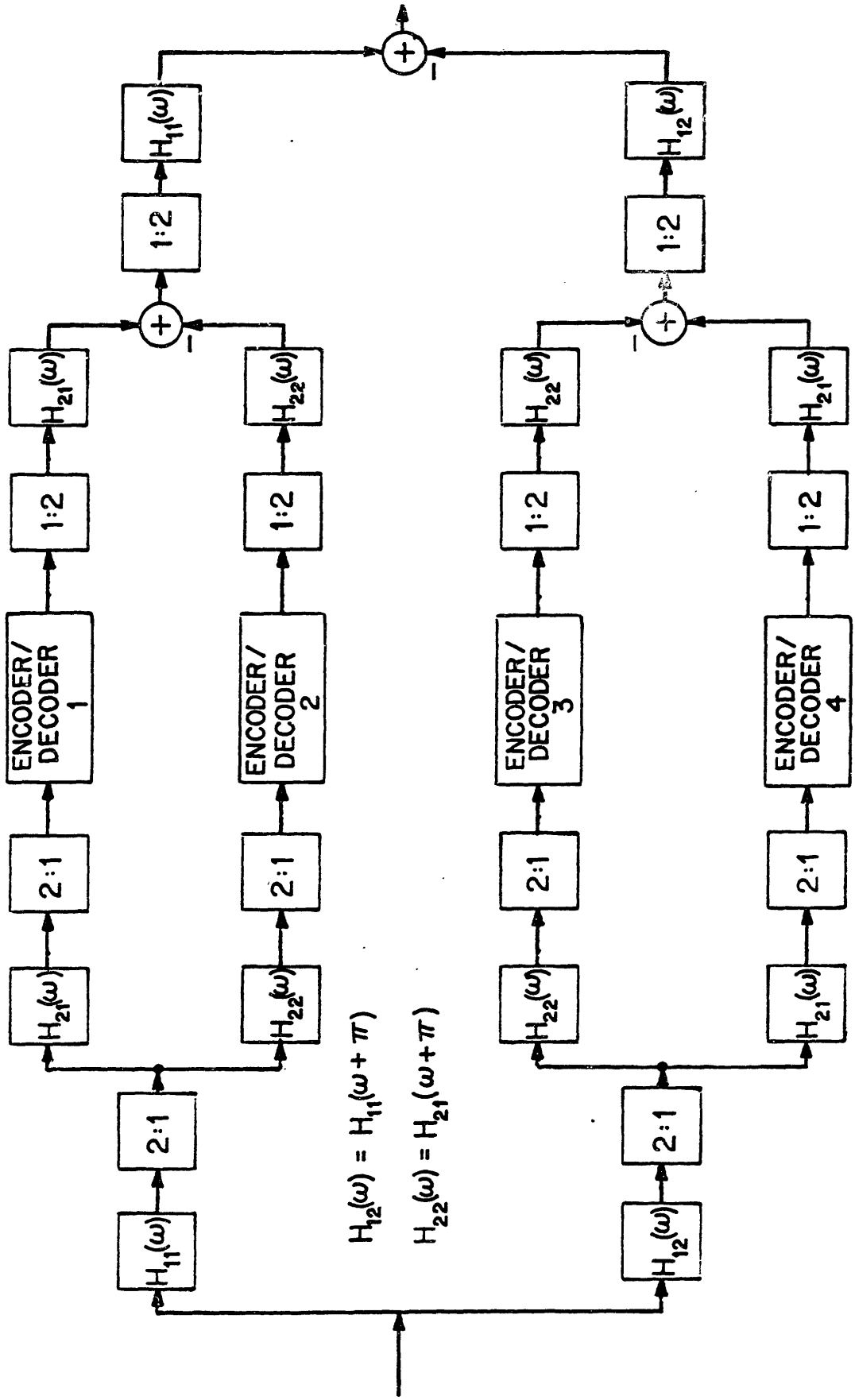

Fig. 2.6 Four-band sub-band coder incorporating QMF's.

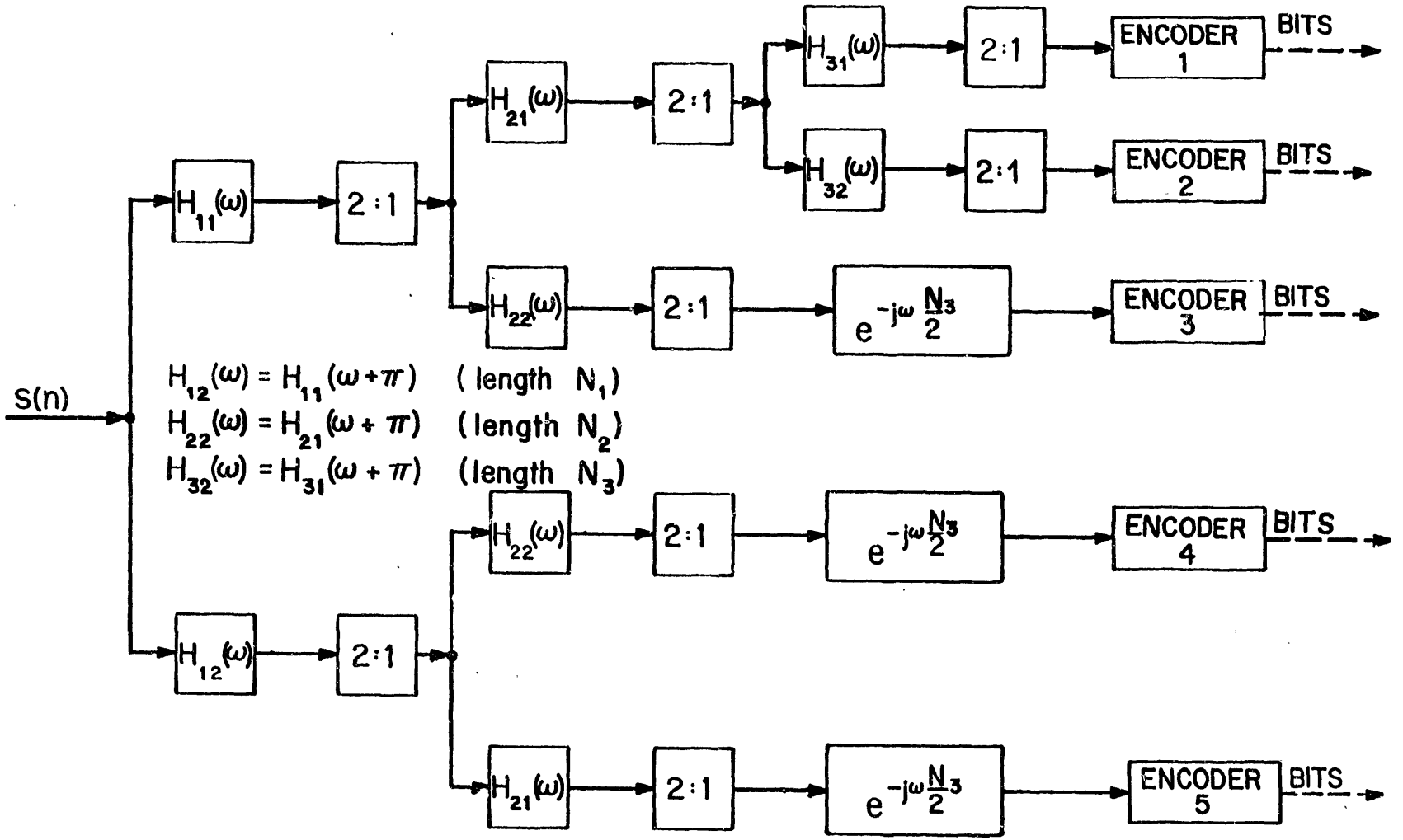

Fig. 2.7(a) Transmitter section of five-band sub-band coder incorporating QMF's.

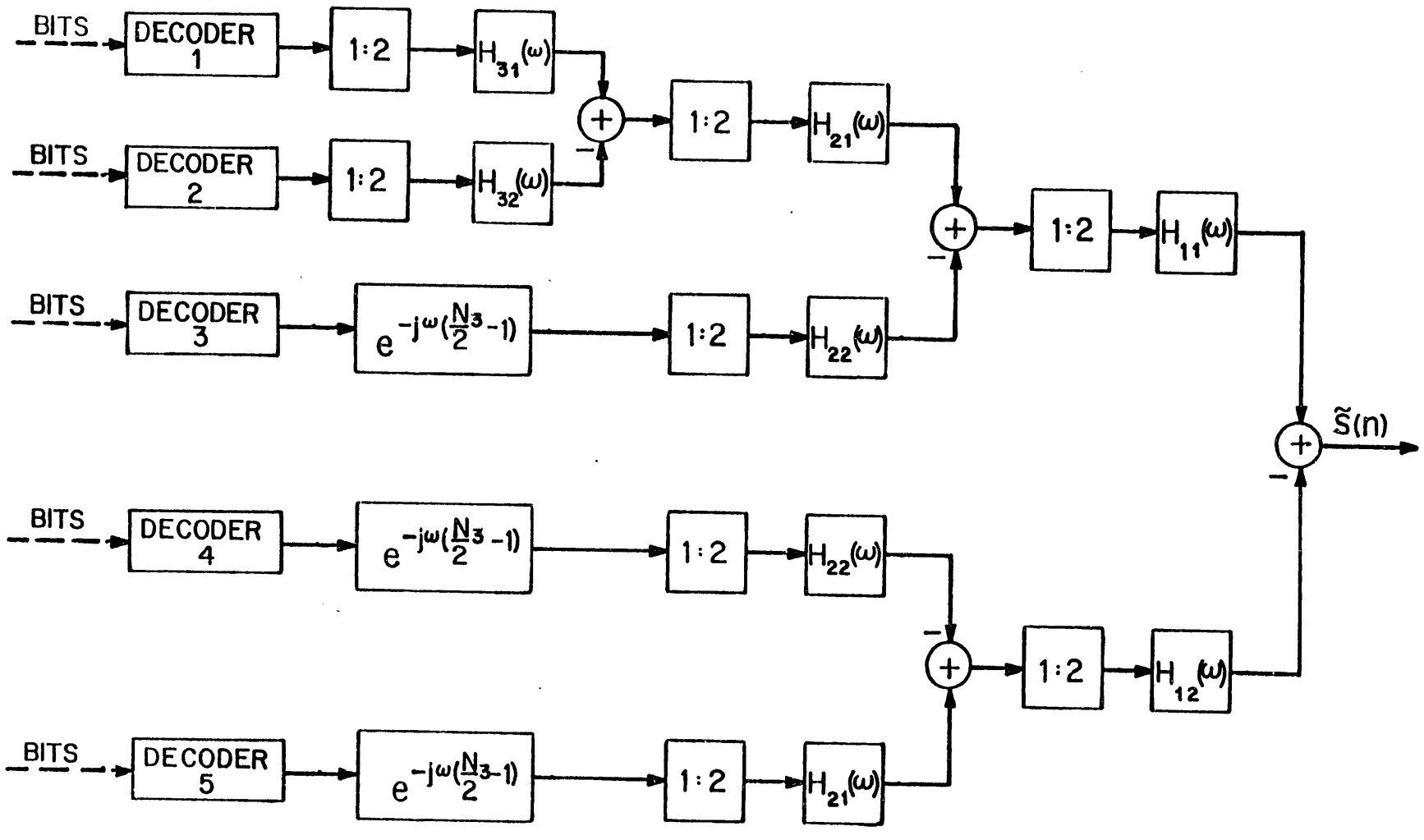

Fig. 2.7(b) Receiver section of five-band sub-band coder incorporating QMF's.

As has just been discussed, when asymmetric trees are used, delay lines can be used as an efficient means of assuring that the desired aliasing cancellation is essentially complete. If the encoder/decoder systems of each sub-band make use of the same side information, such as pitch information, then the delay lines should each be split into two nearly equal portions, one implemented in the transmitter, the other in the receiver. This use of delay lines in sub-band coder systems is illustrated in Fig. 2.7 for a five-band system.

By using the equivalence relations illustrated in Fig. 2.8, one can obtain an equivalent parallel structure for any given tree structure, and thus obtain a structure identical in form to Fig. 2.1. Figures 2.9 and 2.10 illustrate the equivalent parallel forms of the systems of Figs. 2.6 and 2.7, respectively.

At this point, it should be apparent that the use of the QMF technique poses further restrictions on the location and bandwidth of the sub-bands. Each sub-band must have a bandwidth equal to a power of one-half times the total bandwidth. If one wishes to leave gaps between bands to conserve bandwidth (or between dc and the lowest band), one can drop out (not encode) some of the sub-bands. If this is done, the original signal must be pre-filtered to avoid the aliasing effects that would result due to the loss of cancellation effects that would have been provided by the missing sub-bands. In addition, the use of the QMF structure intrinsically assumes that the upper frequency limit of the coding system is equal to half the sampling rate of the input signal. For example, for the highest sub-band generated by the QMF structure to have an upper frequency limit of 3200 Hz, the input to the QMF network must be sampled at 6400 Hz. Often, as in the example just cited, the

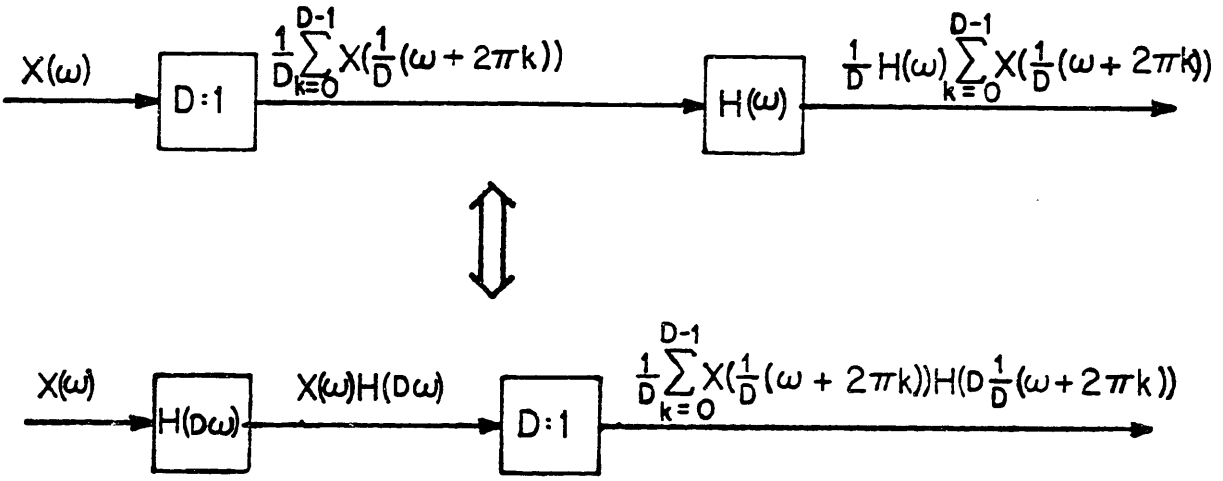

Fig. 2.8(a) Decimator-bandpass ↔ bandpass-decimator equivalence.

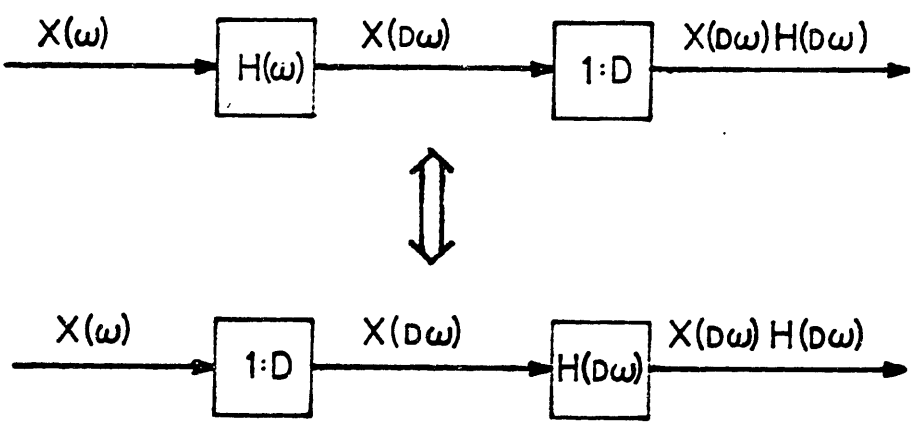

Fig. 2.8(b) Bandpass-interpolator ↔ interpolator-bandpass equivalence.

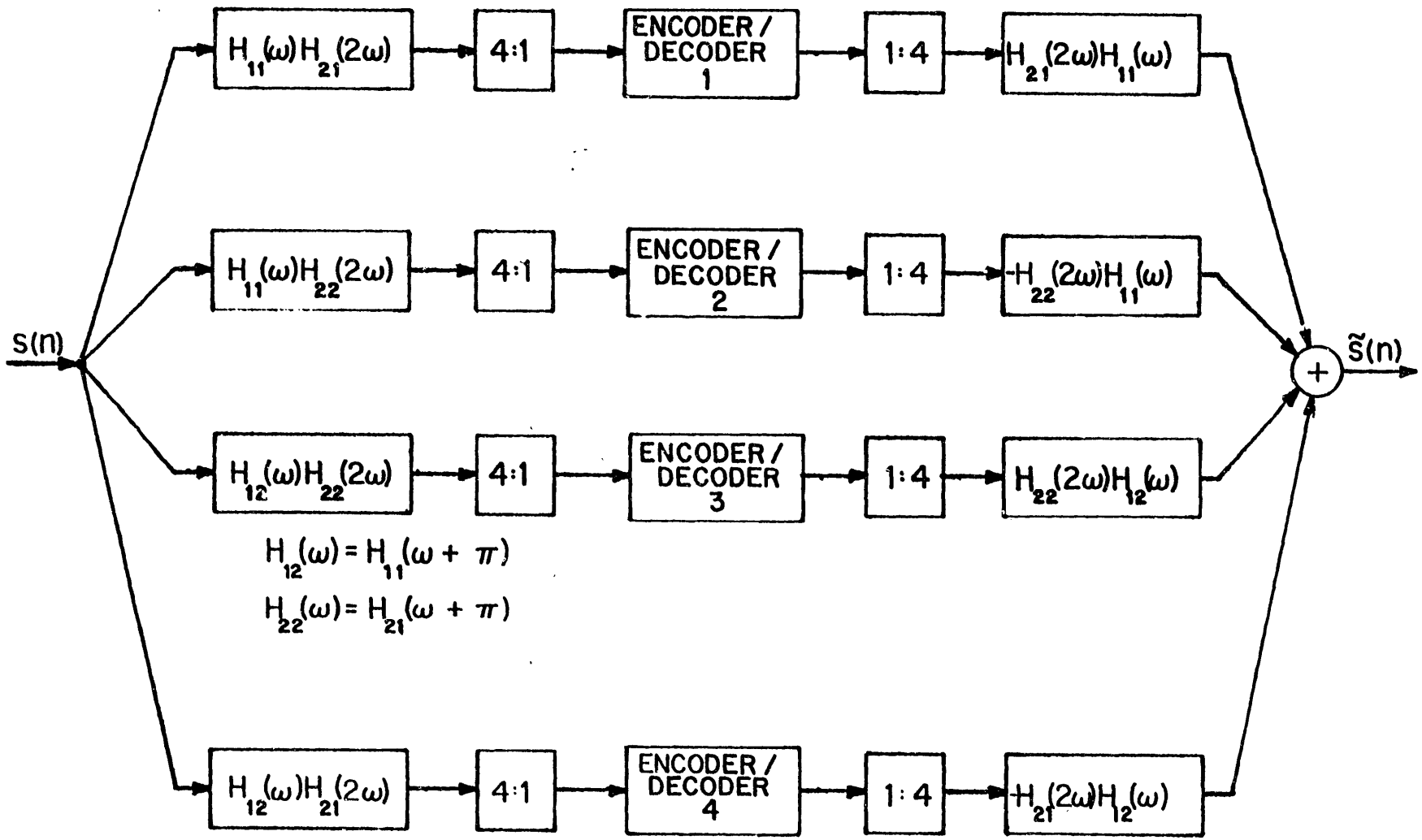

Fig. 2.9 Equivalent parallel structure for coder of Fig. 2.6.

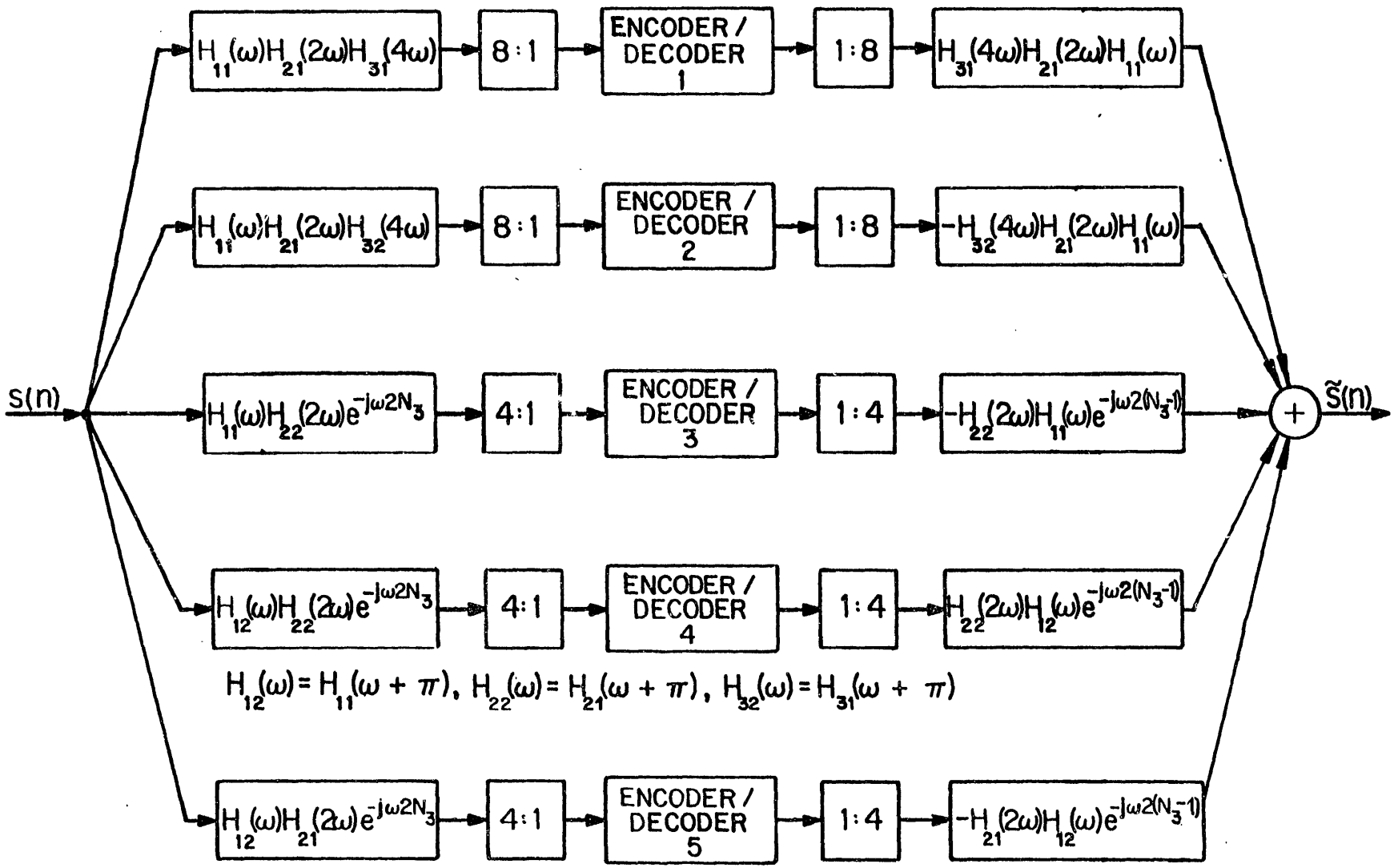

Fig. 2.10 Equivalent parallel structure for coder of Fig. 2.7.

input sampling rate will be somewhat unconventional, and sampling rate conversion systems will be required to handle signals which are sampled at a conventional sampling rate. In the example just cited, the coding system could handle signals sampled at 8 kHz if a 4/5 sampling rate conversion system is used at the input to the transmitter and a 5/4 sampling rate conversion system is used at the receiver output.

2.5 The Use of QMF's to Obtain Octavely Spaced Sub-bands

As was stated in the beginning of this chapter, a desirable manner in which to pick the widths and locations of the sub-bands is so that each sub-band makes an equal contribution to the articulation index (AI). If a QMF network is used to accomplish the band-splitting and frequency translation of the sub-bands, one way to approximately achieve this equal AI contribution with a reasonable number of bands (say four or five) is to use an octave band structure. Figure 2.11 illustrates the bandwidths and locations of the sub-bands for the proposed 9.6 kb/s and 16 kb/s systems. The figure also shows the sub-band widths and locations for the 9.6 kb/s and 16 kb/s systems proposed in Reference [3], which employed conventional integer-band sampling techniques. The frequency axis in this figure is warped to indicate each band's contribution to the AI. Figure 2.12 illustrates the QMF bandsplitting - decimation and interpolation - merging tree structures used in the new 9.6 kb/s sub-band coder to obtain four octavely spaced sub-bands. The networks for the new 16 kb/s sub-band coder are essentially the same, except that five octavely-spaced bands are used. The high-pass filters are used to prevent aliasing effects which would otherwise occur due to the elimination of the lowest sub-band.

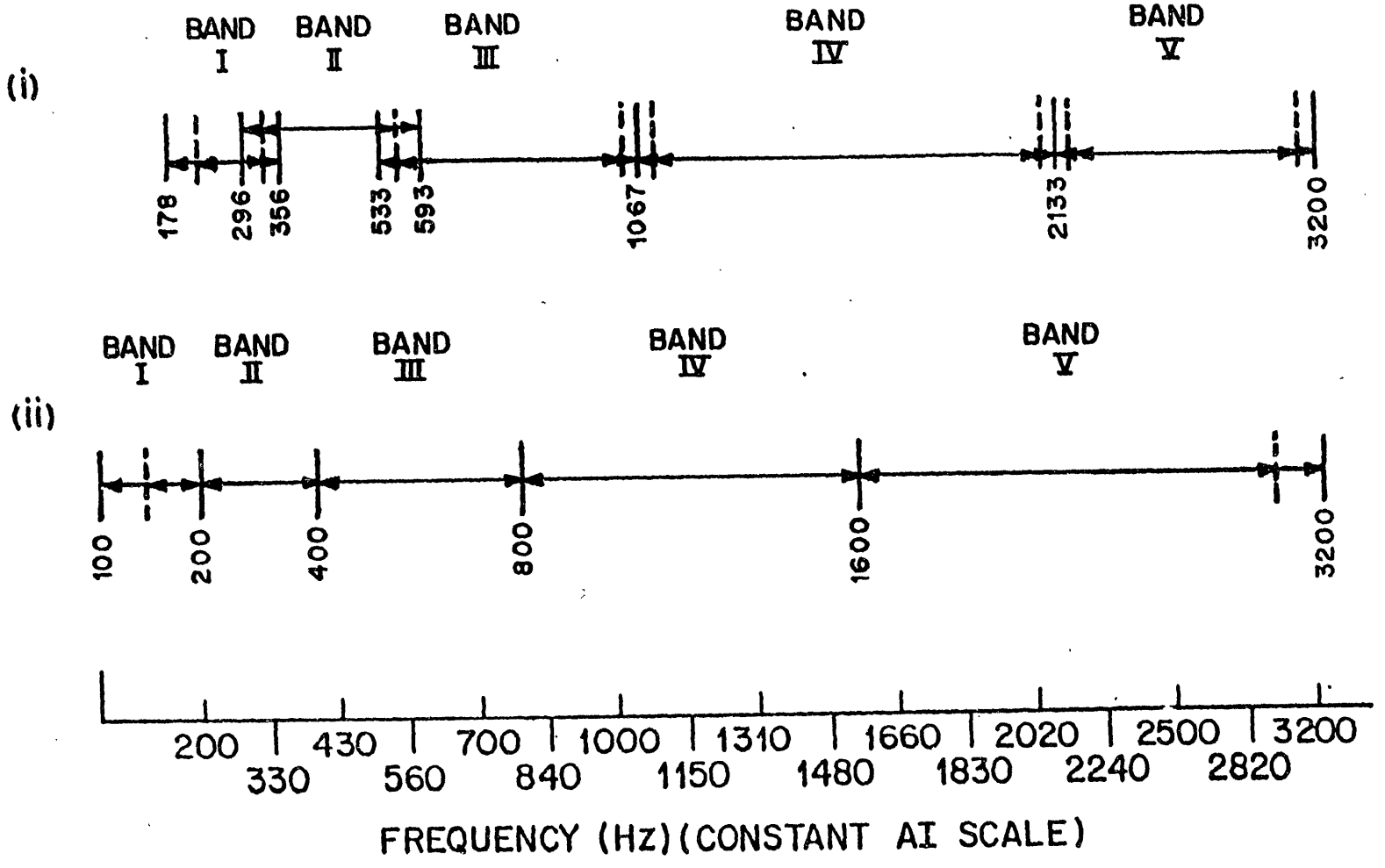

Fig. 2.11(a) Sub-band widths and locations for two 16 kb/s sub-band coders (i) old coder of Reference [3] (ii) new coder proposed in this thesis.

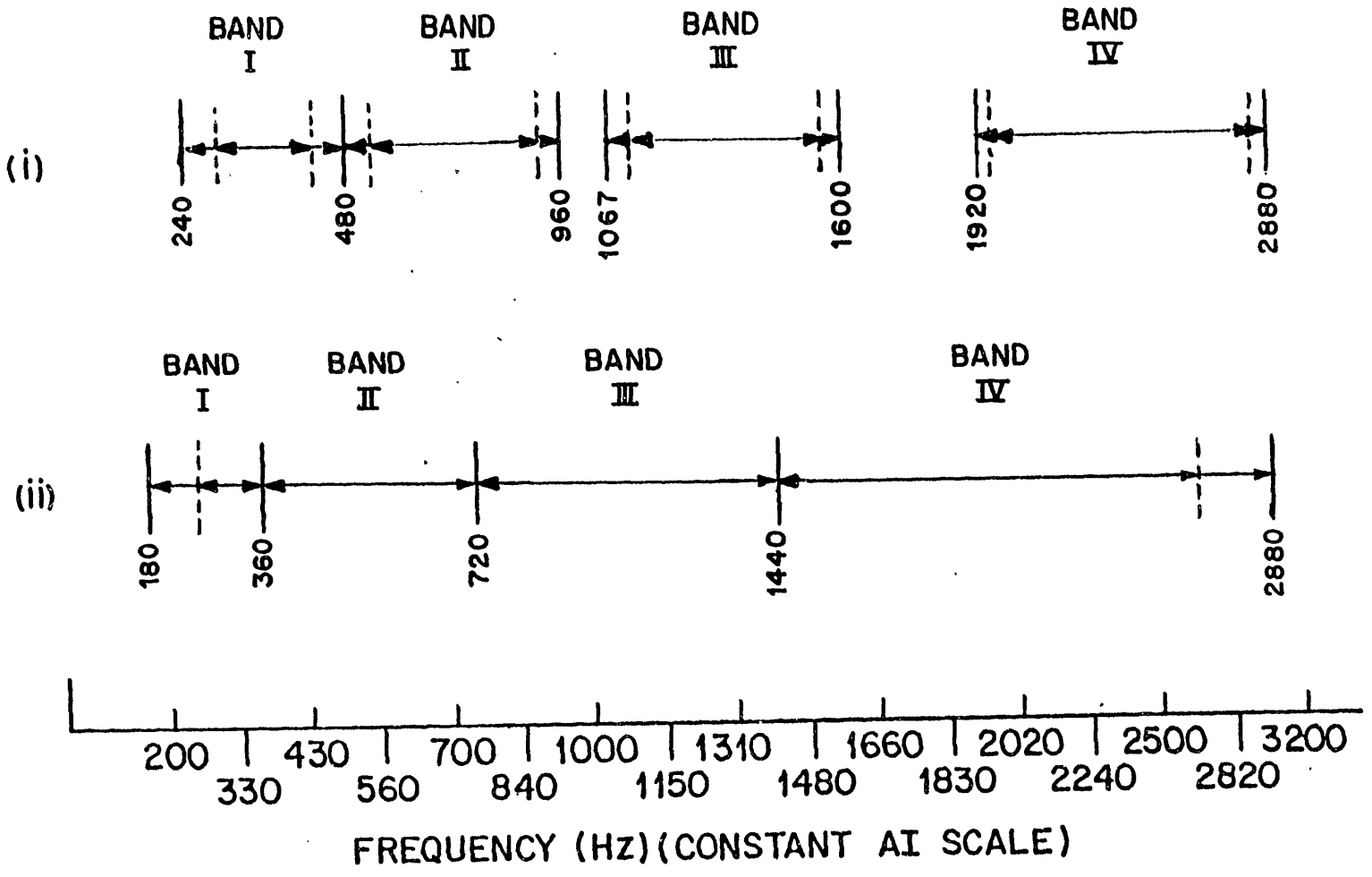

Fig. 2.11(b) Sub-band widths and locations for two 9.6 kb/s sub-band coders (i) old coder of Reference [3] (ii) new coder proposed in this thesis.

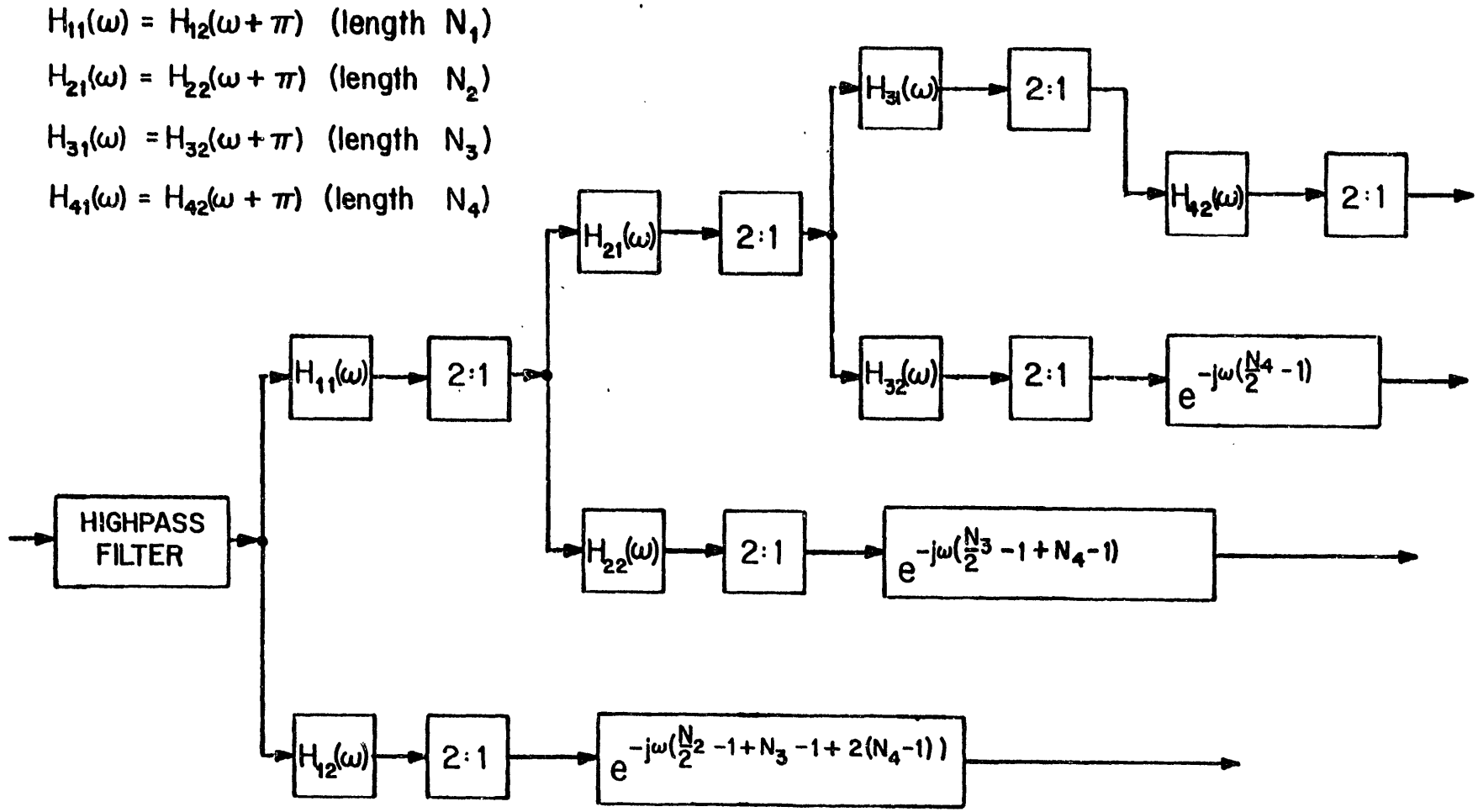

Fig. 2.12(a) Bandsplitting-decimation structure for generating four octavely-spaced sub-bands.

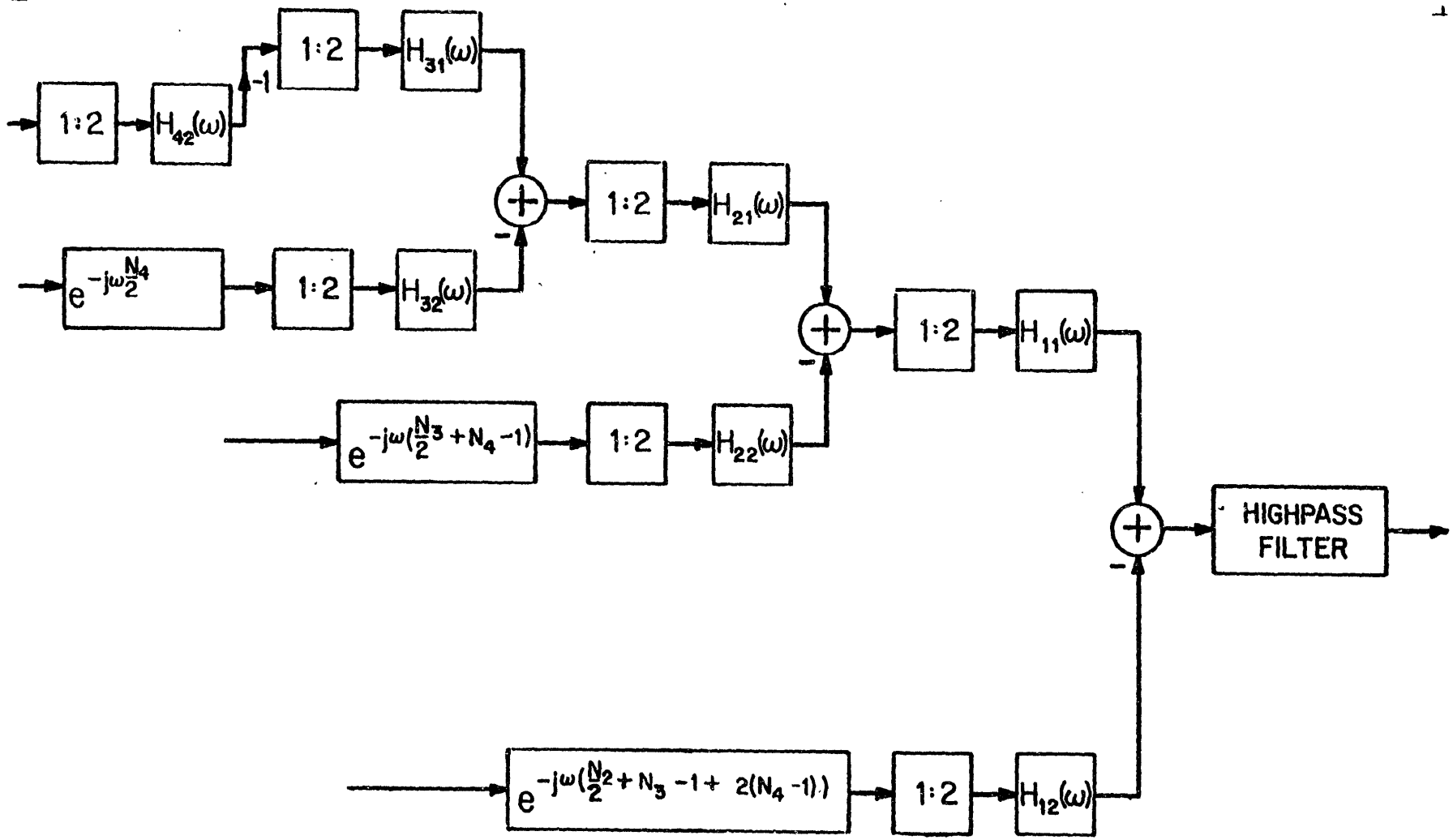

Fig. 2.12(b) Interpolation-merging structure for reconstructing the full band from four octavely-spaced sub-bands.

2.6 Efficient Implementation of QMF-Based Splitting-Decimation and Interpolation-Merging Networks

Croisier et al. [12] have proposed special structures for the efficient implementation of bandsplitting and bandmerging that exploit the special relationship among the QMF's.

Figure 2.13a illustrates the components of the bandsplitting-decimation network for the QMF-based two-band system of Fig. 2.4. From the figure

$$s_1(n) = h_1(n) * s(n) = \{h_E(n) + h_O(n)\} * s(n) \qquad (2.32a)$$

$$s_2(n) = \{(-1)^n h_1(n)\} * s(n) = \{h_E(n) - h_O(n)\} * s(n) \qquad (2.32b)$$

where $h_E(n)$ and $h_O(n)$ were defined in Equations (2.20a) and (2.20b), respectively.

From Equations (2.32a) and (2.32b), an equivalent structure, shown in Fig. 2.13b, is obtained for the bandsplitting network. To save memory, the filters $h_E(n)$ and $h_O(n)$ can share delay lines, as shown in Fig. 2.13c (after Croisier et al. [12]). Since $s_1(n)$ and $s_2(n)$ will be decimated by a factor of two, only the points which are retained after decimation need be computed. Thus, if $h_1(n)$ is N taps long, the network will require N/2 multiplies per input point to generate both $r_1(n)$ and $r_2(n)$.

Similarly, one can obtain an efficient structure to implement the interpolation-bandmerging network for the two-band system of Fig. 2.4. From Fig. 2.14a:

$$\tilde{s}(n) = w_1(n) * 2h_1(n) - w_2(n) * \{2(-1)^n h_1(n)\} \qquad (2.33)$$

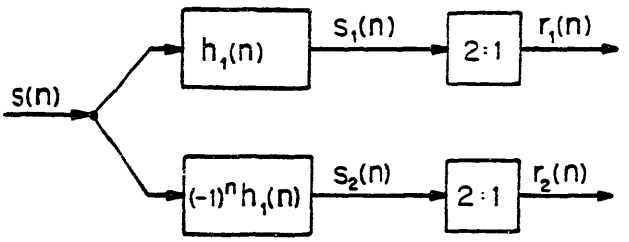

Fig. 2.13(a) Two band bandsplitting-decimation network incorporating QMF's.

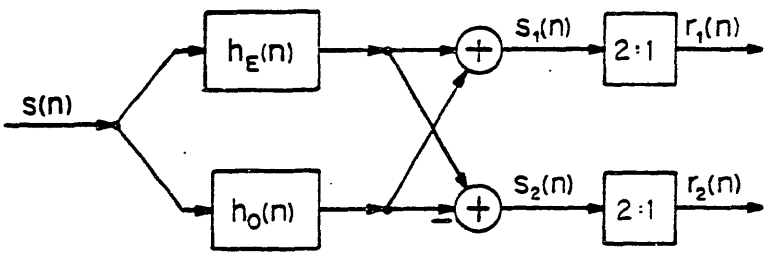

Fig. 2.13(b) Equivalent structure for Fig. 2.13(a).

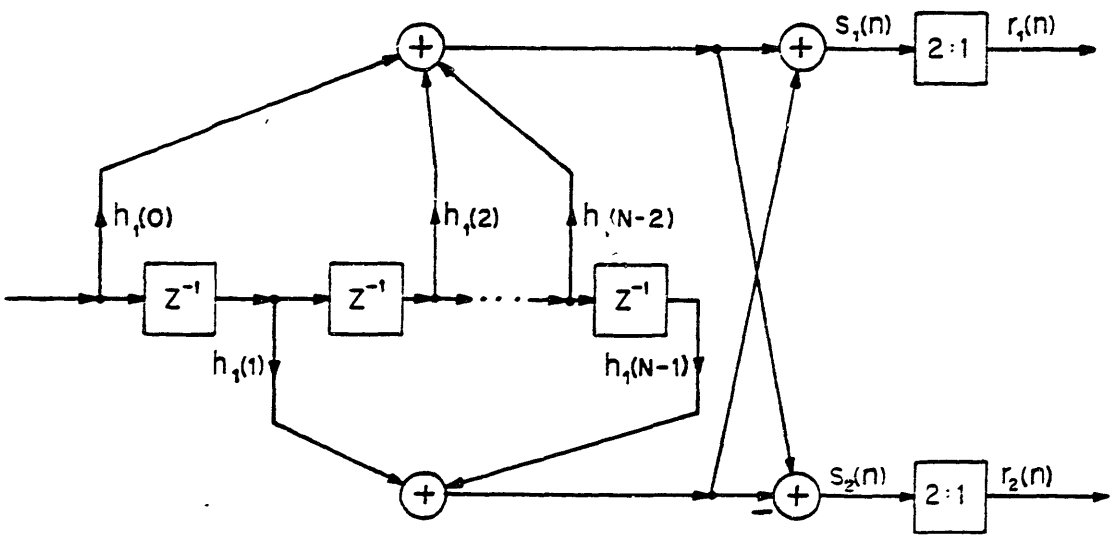

Fig. 2.13(c) Efficient implementation for Fig. 2.13(c) (after Croisier et al. [12]).

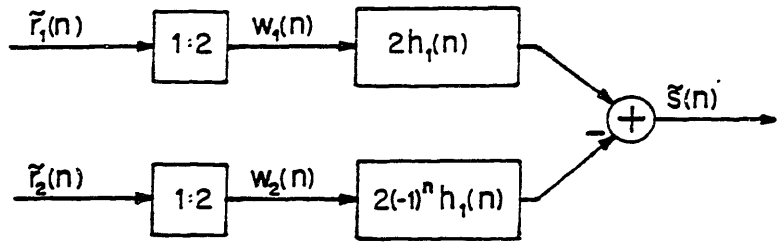

Fig. 2.14(a) Two-band interpolation-bandmerging network incorporating QMF's.

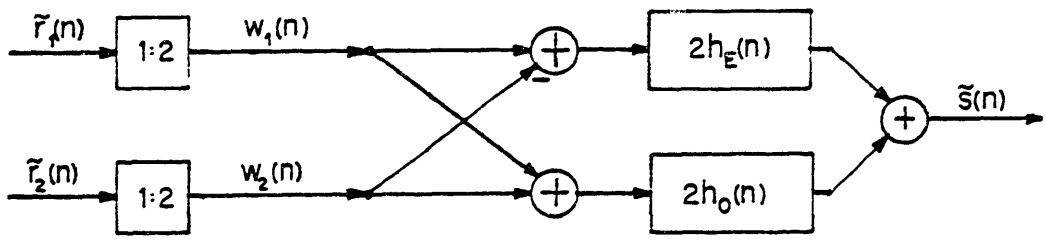

Fig. 2.14(b) Equivalent structure for Fig. 2.14(a).

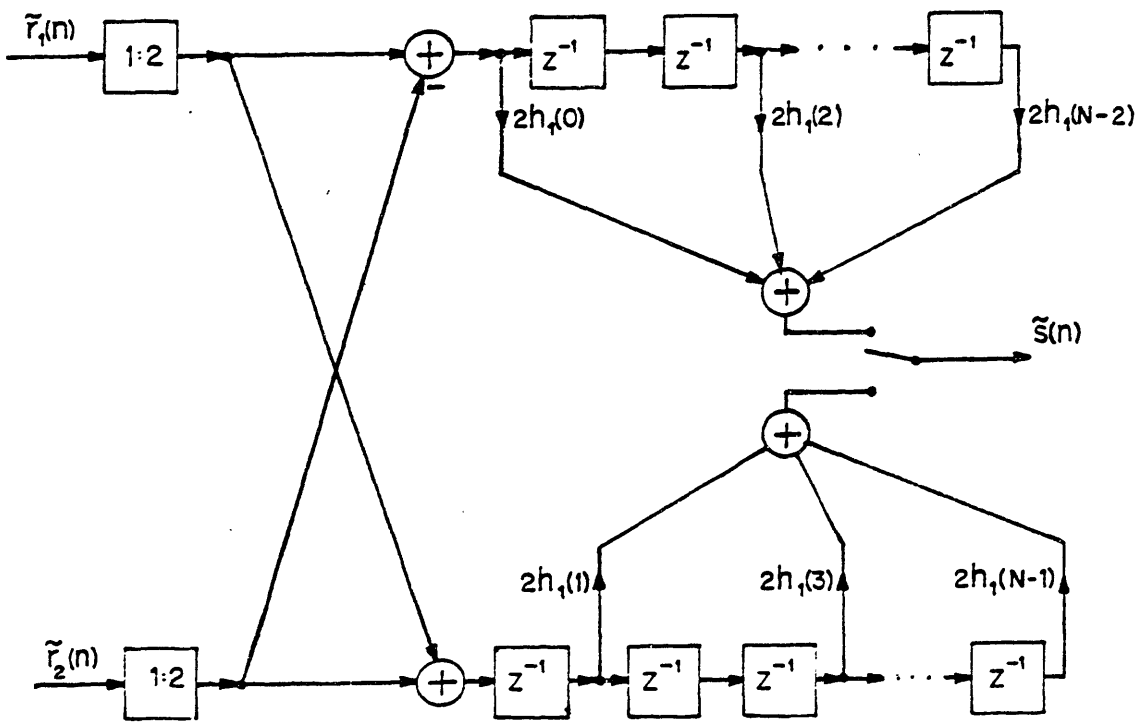

Fig. 2.14(c) Efficient implementation for Fig. 2.14(c) (after Croisier et al. [12]).

$$= w_1(n) * 2\{h_E(n) + h_O(n)\} - w_2(n) * 2\{h_E(n) - h_O(n)\} \qquad (2.34)$$

$$= \{w_1(n) - w_2(n)\} * 2h_E(n) + \{w_1(n) + w_2(n)\} * 2\,h_O(n)$$

From Equation (2.35), an equivalent structure, shown in Fig. 2.14b, is obtained for the bandmerging network. For any given output point $\tilde{s}(n)$, only one of the two outputs of the filters $h_O(n)$ and $h_E(n)$ will be nonzero, and thus the adder used to generate $\tilde{s}(n)$ can be replaced by a switch, as shown in Fig. 2.14c (after Croisier et al. [12]). This property arises from the fact that the inputs to the filters $h_O(n)$ and $h_E(n)$ are interlaced with zeros, and that the impulse responses $h_O(n)$ and $h_E(n)$ are also interlaced with zeros. As a result, it only takes N/2 multiplies to generate each output point $\tilde{s}(n)$.

2.7 Relative Computational Costs of Implementing Conventional vs QMF-Based Bandsplitting-Decimation and Interpolation-Bandmerging Networks

To close this chapter, a comparison is made between the number of multiplies per second required to implement the bandsplitting-decimation and interpolation-bandmerging networks for the 16 kb/s sub-band coder of Reference [3] and the new 16 kb/s sub-band coder that was simulated as part of this thesis project. The old coder of Reference [3] used conventional filters to implement a set of integer-band sampling networks, whereas the new coder used the techniques of the previous section to implement the octave band tree structure of Fig. 2.12. Included in the multiply count for the new coder is the computation associated with the implementation of the high-pass filters and the sampling rate conversion systems discussed earlier. The actual design of these systems will be discussed in Chapter 5.

Table 2.1 details the number of multiplies needed to accomplish

the integer band sampling operations in the old coder, while Table 2.2 lists the number of multiplies needed to implement the sampling rate conversion systems, high-pass filters and the octave band structures of the new coder. As indicated by the tables, the total multiply count for the new coder is about half that of the old coder. It is also interesting to note that a substantial portion of the multiply count for the new coder is due to the high-pass filters and the sampling rate conversion systems.

Table 2.1

Number of Multiplies to Accomplish Bandsplitting-Decimation and Interpolation-Merging in Old 16 kb/s Coder

Sampling Rate: 10.67 kHz

Data Frame Length: 90 samples

Band No.	Filter Length	Decimation Rate	Multiplies/Frame	
			Transmitter	Receiver
1	200	30	300	600
2	200	18	500	1000
3	200	10	900	1800
4	200	5	1800	3600
5	200	5	1800	3600
			5300	10600

Total multiplies/sec: 1.88×10^6

Table 2.2(a)

Number of Multiplies to Accomplish Bandsplitting-Decimation and Interpolation-Merging in New 16 kb/s Coder

Sampling Rate: 6.4 kHz

Data Frame Length: 160 samples

Split No.	Filter Length	Total Equivalent Decimation Rate	Multiplies/Frame	
			Transmitter	Receiver
1	32	2	2560	2560
2	16	4	640	640
3	16	8	320	320
4	16	16	160	160
5	8	32	40	40
			3720	3720

Octave Networks Sub-total multiplies/sec: 2.98×10^5

Table 2.2(b)

Number of Multiplies to Accomplish Highpass Filtering and Sampling Rate Conversion in New 16 kb/s Coder

Highpass Filter Order (IIR Design)	5
Multiplies/Frame (Transmitter and Receiver)	3520
Highpass Filter Sub-total, multiplies/second	1.41×10^5
Sampling Rate Conversion Filter Length	150
Sampling Rate Conversion Ratio	4/5
Multiplies/Frame (Transmitter and Receiver)	12000
Sampling Rate Conversion Sub-total, multiplies/second ..	4.8×10^5
Total multiplies/second (Octave Network + Highpass Filter + Sampling Rate Conversion)	9.18×10^5

CHAPTER 3

THE USE OF PITCH PREDICTION IN SUB-BAND CODING

3.1 Introduction

Many speech coding systems have been proposed which take advantage of the long-time correlations, i. e. pitch structure, associated with voice speech [1], yielding improved performance over their non-pitch-predicting counterparts. Time domain coders use an adaptive predictive filter to exploit these long-time correlations [1,21], whereas frequency domain coders explicitly make use of the fine harmonic structure associated with pitch [1,22].

This chapter begins with a brief discussion of time domain methods for predictive coding, and then focuses on the specific example of pitch predictive coding. This discussion is followed by a presentation of an efficient technique (due to Crochiere [7]) for the implementation of pitch prediction in sub-band coders. This presentation is followed by a discussion of limits on the effectiveness of pitch prediction in sub-band coders due to the nature of the sub-band signals. Taking this discussion into account, the focus of the chapter then turns to the design of the pitch prediction systems. The chapter closes with presentations of an efficient implementation scheme for the pitch prediction systems, and the computational costs of adding such systems to a sub-band coder.

3.2 Predictive Encoding

The principle of predictive encoding is illustrated in Fig. 3.1a. The discrete time signal s(n) is periodically analyzed, and the resulting analysis parameters are quantized for use by both the transmitter and the receiver, in order to assure that the two sub-systems match each other. These quantized analysis parameters are used to control the

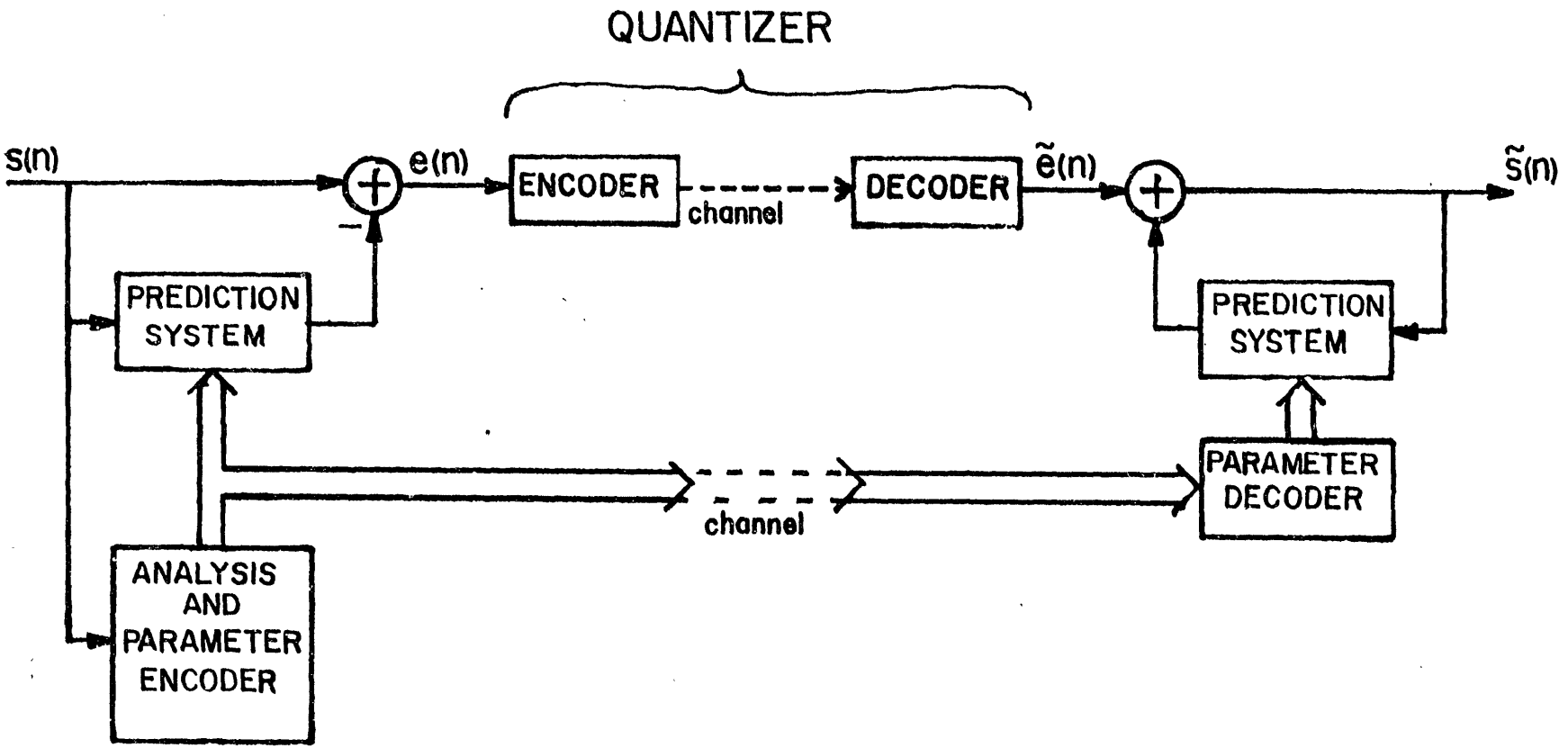

Fig. 3.1(a) Predictive encoding system.

prediction system. Typically, the prediction system is linear and uses only past values of s(n) (i.e. s(n-1), s(n-2), ...) to generate the estimate $\hat{s}(n)$. All prediction systems discussed in this thesis will have this property.

The difference between the actual signal s(n) and the estimate $\hat{s}(n)$, the prediction error e(n) is encoded and transmitted, along with the quantized analysis parameters, for use by the receiver. At the receiver, the prediction error signal is decoded, yielding $\tilde{e}(n)$. This signal is passed through an inverse prediction filter system, yielding the signal $\tilde{s}(n)$, a facsimile of the original signal s(n).

If the prediction estimate $\hat{s}(n)$ is highly correlated with the original signal s(n), then the prediction error variance σ_e^2 will be much lower than the original signal variance σ_s^2. Assuming that no quantizer overload has taken place, the noise energy associated with adaptive quantization is proportional to the input signal variance [1,8-11]. Thus, the noise associated with the quantization of the error signal e(n) will be lower in energy than the noise associated with the direct quantization of s(n). Unfortunately, though, this quantization noise will be filtered by the inverse filter, resulting in an increase in the noise energy level. In addition, this filtering action will result in the overall system noise possessing spectral characteristics similar to the inverse prediction filter frequency response. Figures 3.1b and 3.1c provide an illustration of this noise filtering process. In Fig. 3.1b,* the quantizer has been replaced by an adder which injects the quantization noise signal q(n) into

---

* In this figure, and many of those which will follow, the analysis and parameter encoding system is not shown, and is assumed to be used in the same manner as in Fig. 3.1a.

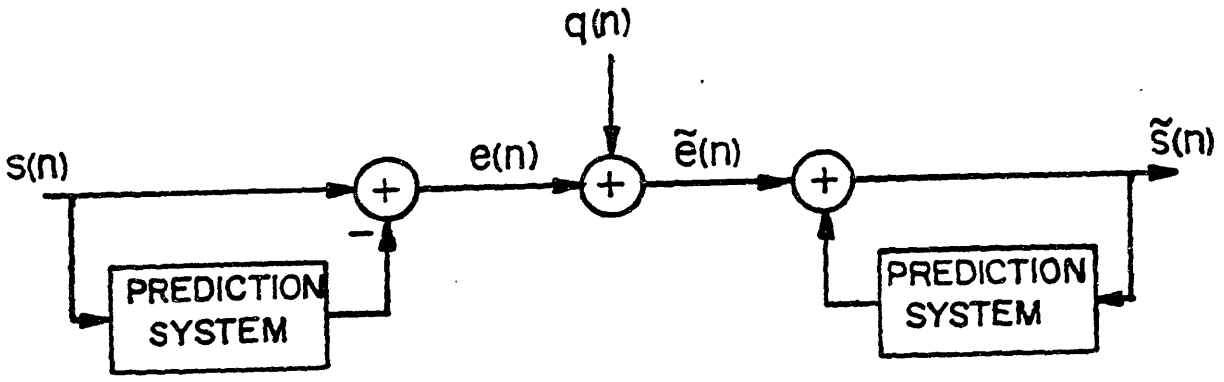

Fig. 3.1(b) Predictive encoding system of Fig. 3.1(a) incorporating quantization noise source model.

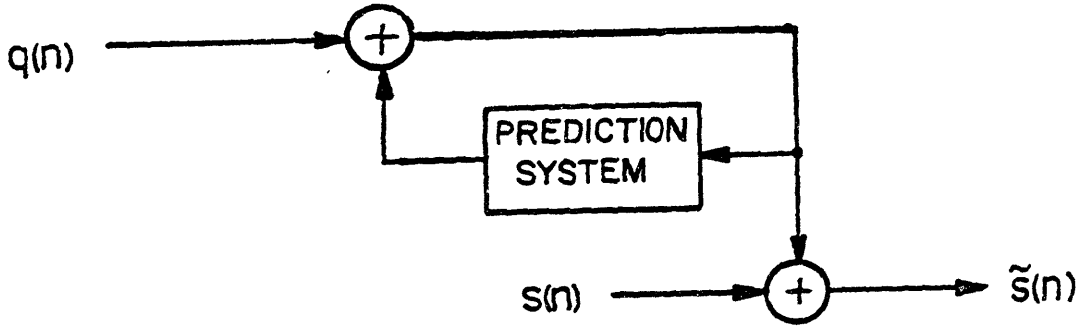

Fig. 3.1(c) Equivalent for the system of Fig. 3.1(b).

the system, where q(n) implicitly depends on e(n) and the particular quantizer which was used. Simple interchanges of the linear systems in Fig. 3.1b yield Fig. 3.1c. By inspection of Fig. 3.1c, one can see that the system noise is a spectrally shaped version of the quantizer noise, and that the inverse prediction filter is the cause of this noise shaping. Depending on the particular prediction filter used, such noise shaping could improve or degrade the subjective performance of the coding system. It is important to reiterate, however, that the reduction in noise energy obtained due to prediction is somewhat lost when the signal is inverse filtered. To prevent these noise accumulation effects, the prediction loop is usually enclosed in a feedback loop at the transmitter, as shown in Fig. 3.2a.*

The absence of noise filtering effects for the system of Fig. 3.2a is demonstrated in Figs. 3.2b and 3.2c. In Fig. 3.2b, the quantizer has been replaced by an adder which injects the quantization noise signal q(n) into the system, where, once again, q(n) implicitly depends on e(n) and the particular quantizer. Equivalently, the quantization noise signal q(n) could be injected at the input to the system, as shown in Fig. 3.2c. From this figure, it is clear that the total system noise is identically equal to the quantization noise.

For the system of Fig. 3.2a, the prediction error variance σ_e^2 will be much lower than the original signal variance σ_s^2 if the estimate $\tilde{\hat{s}}(n)$ is highly correlated with the original signal s(n). Since this system does not have the noise shaping properties of the system of Fig. 3.1a,

---

* Note that for this system, the receiver is identical to the portion of the transmitter enclosed in dotted lines. For this reason, future figures will often show only the transmitter portion of the coding system.

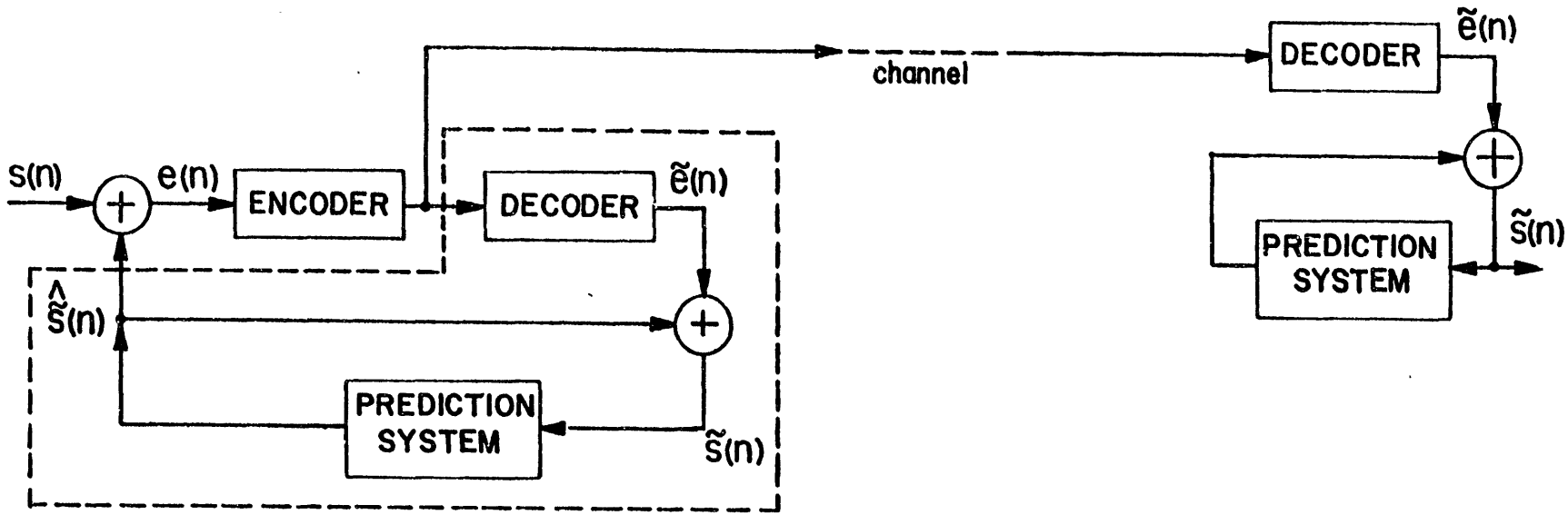

Fig. 3.2(a) Predictive encoding system incorporating feedback around the quantizer.

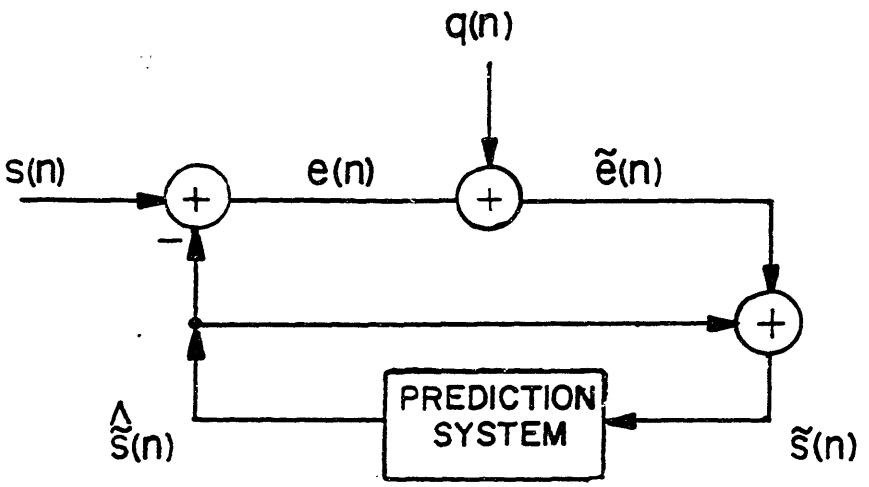

Fig. 3.2(b) Equivalent for system of Fig. 3.2(a), incorporating quantization noise source model.

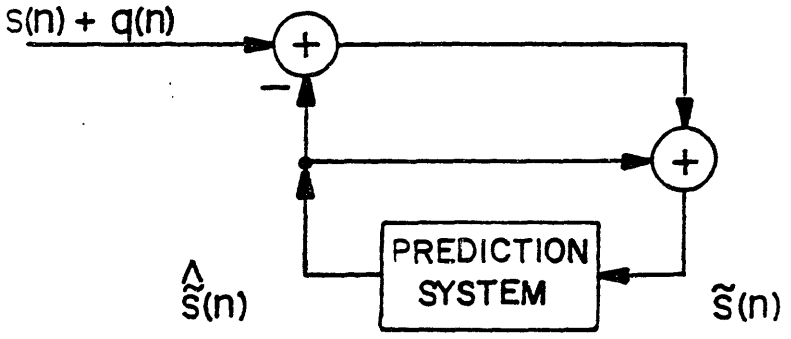

Fig. 3.2(c) Equivalent for system of Fig. 3.2(b).

the ratio of original signal variance σ_s^2 to prediction error variance σ_e^2, known as the prediction gain, provides an indication of the increase in signal-to-noise ratio (SNR) obtainable when predictive encoding is used in conjunction with a given quantizer. Unfortunately, the ratio σ_s^2/σ_e^2 is impossible to calculate without making further assumptions about the quantizer, due to the interdependence of s(n), e(n) and the nonlinear quantizer system. As shown in Reference [18], if the quantization is fine enough to guarantee that the quantization noise will be relatively uncorrelated with the signal s(n) and will have a much lower variance than that of s(n), then the prediction error variance associated with the system of Fig. 3.2a will be approximately the same as the prediction error variance associated with the system of Fig. 3.1a when the two systems have identical input. Using this approximation, the calculation of σ_s^2/σ_e^2 becomes tractable. When coarser quantizers are used, so that the previously stated assumptions break down, the prediction performance will degrade. Fortunately, though, even when rather coarse quantizers are used, experimental results have shown that significant SNR gains are still obtainable when prediction is used [1, 21]. For example, the system of Reference [21] made use of short-time prediction to exploit the formant structure in speech and long-time prediction to take advantage of the pitch structure in voiced speech. This system yielded speech quality comparable to that of a 5 bit/sample log-PCM system, yet it used only 1 bit/sample to encode the prediction error. (The step size for this quantizer was computed every 5 ms and transmitted as side information.)

Before closing this section on the general use of prediction, it is worthwhile to consider a few computational issues. Of particular

interest is the increase in coder complexity that results when prediction is used in conjunction with a given coding system. From Fig. 3.2a, we see that the use of prediction in a feedback loop requires the implementation of the quantizer decoder in the transmitter as well as in the receiver. For some quantizing systems, the decoder is fairly simple as compared to the encoder, but for other systems, such as sub-band coders, the decoder is about as complex as the encoder. For the latter case, the amount of computation for a predicting coder will, therefore, be at least fifty percent greater than the amount of computation required for its non-pitch predicting counterpart. In addition, one must also provide additional computational facilities for the implementation of the prediction system and the analysis and parameter encoding system. The computational requirements of these systems will, of course, depend on the sophistication of the prediction system being used.

3.3 Pitch Prediction

Very often the prediction systems in Figs. 3.1a and 3.1b will make use of the long-time correlations in voiced speech. In its simplest form, a pitch prediction system consists of a weighted delay line, as shown in Figs. 3.3a and 3.3b. The shaped noise associated with the system of Fig. 3.3a is perceptually annoying, so, in practice this configuration is never used. For the weighted delay line pitch prediction system, the analysis system must determine two parameters, the pitch period M and the weighting factor α, which is often referred to as the pitch gain. If $\tilde{M}$ and $\tilde{\alpha}$ are the quantized versions of the parameters M and α respectively, and $\rho(\tilde{M})$ is the normalized autocorrelation between speech segments which differ by a time lag $\tilde{M}$, then the prediction gain for the coding system of Fig. 3.2b is given by [18]:

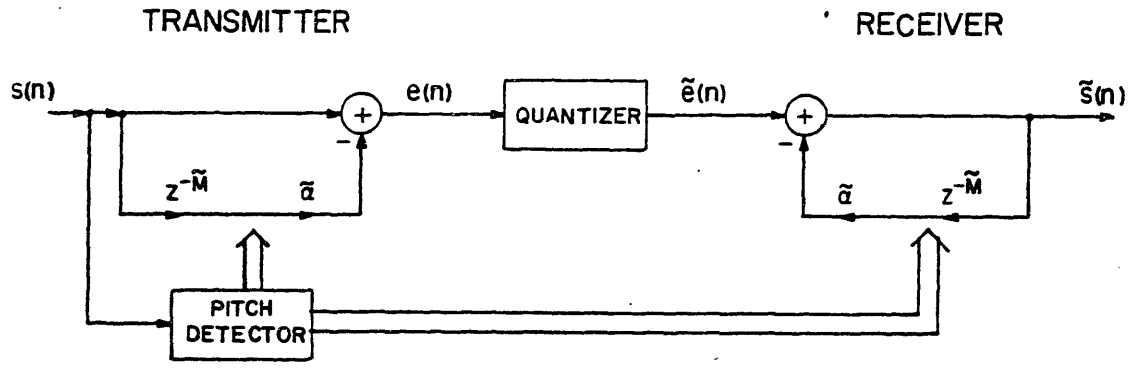

Fig. 3.3(a) Pitch predictive coding system (after Crochiere [7]).

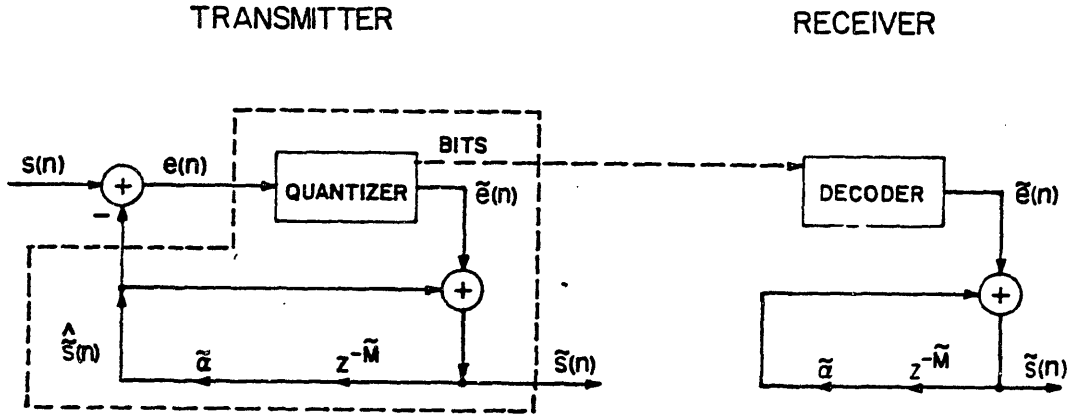

Fig. 3.3(b) Pitch predictive coding system incorporating feedback around the quantizer (after Crochiere [7]).

$$\frac{\sigma_s^2}{\sigma_e^2} = \frac{1}{1 - 2\rho(\tilde{M})\tilde{\alpha} + \tilde{\alpha}^2} \tag{3.1}$$

assuming that the quantizer is fine enough to satisfy the assumptions stated in the previous section.*

The prediction gain will be greater than unity provided that $\tilde{\alpha}$ has a value between 0 and $2\rho(\tilde{M})$, and is maximized when $\tilde{\alpha}$ equals $\rho(\tilde{M})$, yielding:

$$\left[\frac{\sigma_s^2}{\sigma_e^2}\right]_{max} = \frac{1}{1 - [\rho(\tilde{M})]^2} \tag{3.2}$$

The general comments made at the end of the previous section regarding the computational requirements of predictive encoding systems are also valid for the case of coders incorporating pitch prediction. Typically, the analysis system will consist of a pitch detector, which yields pitch period estimates for voiced speech segments, and a pitch gain estimator, which directly computes the normalized autocorrelation for the lag value equal to the quantized pitch period estimate $\tilde{M}$. Fortunately, the accuracy requirements on the pitch estimate are not as stringent for this coding system as they are in a vocoder system. For a vocoder system, the pitch estimate is used in the receiver to control a vocal cord model. Errors in the pitch estimate, such as pitch frequency doubling, can result in regenerated speech which sounds rather unnatural. For systems in which the prediction error is also encoded, errors in the pitch estimate are not quite so catastrophic - indeed, as long as $\rho(\tilde{M})$ is nonzero, and $\tilde{\alpha}$ is between 0 and $2\rho(\tilde{M})$, there will still

---

* Even when these assumptions are not valid, pitch prediction gain calculations are useful in that they can provide an indication of the maximum SNR increase obtainable when pitch prediction is used.

be some gain in SNR due to prediction. Thus, for prediction error encoding systems, fairly simple methods of pitch extraction may be used, such as the techniques proposed in References [23, 24], thus enabling the designer to somewhat limit the computation requirements of the overall system.

3.4 The Use of Pitch Prediction in Sub-band Coders

So far, it has been assumed that the quantizer acts instantaneously upon its input. In general, though, the quantizer system might have some delay associated with it. This delay may be taken into account in the system of Fig. 3.3b by adding delays and advances of I samples to the appropriate signal paths, where I is the delay associated with the quantizer. The resulting system is shown in Fig. 3.4. The delay in the pitch prediction path need only be $\tilde{M}$-I samples in length, since $\tilde{s}(n)$ is a facsimile of the delayed signal, s(n-I). Since phase advances cannot be implemented in causal systems, the minimum allowable pitch period for which prediction is realizable is given by:

$$\tilde{M}_{min} \geq I$$

If the pitch period of a given speech signal falls below $\tilde{M}_{min}$, then some prediction gain may still be attainable by doubling or tripling the pitch prediction delay, $\tilde{M}$.

At this point, recall that sub-band coders which utilize symmetric FIR filters have a linear phase response. Thus, the quantizer with memory system of Fig. 3.4 can be replaced by a sub-band coder whose overall delay is I samples. As shown in Fig. 3.5, one can use a separate pitch prediction loop, and, if desired, a separate value of pitch gain for each sub-band channel. As will be discussed later, using

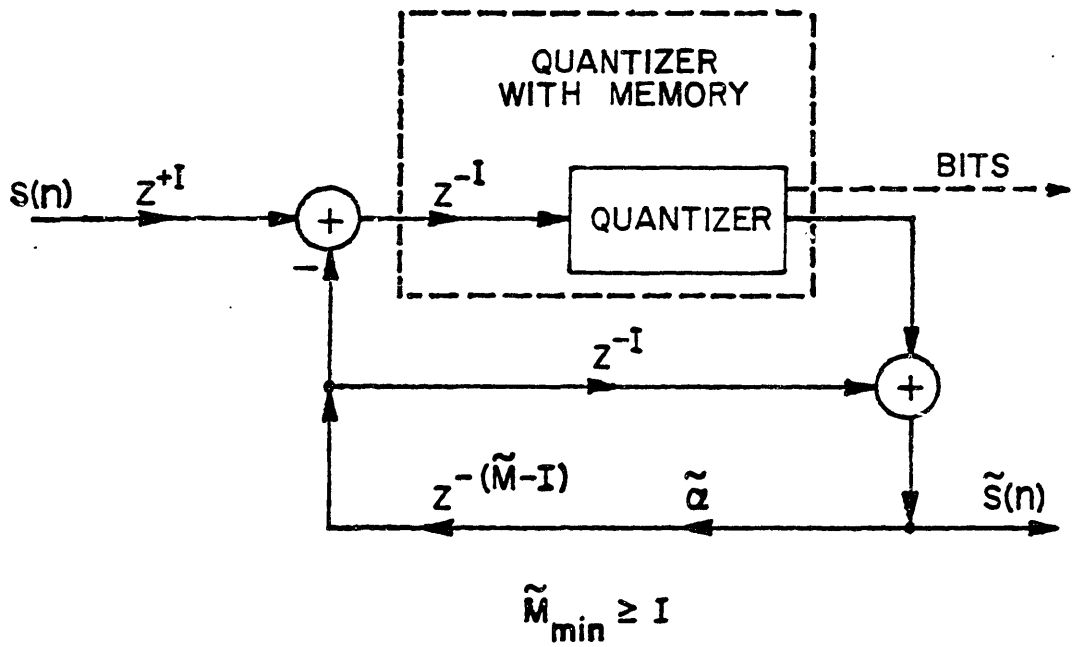

Fig. 3.4 Block diagram of a pitch predictive coder with a quantizer with delay I, $I \leq M_{min}$. (after Crochiere [7])

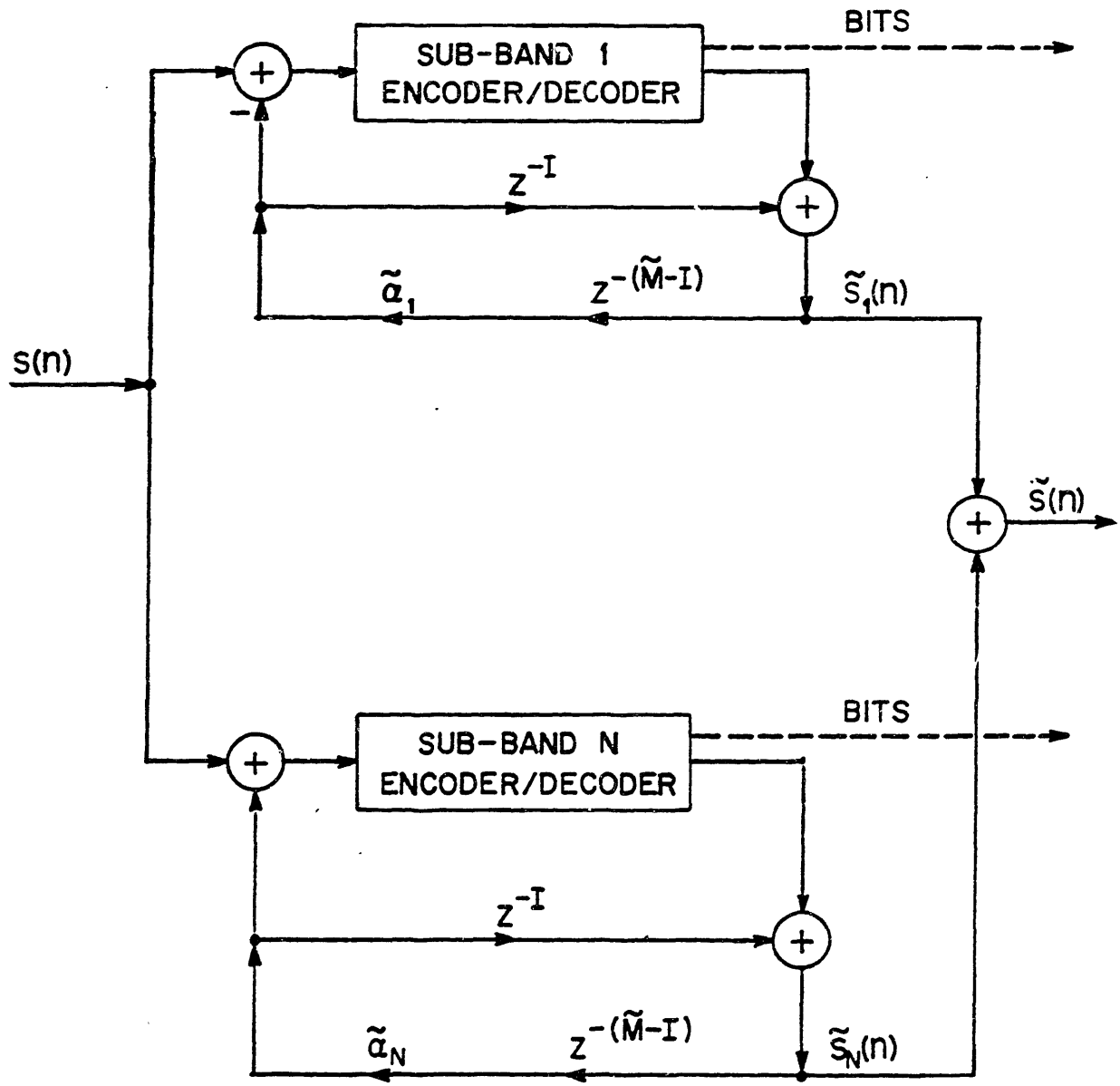

Fig. 3.5 Sub-band coder with separate pitch prediction loop around each sub-band (after Crochiere [7]).

separate pitch gain values for each sub-band channel can provide for a better characterization of the speech signal.

Figure 3.6 gives a more detailed illustration for a single sub-band i in this system configuration. The band-pass decimation block provides for the appropriate band limiting and down-sampling of the signal $e_i(n)$, as discussed in Chapter 2. The output $d_i(n)$ of the band-pass decimator is quantized by the encoder-decoder system, forming a quantized signal $\tilde{d}_i(n)$, as well as the bits to be transmitted. The operation of quantization systems which are typically used in sub-band coders will be discussed further in the next chapter. The signal $\tilde{d}_i(n)$ is interpolated and band-pass translated to the original sampling rate by the band-pass interpolator to form the signal $\tilde{e}_i(n)$. Since this signal is bandlimited to the frequency range of sub-band i, $\tilde{s}_i(n)$ is a facsimile of only that portion of the original delayed signal s(n-I) which is associated with the frequency range of sub-band i.*

A drawback with this particular implementation of pitch prediction in sub-band coding is that the coded sub-band signals must be reconstructed at the original sampling rate. A significant increase in the computational requirements of the coding system is needed to implement this process. In the next section, a technique proposed by Crochiere [7] will be described for implementing pitch prediction in sub-band coding in a more efficient manner.

3.5 Pitch Prediction of Band-pass Decimated Speech

The inefficiency of the system of Figs. 3.5 and 3.6 resulted from the rather naive application of a particular pitch prediction system

---

* To keep our discussion as uncomplicated as possible, let us assume (for now) that any aliasing effects are negligible. This issue will be treated later in this chapter.

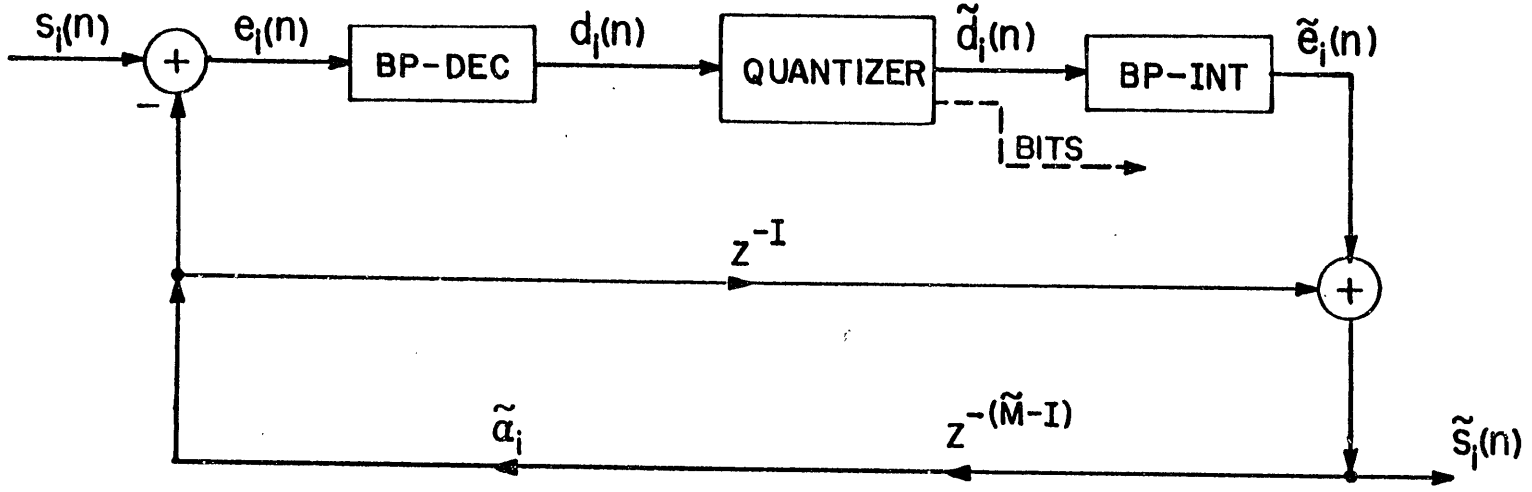

Fig. 3.6 Band i of the pitch predicting sub-band coder of Fig. 3.5 (after Crochiere [7]).

(i. e. a weighted delay line) to a fairly complicated coding system. This resulted in the need to duplicate the entire decoder portion of the sub-band coder in the transmitter. It would be preferable to apply predictive coding techniques to the sub-band signals at the low sampling rate, as illustrated in Fig. 3.7. Conceptually, the prediction system would generate estimates using pitch information by band-pass interpolating the sub-band signal input to the original, higher, sampling rate, delaying the signal by a pitch period, weighting the signal by the pitch gain, and then band-pass decimating the signal back to the lower sampling rate.

Since the band-pass filters have some delay associated with them, say I samples, the delay line should be only $\tilde{M}$-I taps long. The application of the pitch gain weighting at the low sampling rate will cut down the number of multiplies needed to implement our system. One sub-band of a predictive coder using the pitch prediction system described above is shown in Fig. 3.8. The sub-system enclosed in the dotted lines in Fig. 3.8 realizes a band-pass translated phase shift, and is shown in greater detail in Fig. 3.9. Note that the band-pass filter has been eliminated from the decimation stage, since the input to the decimator has already been bandlimited by the interpolating filter. An efficient implementation technique for this phase shifter (due to Crochiere et al. [25]) will be presented later in this chapter.

In order to demonstrate that the proposed pitch prediction system performs the desired function, one can show that the systems of Fig. 3.6 and Fig. 3.8 are equivalent. In order to do so, it is necessary to assume that all band-pass decimation blocks and all band-pass interpolation blocks are identical, and that any aliasing which might occur is negligible.

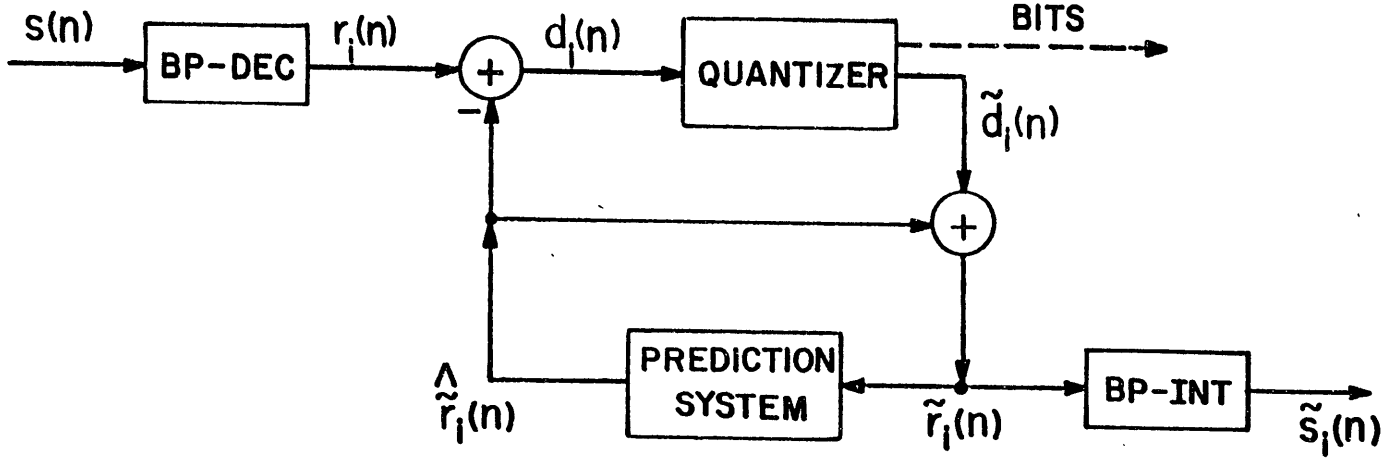

Fig. 3.7 Predictive encoding of downsampled sub-band signals.

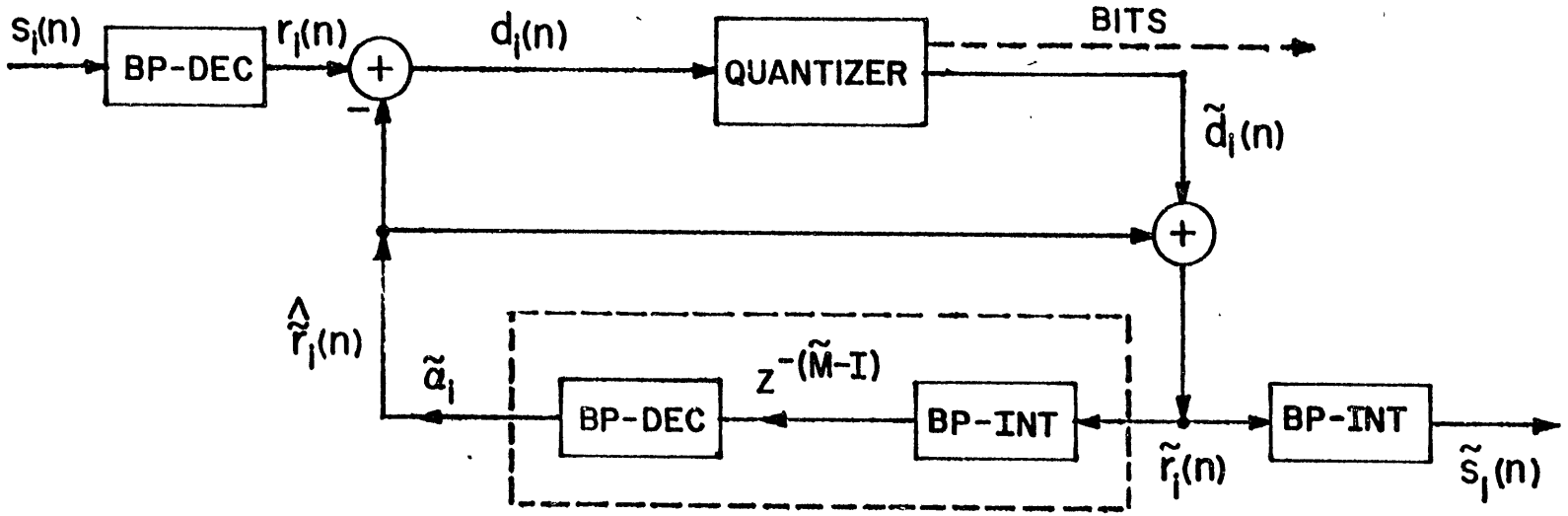

Fig. 3.8 One band of sub-band coder incorporating pitch prediction of downsampled sub-band signals (after Crochiere [7]).

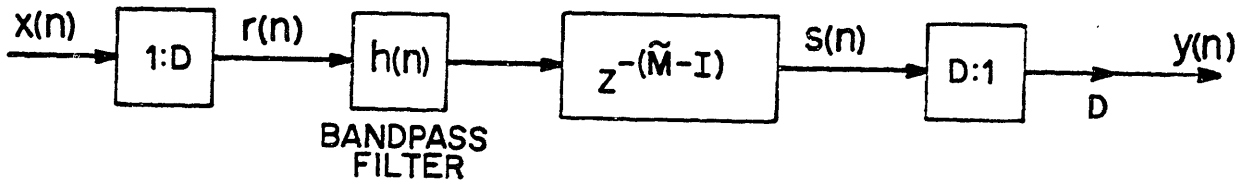

Fig. 3.9 Detailed view of digital phase shifter (after Crochiere [7]).

One can obtain the system of Fig. 3.10 from the system of Fig. 3.8 by shifting the band-pass decimation and band-pass interpolation blocks across the appropriate branches of the circuit. Such shifts of subsystems do not affect the overall system function since the band-pass decimation and band-pass interpolation blocks perform linear operations. Note that in Fig. 3.10, $\tilde{e}_i(n)$ is bandlimited, so the input to the cascade of a band-pass decimation block followed by a band-pass interpolation block will also be bandlimited. Thus, the cascaded blocks can be replaced by a delay of I samples, as indicated in the figure. Finally, one can obtain the system of Fig. 3.6 from the system of Fig. 3.10 by sliding the band-pass decimation blocks through the input difference operator.

3.6 The Practical Use of Pitch Prediction in Sub-band Coders

Before discussing the actual design of the phase shifters, it is worthwhile to first examine certain issues that have been raised in previous sections but have been ignored until now.

In section 3.4 it was stated that when using a separate pitch prediction loop for each sub-band it might be desirable to compute and use a separate pitch gain value in each loop. If one only considered the simple (but generally accepted) model for speech production illustrated in Fig. 3.11 (after Schafer and Rabiner [26]), it would appear that there should be no performance difference whether or not a separate pitch gain value was computed and used for each prediction loop. However, if such a model were always valid, we would expect to see a uniform harmonic structure across the total frequency range of short-time spectra of voiced speech segments. In reality, the harmonic structure of voiced speech is sometimes interrupted in various regions of the frequency

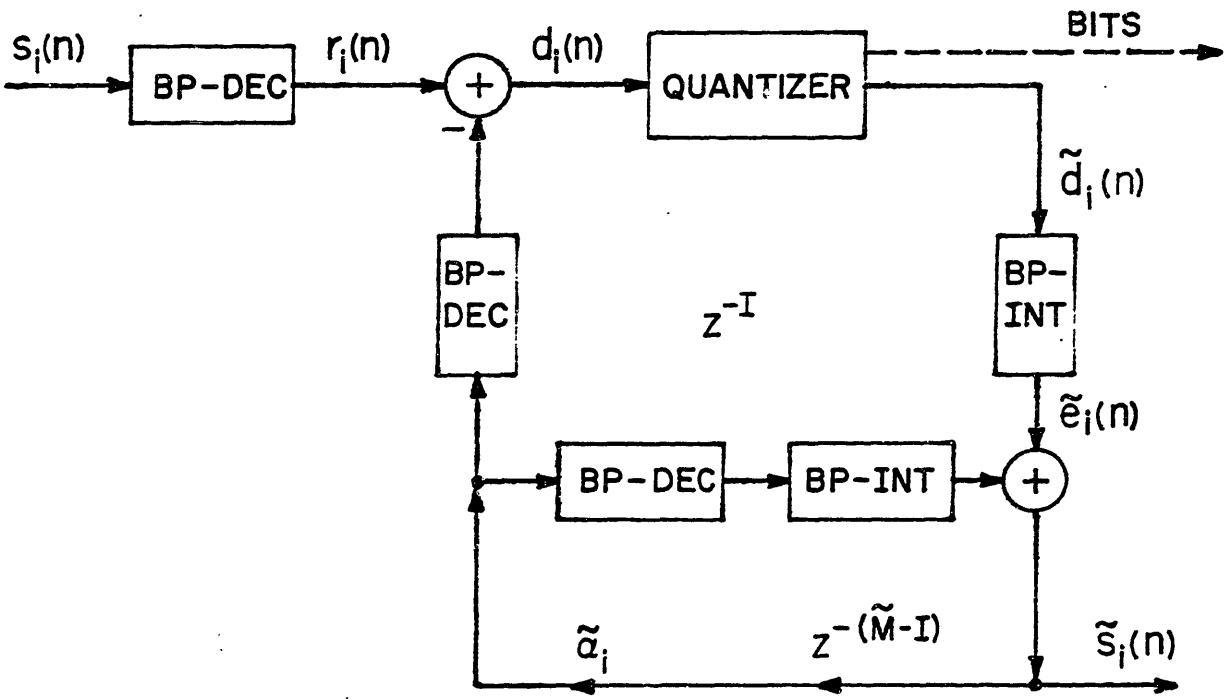

Fig. 3.10 Equivalent for system of Fig. 3.8 (after Crochiere [7]).

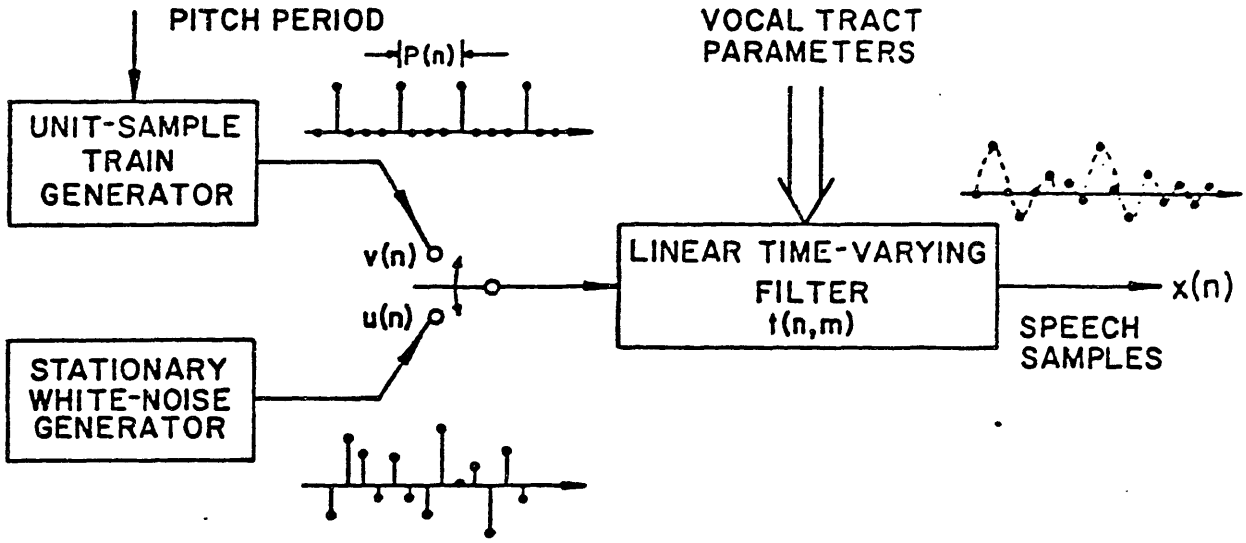

Fig. 3.11 Terminal-analogue model of the vocal system (after Schafer and Rabiner [26]).

domain, as illustrated in Fig. 3.12 (after Fujimura [27]). This phenomenon is sometimes referred to as "devoicing" [27]. Devoicing occurs most often in the higher frequency regions (above 1 kHz) of voiced speech spectra, as seen in the last two spectra of Fig. 3.12. Occasionally, devoicing can occur in an intermediate frequency region, while the higher frequency region remains voiced, as seen in the third spectrum of Fig. 3.12. Now suppose a voiced speech segment in which there is high frequency (say, above 1.5 kHz) devoicing is to be encoded with a pitch predicting sub-band coder. Assume that the coder computes only one pitch gain value for use by all the sub-band pitch prediction loops. Since voiced speech has a higher energy content at low frequencies than at high frequencies, any pitch period and pitch gain computations made on the original full bandwidth signal would be valid for the lower frequency regions of the speech segment, but not for the higher frequency regions, where, due to devoicing, there is little or no long-time correlation present. Thus, if the full bandwidth pitch gain value is used in the higher frequency sub-band prediction loops, the input energy to each higher frequency sub-band quantizer would increase, resulting in a decrease in SNR for those bands, as compared with not using pitch prediction in those bands at all.

One way to prevent devoicing effects from adversely affecting the performance of the pitch predicting sub-band coder would be to compute separate pitch gain values for each sub-band. Unfortunately, this would increase the coder computation requirements and reduce the amount of transmission bandwidth available for the encoded signal points, since more side information would have to be transmitted.

A far simpler alternative would be to attenuate the full bandwidth

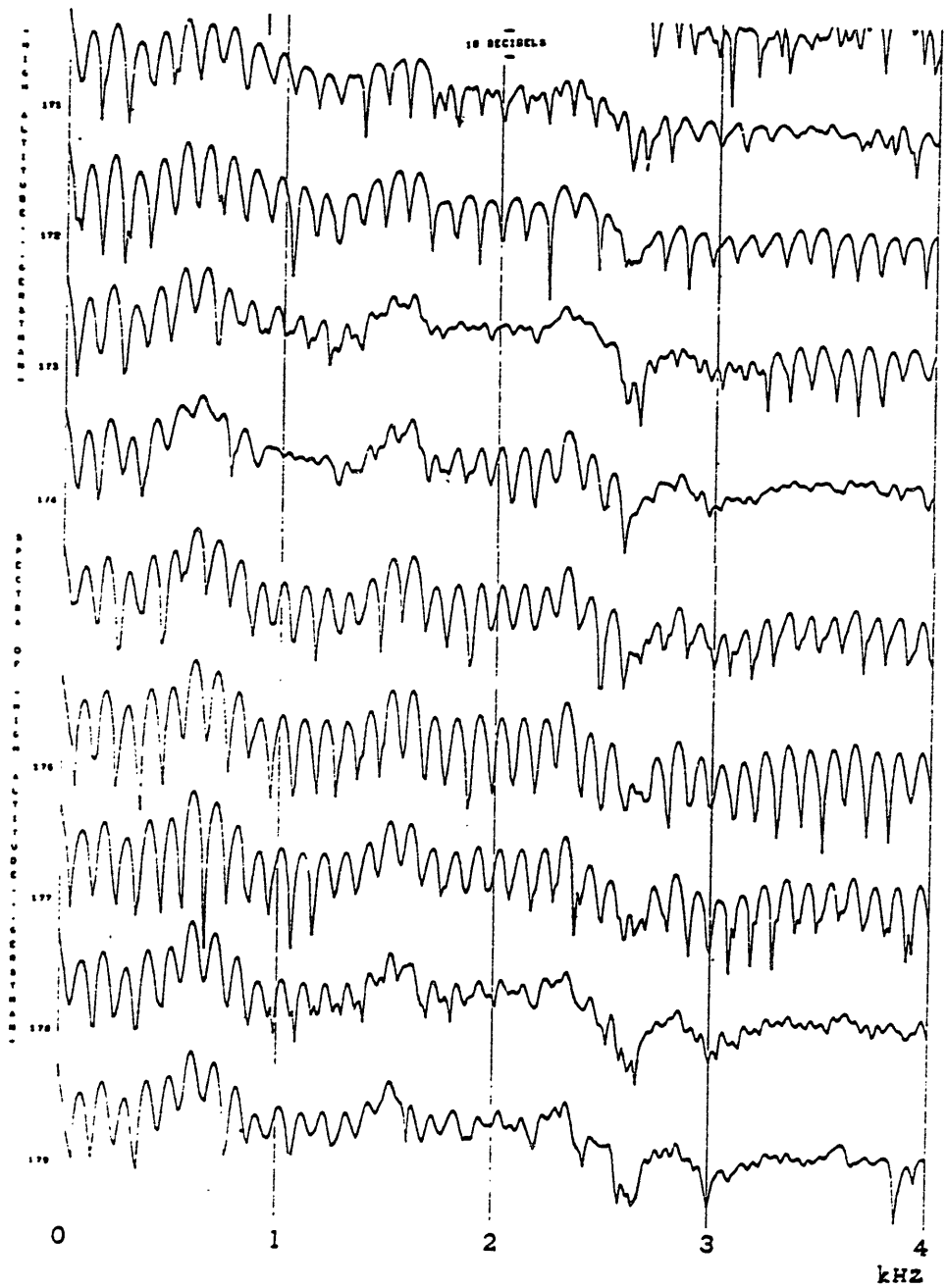

Fig. 3.12 A series of amplitude spectra representing a vowel segment [ae]. Time runs from top to bottom (after Fujimura [27]).

pitch gain by predetermined fixed weighting factors associated with each sub-band. From the previous discussions on devoicing, one would expect that unity would be a suitable pitch gain weighting for the lowest sub-bands and that progressively smaller values should be used for higher sub-bands. This technique was implemented in the sub-band coders simulated as part of this thesis by setting the pitch gain value $\tilde{\alpha}_i$ in the i^{th} sub-band equal to $w_i\tilde{\alpha}$, where w_i is the fixed pitch gain weighting factor for that sub-band, and $\tilde{\alpha}$ is the quantized pitch-gain value for the current speech segment. The actual weighting factors used and their selection will be discussed in Chapter 5.

There are several drawbacks with using fixed pitch gain weighting factors. First of all, there can still be some reduction in SNR, compared to not using pitch prediction at all, when devoicing occurs. Second, when the devoicing phenomenon is absent from a voiced speech segment, the use of the pitch gain weighting factors will force the effective pitch gains for each sub-band to be smaller than the optimal values, resulting in a reduction in the SNR improvement due to pitch prediction. For example, suppose a speech segment with a pitch gain of 0.95 is to be encoded, that a fixed pitch gain weighting factor of 0.4 is being used for a particular sub-band (yielding an effective pitch gain of 0.38) and that there are no devoicing effects for that particular segment. From Equation (3.2), the maximum theoretical pitch gain obtainable is about 10 dB, but the upper prediction gain limit for the sub-band of interest is only 3.74 dB, due to the use of the fixed pitch gain weighting factor. In fact, the maximum prediction gain obtainable when using a weighting factor of 0.4 is only 4.44 dB.

In Chapter 6, more sophisticated methods of pitch gain selection

will be suggested which might offer improved performance over the use of fixed weighting factors, but do not have the drawbacks of direct computation and transmission of a pitch gain value for each sub-band.

Another issue on which discussion has been postponed is the effect of aliasing on the performance of our prediction system. Thus far, it has been assumed that both the sub-band signals and the phase shifting filters are totally unaffected by aliasing. It is now time to reevaluate that assumption.

For signals confined to the middle of a sub-band, the past assumptions are certainly quite reasonable. In general, the band-splitting filters that are used have stop-band attenuation levels sufficient to guarantee that any aliasing terms at the middle of the sub-band will be too small to disturb the harmonic structure associated with voiced speech.

For signals near the sub-band edges, one would expect some aliasing to interfere with the pitch harmonic structure. However, the importance of this interference is dependent on the type of bandsplitting filter used to generate the signal. When Quadrature Mirror Filters are used, the energy level of the signal region corrupted by aliasing will be comparable to the energy level in the rest of the sub-band, since the response of the filter is down only 3 dB at the sub-band edges. In this case, the loss of harmonic structure is not unlike the devoicing effect discussed earlier. As in the case of devoicing, one would expect that trying to subtract off an invalid "estimate" of the aliasing corrupted signal region would actually increase the energy to the quantizer, resulting in a decrease in SNR. Unlike the devoicing phenomena, which occur intermittently, signal corruption by aliasing at the band edges is constantly occurring. Thus, a reasonable way to deal with the aliasing

corrupted signal regions would be to attenuate the response of the prediction system at the sub-band edges, so as to prevent erroneous estimates of the corrupted sub-band signals from being generated. As will be seen in the next section, attenuation of the prediction system response at the sub-band edges is readily accomplished by proper design of the phase shifter band-pass filter.

When conventional bandsplitting filters are being used, such as the one illustrated in Fig. 2.3, the energy level of the aliasing corrupted signal region will be considerably lower than the energy level in the rest of the sub-band, since the response of the filter is down 12 dB at the sub-band edges. In addition, the transition regions of these filters are fairly narrow, so the aliasing corrupted signal region will be fairly narrow.

Therefore, erroneous prediction of these aliasing corrupted signal regions should have a negligible effect on the overall performance of the prediction system.

3.7 Considerations in the Design of Band-pass Filters for Use in Digital Phase Shifters

An important consideration in the design of the phase shifter band-pass filter is the choice of filter length. The filter is required to have an integer delay I, so a symmetric FIR filter with an odd number of taps should be used. The delay I sets the minimum implementable prediction delay, $\tilde{M}_{min}$. When the pitch period falls below $\tilde{M}_{min}$, then some multiple of the pitch period can be used in the prediction system, in effect, using the corresponding samples of an older pitch period to generate our new estimates. This strategy might cause some loss in prediction performance, since the correlation between samples many pitch periods apart may not be as strong as the correlation between samples one pitch

period apart. In order to limit the use of this strategy, fairly short filters must be used. For example, if the system will handle a pitch frequency range of 50-450 Hz, then the minimum pitch period the system will have to handle is 2.22 ms, which corresponds to approximately 14 samples at a 6400 Hz sampling rate. If the prediction system is required to use no more than four times the pitch period as the prediction delay, then the band-pass filter cannot be longer than 111 taps. If the prediction system is required to use no more than twice the pitch period as the prediction delay, then the band-pass filter cannot be longer than 55 taps.

Given these restrictions on the choice of the band-pass filter length, the task at hand is to select the band-pass filter which will provide the best performance in the coding system. As an aid for achieving this goal, it is useful to calculate the phase shifter transfer function in terms of the band-pass filter frequency response. It is also useful to calculate the phase shifter transfer function for the special case where the band-pass filter is ideal, so as to obtain a better appreciation of the ultimate design goals. The response of a phase shifter using an allowable band-pass filter will deviate from the ideal phase shifter response. From the discussions of the previous section on the nature of the signals to be estimated, one would expect some deviations from the ideal to be less harmful to the actual performance of the prediction system than others. Given a choice of filter length, this information can be used to select the band-pass filter best suited for use in our system.

The transfer function of the phase shifter of Fig. 3.9 can be shown to have the form:

$$T(\omega) = \frac{Y(\omega)}{X(\omega)} = \sum_{\ell=0}^{D-1} H\left(\frac{\omega + 2\pi\ell}{D}\right) e^{-j\left(\frac{\omega - 2\pi\ell}{D}\right)(\tilde{M}-I)} \qquad (3.3)$$

Equation (3.3) can be obtained using the following relationships among the signals x(n), r(n), s(n) and y(n) indicated in Fig. 3.9:

$$R(\omega) = X(\omega D) \qquad (3.4)$$

$$S(\omega) = H(\omega)\, e^{-j\omega(\tilde{M}-I)} R(\omega) \qquad (3.5)$$

$$Y(\omega) = \sum_{\ell=0}^{D-1} S\left(\frac{\omega + 2\pi\ell}{D}\right) \qquad (3.6)$$

Substituting (3.4) into (3.5) yields:

$$S(\omega) = H(\omega)\, e^{-j\omega(\tilde{M}-I)} X(\omega D) \qquad (3.7)$$

Substituting (3.7) into (3.6):

$$Y(\omega) = \sum_{\ell=0}^{D-1} H\left(\frac{\omega + 2\pi\ell}{D}\right) e^{-j\left(\frac{\omega + 2\pi\ell}{D}\right)(\tilde{M}-I)} X(\omega + 2\pi\ell) \qquad (3.8)$$

Using the periodicity property of the discrete-time Fourier transform, Equation (3.3) follows directly from Equation (3.8).

Now suppose $H(\omega)$ is an ideal band-pass filter with delay I designed to isolate band r of the integer band sampling process, i.e. the ideal frequency response of $H(\omega)$ for $|\omega| \le \pi$ is given by:

$$H(\omega) = \begin{cases} e^{-j\omega I} & \frac{\pi}{D} r \le |\omega| < \frac{\pi}{D}(r+1) \qquad (3.9a) \\ 0 & |\omega| < \frac{\pi}{D} r,\ \frac{\pi}{D}(r+1) \le \omega \le \pi \qquad (3.9b) \end{cases}$$

Note that if r is even, then for $0 \le \omega < \pi$, the only nonzero term in the summation of (3.3) is for $\ell = r/2$, and for $-\pi \le \omega < 0$, the only nonzero term in the summation of (3.3) is for $\ell = D - r/2$ (or 0, when $r = 0$).

If r is odd, then for $0 \leq \omega < \pi$, the only nonzero term in the summation of (3.3) is for $\ell = D - \frac{(r+1)}{2}$, and for $-\pi \leq \omega < 0$, the only nonzero term in the summation of (3.3) is for $\ell = \frac{r+1}{2}$.

Using the above observations, one can obtain the ideal phase shifter transfer function:

For r even,

$$T(\omega) = \begin{cases} e^{-j\pi r\tilde{M}/D}\ e^{-j\omega\tilde{M}/D}, & 0 \leq \omega < \pi \quad (3.10a) \\ e^{j\pi r\tilde{M}/D}\ e^{-j\omega\tilde{M}/D}, & -\pi \leq \omega < 0 \quad (3.10b) \end{cases}$$

For r odd,

$$T(\omega) = \begin{cases} e^{j\pi(r+1)\tilde{M}/D}\ e^{-j\omega\tilde{M}/D}, & 0 \leq \omega < \pi \quad (3.11a) \\ e^{-j\pi(r+1)\tilde{M}/D}\ e^{-j\omega\tilde{M}/D}, & -\pi \leq \omega < 0 \quad (3.11b) \end{cases}$$

Figure 3.13 illustrates the relationship between the phase terms at the high and sub-band sampling rates when an ideal band-pass filter is employed in the phase shifter for the cases r = 1 and r = 2.

Real world band-pass filters do not have ideal characteristics, and so Equation (3.3) must be used to predict the effects that the pass-band ripple, finite transition region width and finite stop-band attenuation of a given filter have on the phase shifter.

The frequency response of a symmetric FIR filter of length N = 2I + 1 is given by:

$$H(\omega) = A(\omega)\ e^{-j\omega I} \quad (3.12)$$

where $A(\omega)$ is real valued and may be either positive or negative [16, 17, 18].

Substituting Equation (3.12) into Equation (3.3) yields:

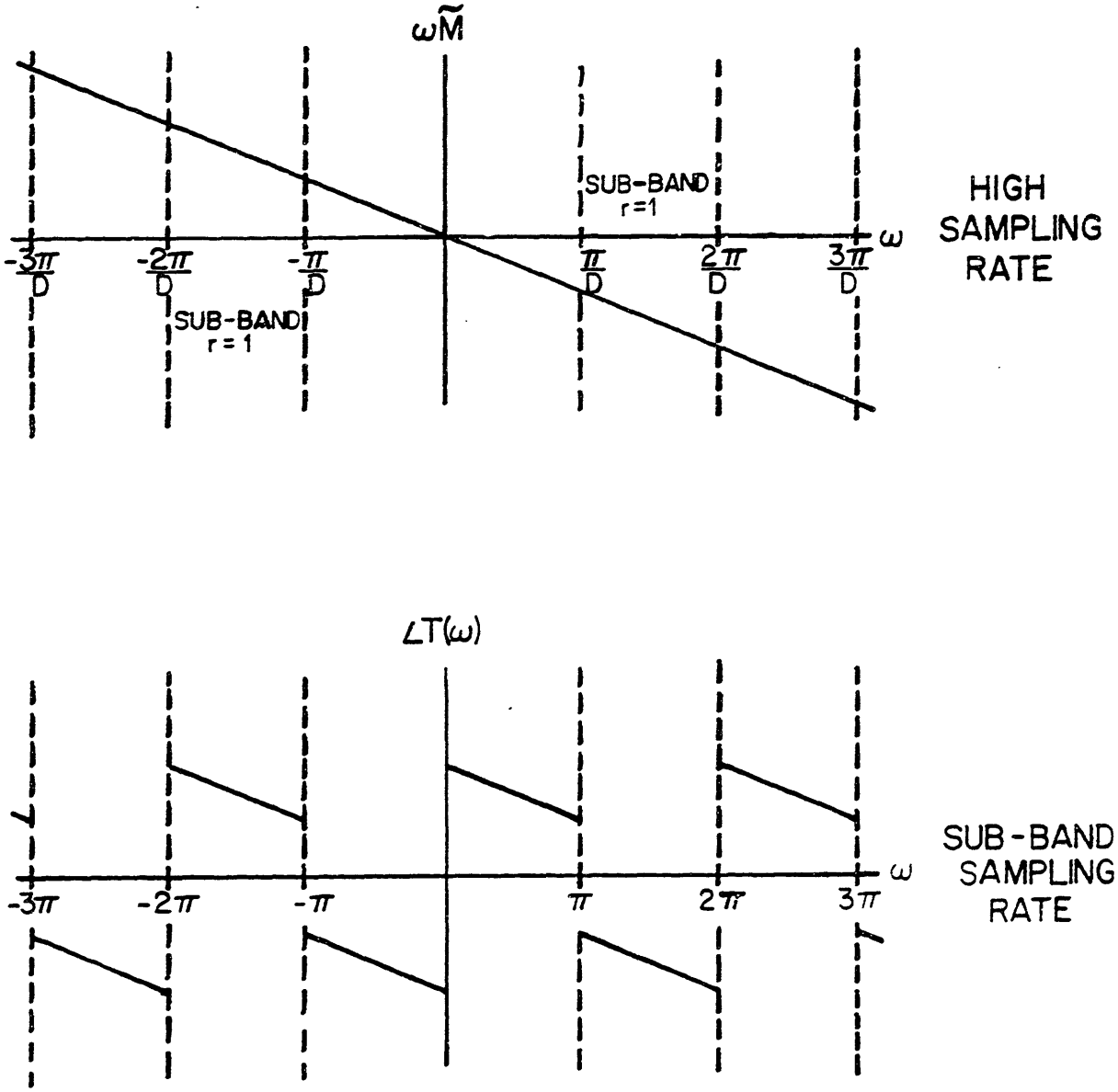

Fig. 3.13(a) Relationship of the linear phase shift at the high sampling rate to the phase shift at the sub-band sampling rate for the r = 1 sub-band.

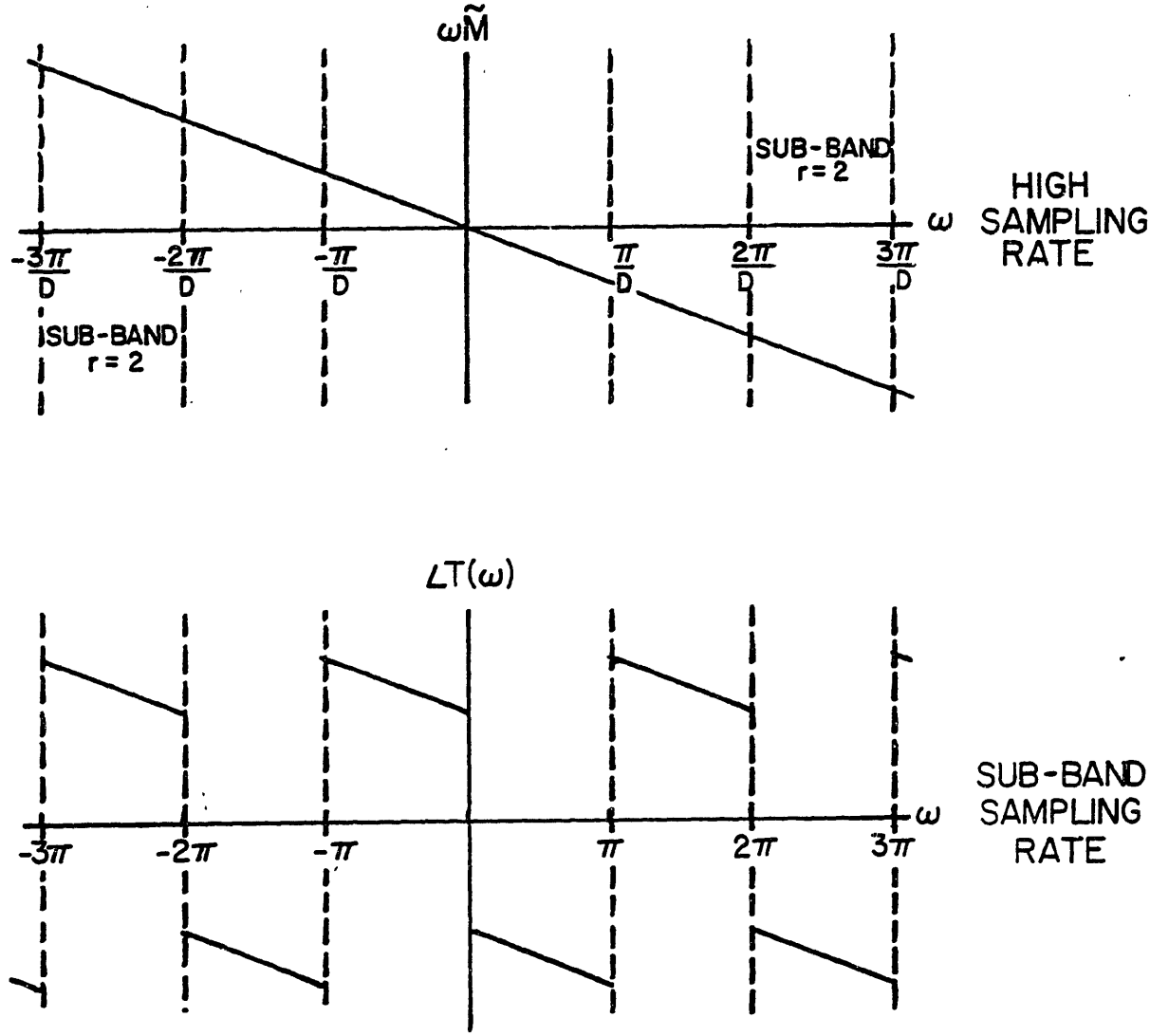

Fig. 3.13(b) Relationship of the linear phase shift at the high sampling rate to the phase shift at the sub-band sampling rate for the r = 2 sub-band.

$$T(\omega) = \sum_{\ell=0}^{D-1} A\left(\frac{\omega + 2\pi\ell}{D}\right) e^{-j\left(\frac{\omega + 2\pi\ell}{D}\right)\tilde{M}} \qquad (3.13)$$

Figure 3.14a shows $A(\omega)$ for a band-pass filter designed to isolate the r = 2 sub-band in a D = 4 integer band sampling scheme. Figure 3.14b shows each of the four $A(\frac{\omega + 2\pi\ell}{D})$ terms of the summation of Equation (3.13).

In the frequency regions marked "PB" in Fig. 3.14b, the summation of (3.13) will be dominated by a single term. In these regions, the phase shifter's deviation from the ideal response will be caused by the pass-band ripple associated with the dominant term and the stop-band ripple associated with each of the small terms.

Suppose, for the moment, one was interested in estimating the effect of the pass-band ripple of the dominant term in the "PB" region on the performance of the phase shifter as a prediction system. For the purposes of this estimation, it is reasonable to make certain assumptions in order to identify the prediction performance degradation due solely to the pass-band ripple. These assumptions are:

- The quantization is fine enough to permit the standard estimations which led to the prediction gain Equations (3.1) and (3.2).
- The sub-band signals in the "PB" region are essentially free from aliasing effects.
- The small terms of the summation of (3.13) are negligible.
- The sub-band is wide enough to render problems arising from the particular alignment of the pitch harmonic structure negligible.

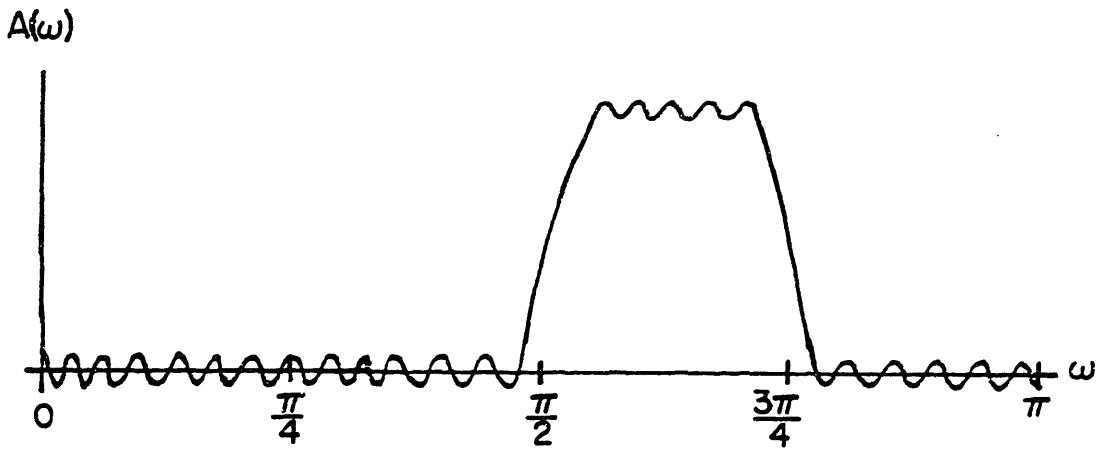

Fig. 3.14(a) Bandpass filter response for r = 2, D = 4 sub-band system.

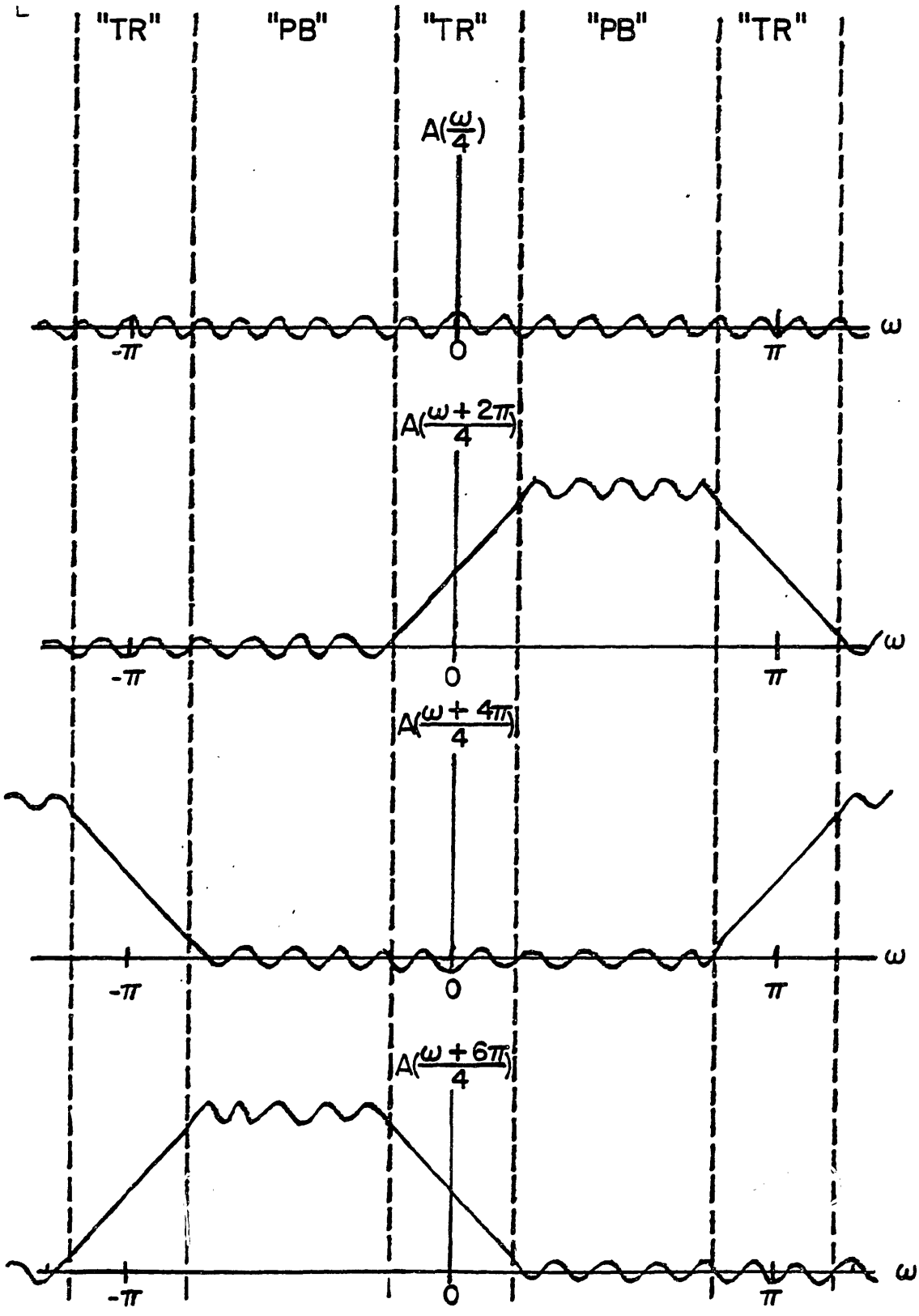

Fig. 3.14(b) Resulting terms of sum in Equation (3.13) using filter of Fig. 3.14(a) (see text).

Using these assumptions* and the fact that the phase of the dominant term of the summation of (3.13) is identical to the ideal phase shifter phase response, one can treat the effect of the pass-band ripple on the prediction performance of the phase shifter to be equivalent to the effect on the prediction performance of the system of Fig. 3.3b when a frequency dependent perturbation is applied to the pitch gain. As was discussed in Section 3.2, the prediction gain of this system can be calculated by computing the ratio σ_s^2/σ_e^2 for the system of Fig. 3.3a. If the ripple perturbation is estimated by using a pitch gain of the form:

$$\tilde{\alpha}(1 + \beta \cos \omega K)$$

then the ratio σ_s^2/σ_e^2 can be calculated using the system of Fig. 3.15. For calculation purposes, a suitable test input to the system is a decaying impulse train, with "pitch period" $\tilde{M}$ and "pitch gain" $\tilde{\alpha}$, as shown in the figure.

In the system of Fig. 3.15, for a given "pitch gain" $\tilde{\alpha}$ and ripple amplitude $|\beta|$, the output signal energy will be maximized (corresponding to a minimization of the prediction gain) when K equals M and β is less than zero. Under these conditions, the pitch gain ripple will tend to somewhat cancel the pitch harmonic structure in the estimate signal $\hat{s}(n)$. Figure 3.16 illustrates this effect of $\tilde{\alpha} = 0.8$ and two values of β, $\beta = 0$ and $\beta = -0.5$. Note that the $\beta = -0.5$ case is a rather extreme example used for illustration purposes, since no practical filter would have that much ripple.

Now suppose $\tilde{\alpha} = 0.95$, and consider the resulting prediction gain values for $\beta = 0$ and $\beta = -0.090$. For the case $\beta = 0$, the prediction gain

---

* The effects of the last two assumptions have not been addressed yet, but will be treated later in this chapter.

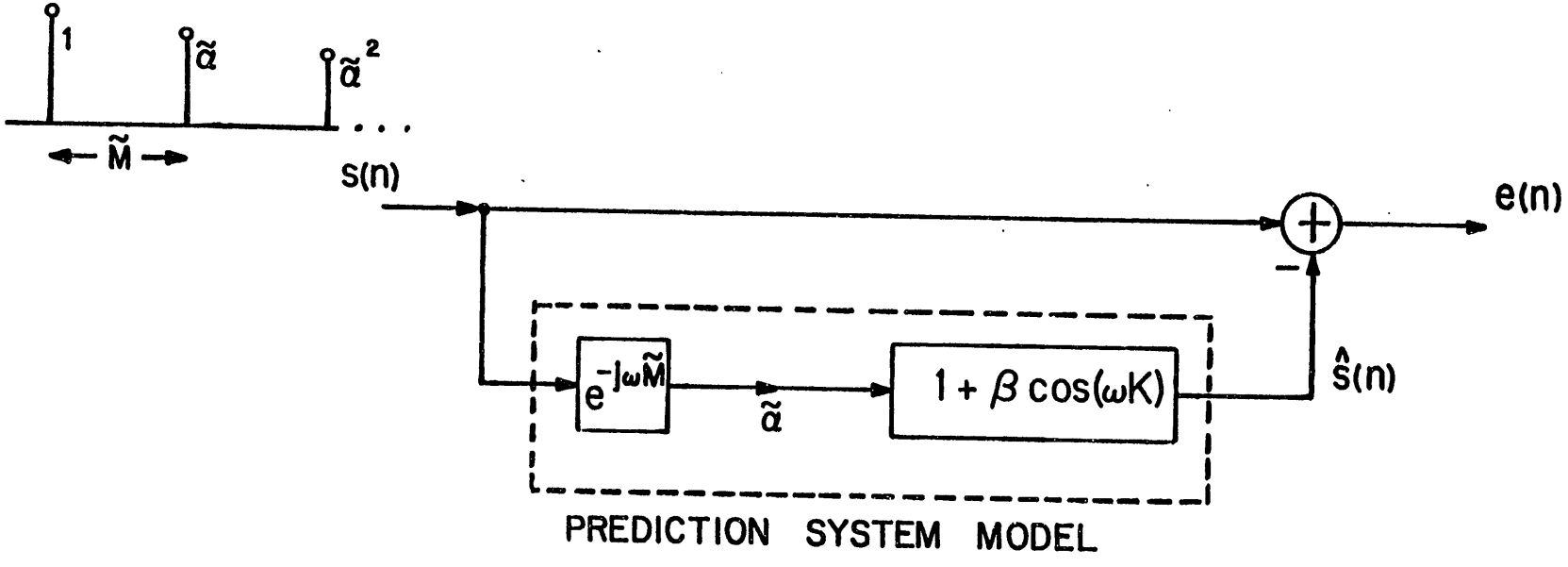

Fig. 3.15 Model for determining the effect of filter passband ripple on the pitch prediction system performance.

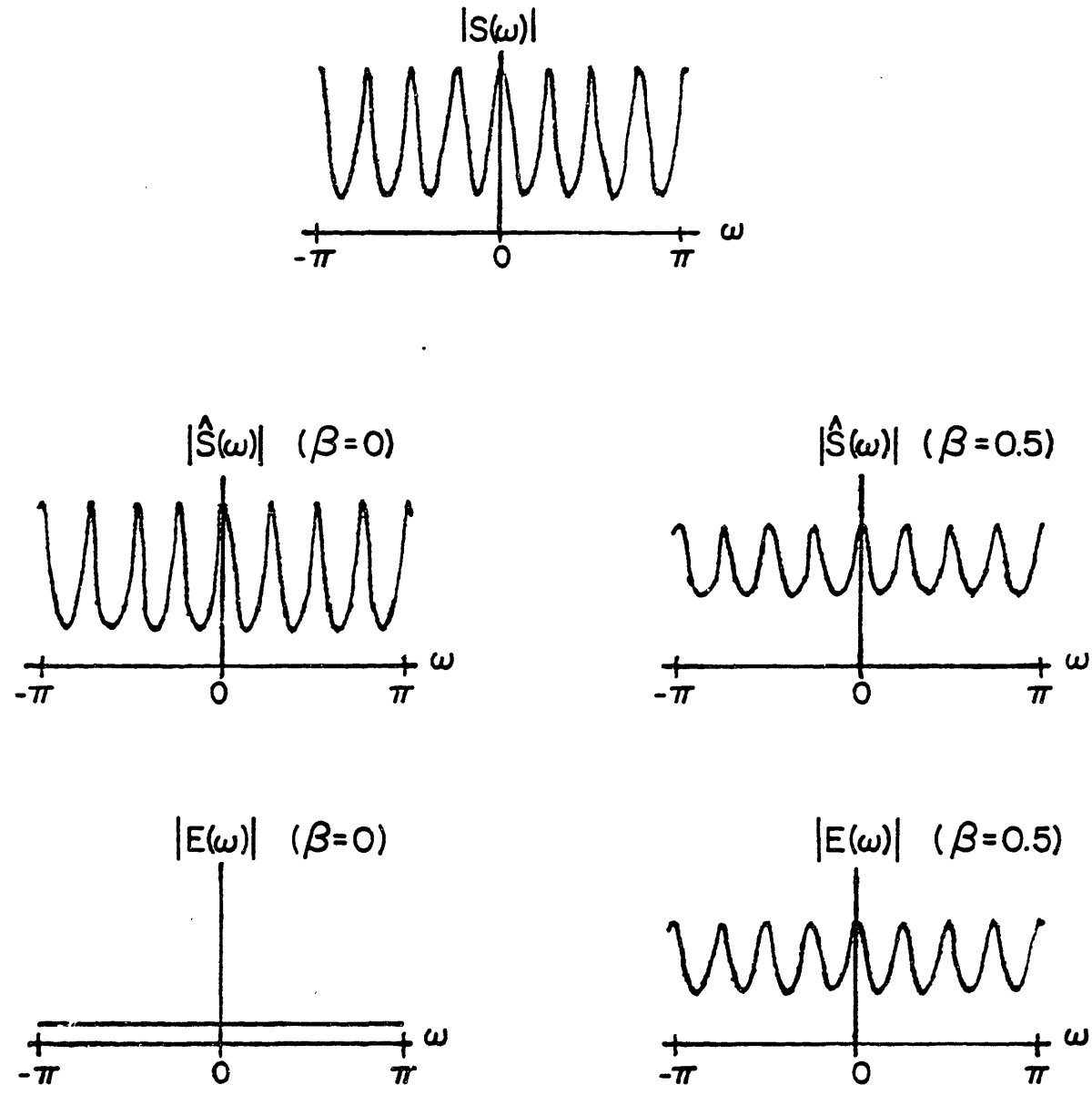

Fig. 3.16 Effect of passband ripple on pitch prediction performance when ripple structure is aligned with pitch harmonic structure.

is 10.11 dB. For the case $\beta = -0.090$, which is equivalent to $\pm$ 0.75 dB of filter ripple, the prediction gain is 9.48 dB, for a total loss in prediction gain of about 0.6 dB. For higher pitch gain values, the prediction system should provide a greater degree of energy cancellation, so any ripple will result in a more significant degradation in prediction gain. For example, when $\tilde{\alpha} = 0.99$ and $\beta = 0$, the prediction gain is 17.01 dB. When $\beta = -0.090$, the prediction gain is lower by about 1.7 dB to 15.29 dB.

In the frequency regions marked "TR" in Fig. 3.14b, the summation of (3.13) will be dominated by two terms. In these regions, the phase shifter's deviation from the ideal response will be caused by the interaction between the transition regions associated with the dominant terms, as well as the stopband ripple of the smaller term. To simplify the discussion, once again the assumption will be made that these smaller terms are negligible.

The two dominant terms in the "TR" regions are images of the band-pass filter's transition region. The magnitude responses of these terms are, in fact, mirror images of each other. The phase response of one of these two terms is always equal to the ideal phase shifter response; henceforth this term will be referred to as the desired term. The phase response of the other, interfering, term will differ from the ideal phase response by a constant. As shown in Equation (3.13), this constant phase difference is determined by the sub-band number r, of interest (which will determine the desired and interfering terms, as indicated by the ideal response summarized by Equations (3.10) and (3.11)), the sampling conversion ratio D, and the pitch period $\tilde{M}$. In fact, for any given sub-band number r and sampling conversion ratio D, there

will be D possible values of phase difference, corresponding to the different angle values of $2\pi\tilde{M}/D$. If the phase difference between the two dominant terms is great, there will be a large deviation in the phase shifter's phase response from the ideal. At the same time, this large phase difference will cause the two dominant terms to somewhat cancel each other, resulting in a dip in the phase shifter's magnitude response. At the other extreme, if the phase difference between the two dominant terms is zero, then the phase shifter phase response will equal the ideal. Since the two terms will add in phase, there will be no dip in phase shifter magnitude response if the band-pass filter response is down 6 dB at the sub-band edge.

Figure 3.17 illustrates the magnitude response of a band-pass filter designed to isolate the r = 1 sub-band in a D = 8 sampling conversion ratio system. From Equation (3.13) and our discussions regarding the ideal case, we may conclude that $\ell = D - \frac{(r+1)}{2} = 7$ is the desired term in the summation of (3.13) for $0 < \omega < \pi$. The $\ell = 1$ term will be the interfering term near $\omega = 0$. The $\ell = 0$ term will be the interfering term near $\omega = \pi$. Figure 3.18 illustrates the resulting phase shifter magnitude and phase response that would be obtained using this filter for pitch periods $\tilde{M} = 40$, 43, and 46. Dotted lines are used in this figure to indicate the ideal phase response.

The previous discussion and the examples illustrated in Figs. 3.17 and 3.18 show that when the true phase shifter phase response deviates from the ideal in the "TR" regions due to the influence of the out of phase interference term, there will be an attenuation of the phase

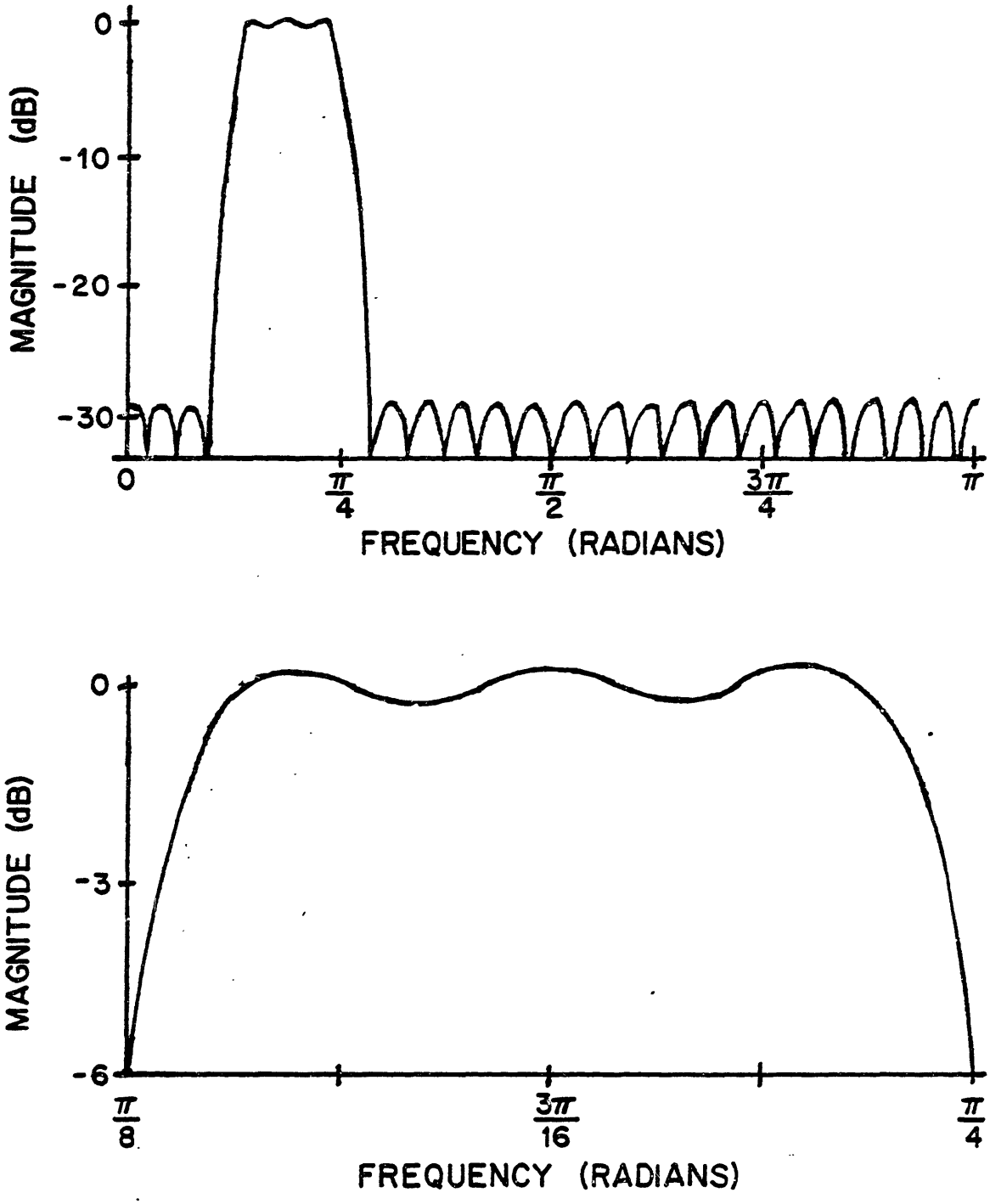

Fig. 3.17 Magnitude response of a bandpass filter designed to isolate the r = 1 sub-band in a D = 8 bandpass interpolator.

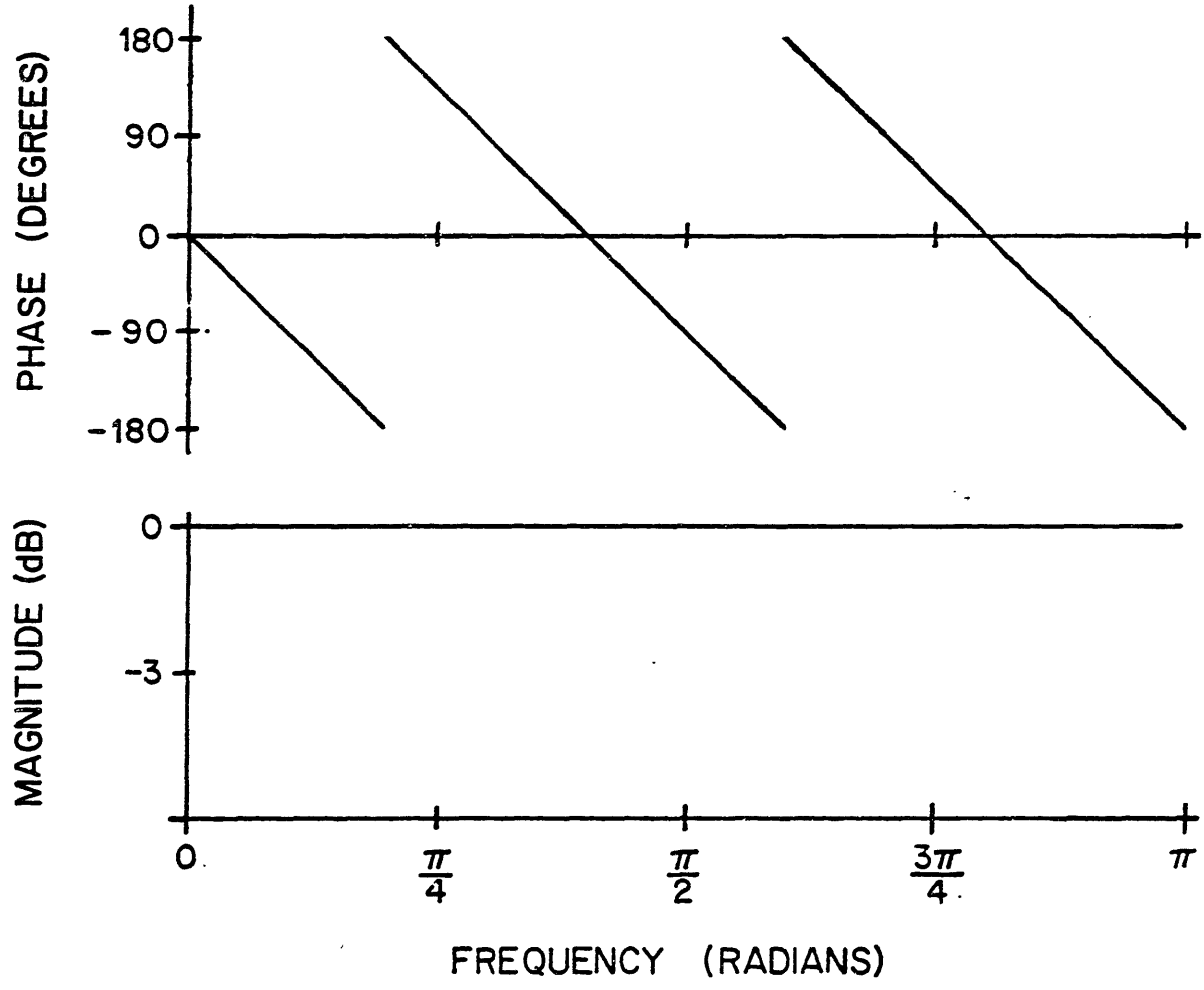

Fig. 3.18(a) Phase shifter response for D = 8, r = 1, M = 40, using the bandpass filter of Fig. 3.17.

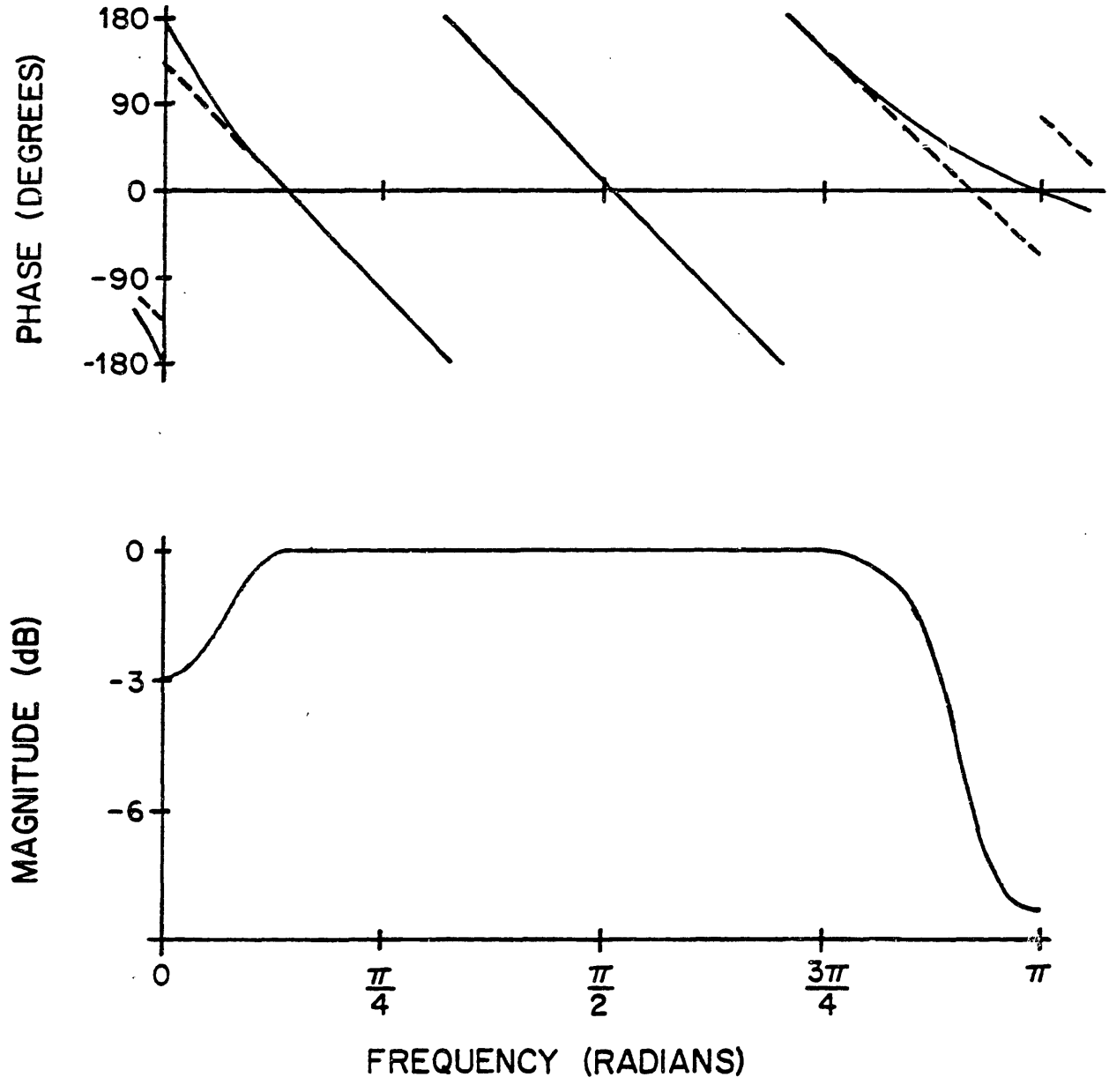

Fig. 3.18(b) Phase shifter response for D = 8, r = 1, M = 43, using the bandpass filter of Fig. 3.17.

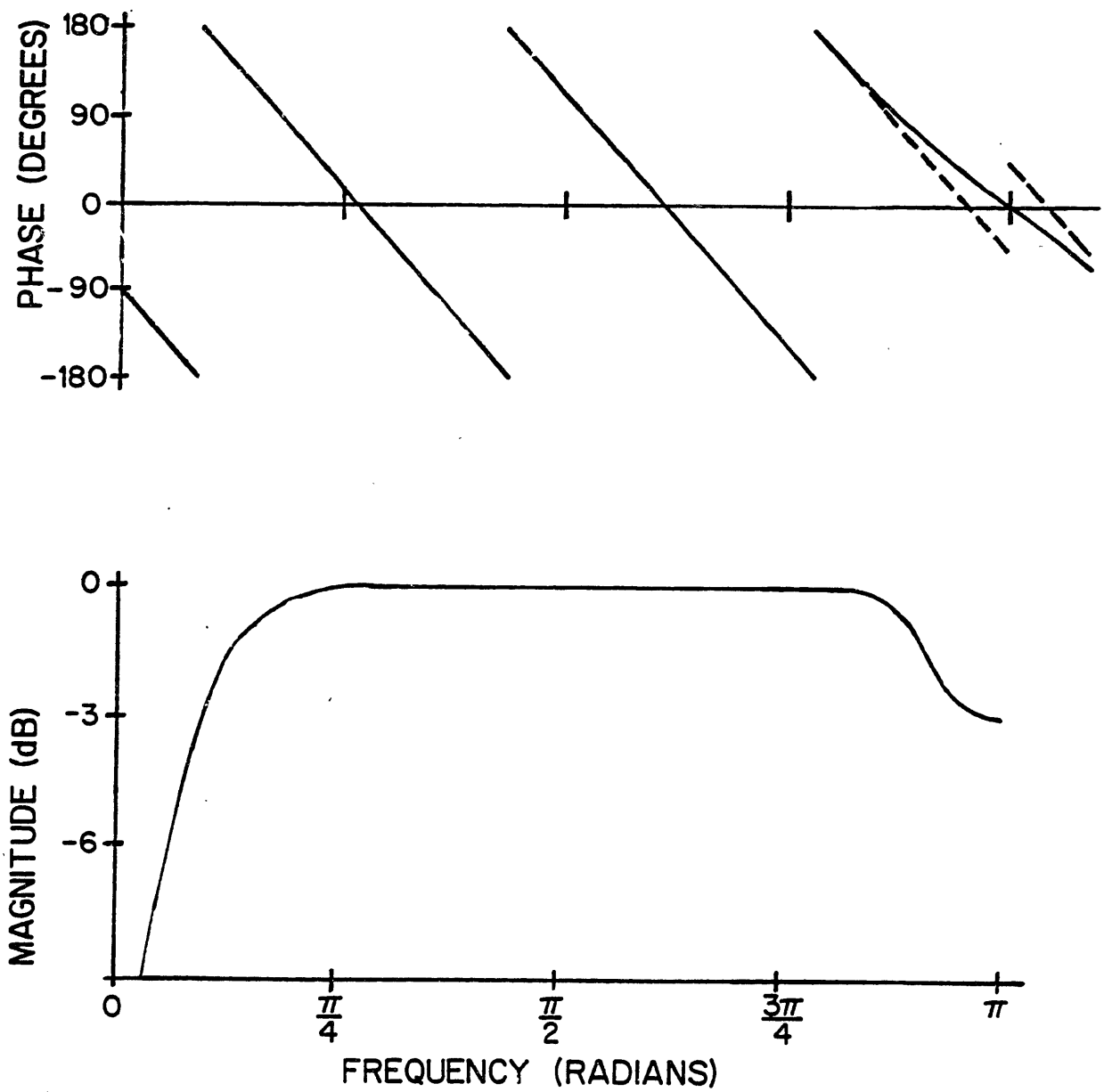

Fig. 3.18(c) Phase shifter response for D = 8, r = 1, M = 46, using the bandpass filter of Fig. 3.17.

shifter magnitude response as well.* This attenuation factor will tend to increase as the deviation from the ideal phase response increases, as illustrated in the examples. Thus, invalid estimates of signals in the "TR" regions caused by the out-of-phase interference term will be appropriately attenuated, preventing a significant loss in prediction performance. If greater attenuation of the phase shifter's magnitude response in the "TR" regions is desired, as in the case where the sub-band edge signals are significantly corrupted by aliasing, a band-pass filter with a larger amount of attenuation at the sub-band edges can be used. For example, if the filter of Fig. 3.17 is replaced by a filter with 12 dB of attenuation at $\omega = \frac{\pi}{8}$ and $\omega = \frac{\pi}{4}$, the phase shifter response would be down 6 dB at $\omega = 0$ and $\omega = \pi$ for the M = 40 case, down 9 dB at $\omega = 0$ and 11.3 dB at $\omega = \pi$ for the M = 43 case, and down 9 dB at $\omega = \pi$ for the M = 46 case. (Of course, the notch at $\omega = 0$ for the M = 46 case would still occur.)

The stopband ripple associated with the small terms of the summation of (3.13) can affect the phase shifter response in both "PB" and "TR" regions. Unfortunately, since each of the terms of the summation of (3.13) has a different phase associated with it, it is difficult to determine in general how the stopband region terms will accumulate. Thus, it is difficult to predict, in general, the exact influence of the band-pass filter's stop-band region on the phase shifter performance. However, it is possible to make a few general observations. In particular, it is somewhat enlightening to contrast the require-

* Note that the converse is not always true. As shown in Fig. 3.18c, when the two dominant terms are 180° out-of-phase, there will be a notch in the phase shifter's magnitude response due to the perfect cancellation of terms at the band edge, but the phase response will be ideal.

ments on the stop-band region of a band-pass filter designed for use in a bandsplitting network with the requirements on the stop-band region of a band-pass filter designed for use in a phase shifter network. Recall from the discussions of Chapter 2 that band-pass filters intended for use in band-splitting networks should have a sloped stop-band attenuation characteristic. This sloped characteristic is useful for providing proper isolation between the sub-bands, since the long-time average spectrum of speech falls off with frequency. In the case of band-pass filters designed for use in a phase shifter network, there is no need for the stop-band region to be sloped. Using this fact and the previous discussions on the pass-band ripple requirements, one may conclude that equiripple filters are quite suitable for use in phase shifter networks. Recall also from Chapter 2 that it is often important to use, in band-splitting networks, band-pass filters with a considerable amount of stop-band attenuation, in order to prevent a perceptually annoying level of aliasing from occurring.* In contrast, no signal aliasing occurs in phase shifter networks, so the band-pass filter stop-band attenuation requirements are determined solely by the resulting phase and magnitude perturbations in the phase shifter response. One would suspect that filters with larger stop-band attenuations should be used to maintain a given fidelity (to the ideal mid-band phase shifter response) criterion when larger sampling conversion ratios (D) are used, since the number of undesirable terms in the summation on (3.13) increases with D.

Table 3.1 summarizes the important features of the filters which were designed for use in the phase shifters of the 9.6 kb/s and 16 kb/s

---

* This is assuming, of course, that the filter bank is not of the QMF design.

Table 3.1

Some vital characteristics of the five band-pass filters designed for use in the pitch prediction phase shifters of the 9.6 kb/s and 16 kb/s sub-band coding systems implemented.

bandpass filter number	I	II	III	IV	V
filter length	111	83	55	27	27
minimum lag predictable (samples)[1]	56	42	28	14	14
sub-band frequency range (radians)	$\frac{\pi}{32}$ to $\frac{\pi}{16}$	$\frac{\pi}{16}$ to $\frac{\pi}{8}$	$\frac{\pi}{8}$ to $\frac{\pi}{4}$	$\frac{\pi}{4}$ to $\frac{\pi}{2}$	$\frac{\pi}{2}$ to π
sampling conversion ratio ("D")	32	16	8	4	2
$\frac{\text{filter passband width}}{\text{sub-band width}}$	.36	.46	.64	.64	.91
passband ripple (dB)	$\pm$.36	$\pm$.37	$\pm$.30	$\pm$.30	$\pm$.30
filter attenuation at sub-band edges (dB)	6.0	6.0	6.0	6.0	6.0
$\frac{\text{total transition bandwidth}^2}{\text{sub-band width}}$	.64	.44	.34	.34	.08
stop-band attenuation (dB)	23.2	23.1	25.0	24.8	24.9

1. Expected pitch frequency range is 50 - 450 Hz, which corresponds to a pitch period range of 2.22 - 20 ms, or 14 - 128 samples at the 6400 Hz sampling rate of the 16 kb/s coder, and 13 - 115 samples at the 5760 Hz sampling rate of the 9.6 kb/s coder.

2. In this table, "total transition bandwidth" is the total bandwidth of the interfering transition region image.

pitch predictive sub-band coder systems which were simulated. The frequency response of these filters is shown in Fig. 3.19.

The filter lengths were chosen as a compromise between minimum lag predictable and the relative size of the pass-band region as compared to the sub-band width. As shown in the table, the pitch period will have to be doubled, tripled, or even quadrupled to obtain a lag length which the phase shifter can handle when the longer filters are used. These long filter lengths were used due to the fairly narrow transition regions which were required in the narrowest sub-bands. Unfortunately, even with these fairly long filters, the pass-band regions in the narrowest sub-bands are quite small. As a result, the predictive coder performance could be adversely affected by the relative alignment of the pitch harmonic structure and the sub-band edges. For example, if two succeeding pitch harmonics lie at either edge of a sub-band, then only the low energy "valley" will fall into the middle of the sub-band. Since the prediction system performs a whitening action (i.e. energy in spectral peaks gets reduced, energy in spectral valleys gets increased), its use will cause an increase in the input energy to that sub-band's quantizer, resulting in a decrease in SNR. Finally, the band-pass filters used in the phase shifters of the narrowest sub-bands do not have the large stop-band attenuation that is necessary for filters that are to be used in systems with large values of D.

Despite all these factors which somewhat limit the effectiveness of pitch predictive coding in the lower sub-bands, it will be seen in Chapter 5 that the use of pitch prediction does indeed provide an improvement in both the subjective and objective quality of sub-band coded speech.

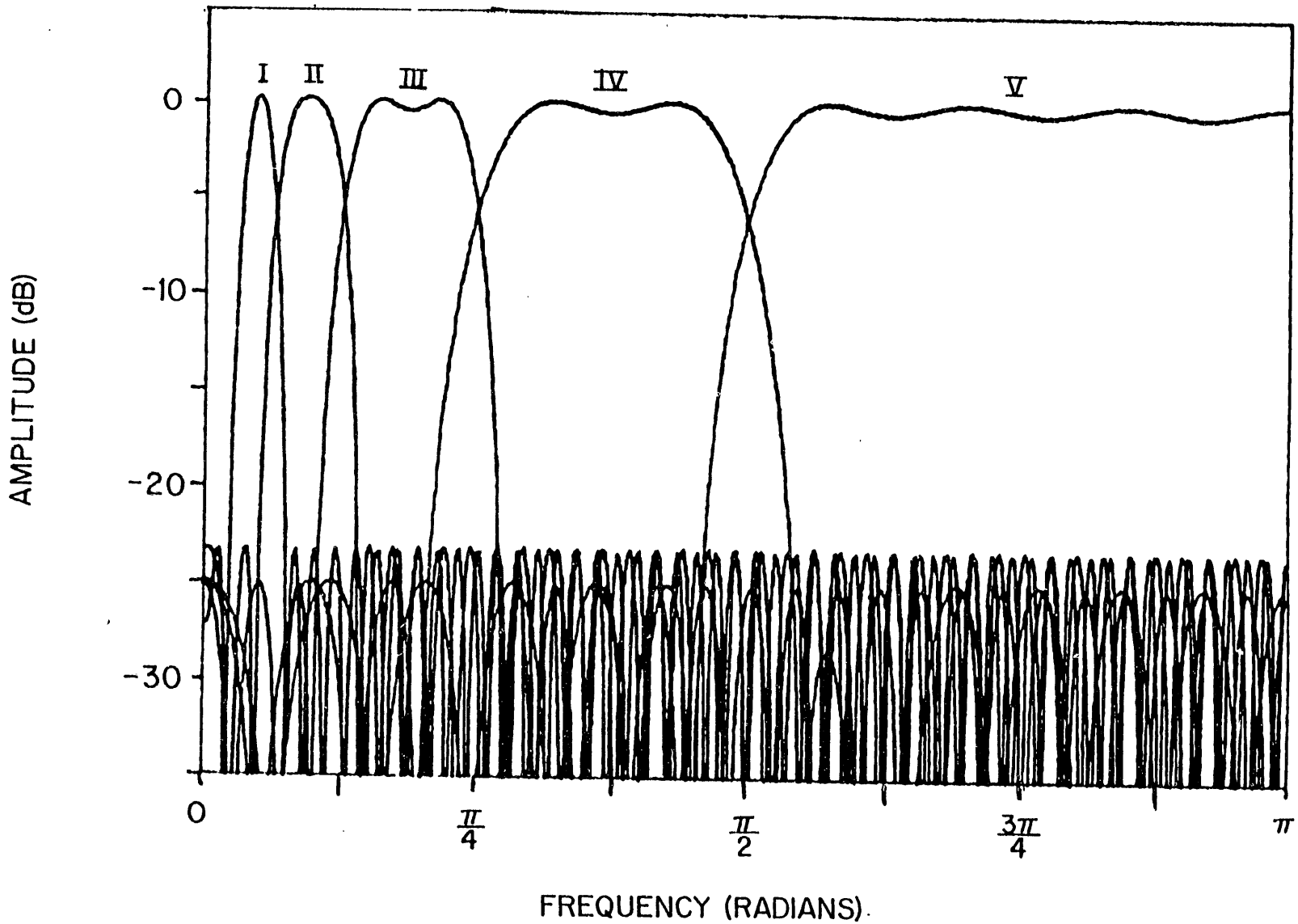

Fig. 3.19 Magnitude response of the bandpass filters used to implement the pitch predicting phase shifters in the proposed 9.6 kb/s and 16 kb/s sub-band coders.

3.8 Efficient Implementation of the Phase Shifter

This section presents an efficient implementation scheme (due to Crochiere et al. [25]) for the phase shifter.

Figure 3.20a shows the same detailed view of the phase shifter as Fig. 3.9. Suppose the delay $\widetilde{M} - I$ is expressed as $qD - L$, where L is restricted to lie between 0 and D - 1, inclusive, as shown in Fig. 3.20b. The delay of qD samples at the high sampling rate can be more efficiently implemented by using instead a delay of q samples at the lower sampling rate, as shown in Fig. 3.20c. The task is now reduced to finding an efficient implementation for the sub-system in the dotted lines in Fig. 3.20c, where h(n) and D are previously specified, and the phase advance L is known to take on integer values between 0 and D - 1, inclusively. If the output y(n) is expressed in terms of the input x(n-q), the parameters D and L, and the impulse response h(n), while taking care to omit multiplies by zero and points which will not be used, then the resulting expression yields an efficient implementation scheme.

From Fig. 3.20c:

$$y(n) = Dw(nD) \tag{3.14}$$

$$w(n) = u(n+L) \tag{3.15}$$

$$u(n) = v(n) * h(n) \tag{3.16}$$

$$v(n) = \begin{cases} x\left(\frac{n-q}{D}\right), & n = 0, \pm D, \pm 2D, \cdots \quad (3.17a) \\ 0, & \text{otherwise} \quad (3.17b) \end{cases}$$

Combining (3.15) and (3.16):

$$w(n) = v(n) * h(n+L) = \sum_{k=-L}^{N-L-1} v(n-k)h(k+L) \tag{3.18}$$

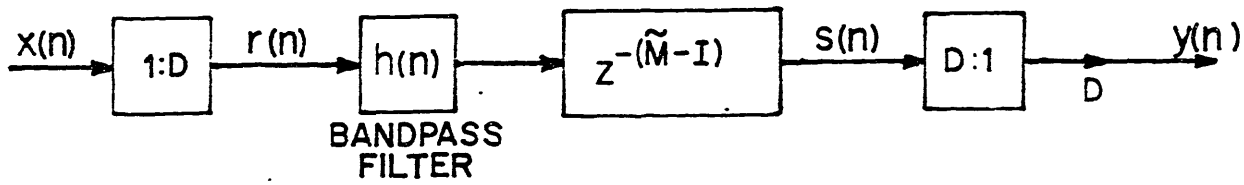

Fig. 3.20(a) Detailed view of digital phase shifter (after Crochiere [7]).

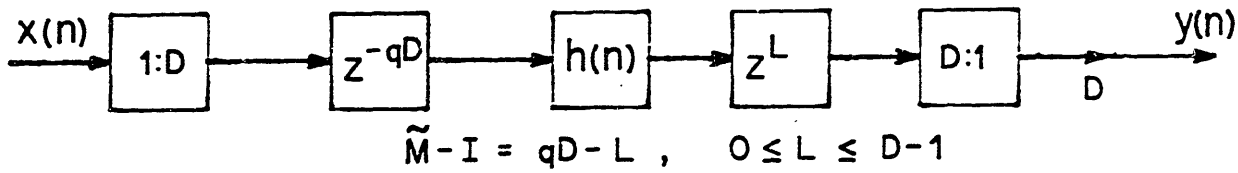

Fig. 3.20(b) Equivalent for system of Fig. 3.20(a).

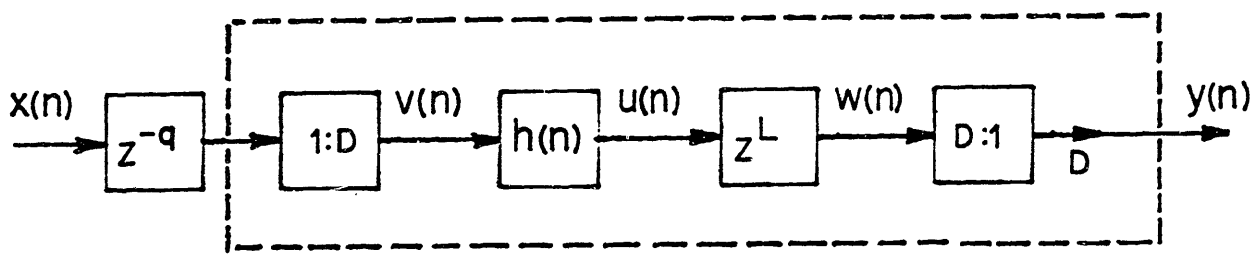

Fig. 3.20(c) Equivalent for system of Fig. 3.20(b).

Using this result and (3.14):

$$y(n) = D \sum_{k=-L}^{N-L-1} v(nD - k)\, h(k + L) \qquad (3.19)$$

Equation (3.17) shows that the only nonzero terms in the summation of (3.19) correspond to values of k which are multiplies of D. Thus, setting:

$$k = k'D$$

(3.19) can be rewritten as:

$$y(n) = D \sum_{k'=0}^{Q-1} v((n-k')D)\, h(k'D+L) \qquad (3.20)$$

where

$$Q - 1 = \left\lfloor \frac{N - L - 1}{D} \right\rfloor \qquad (3.21)$$

and $\lfloor x \rfloor$ is defined as the greatest integer less than or equal to x.

Finally, combining (3.14) and (3.20) yields:

$$y(n) = D \sum_{k'=0}^{Q-1} x(n-q-k')\, h(k'D+L) \qquad (3.22a)$$

$$= x(n-q) * g_L(n) \qquad (3.22b)$$

where

$$g_L(n) = Dh(nD + L) \qquad (3.22c)$$

Thus, the desired output y(n) can be obtained by passing the input x(n-q) through the appropriate FIR filter $g_L(n)$ of length Q. Note that if h(n) was the impulse response of an ideal zero phase band-pass filter, i.e. a modulated sinc $(\frac{\pi n}{D})$ function, then:

$$h(nD) = \frac{1}{D}\,\delta(n) \qquad [16, 17] \qquad (3.23)$$

Thus, for L = 0,

$$y(n) = x(n - q) * g_o(n) \tag{3.24}$$

$$= x(n - q) * \delta(n) \tag{3.25a}$$

$$= x(n - q) \tag{3.25b}$$

as expected.

In the next section, estimates will be made on the increase in computational load due to the addition of pitch prediction in a given sub-band coder.

3.9 Computational Costs of Implementing Pitch Prediction

Table 3.2 indicates the number of multiplies per second required to implement the pitch prediction loops in the proposed 16 kb/s sub-band coder. The totals include the two extra multiplies per predicted sample needed to scale the output of the phase shifter by the pitch gain $\tilde{\alpha}$ and the pitch gain weighting factor w_i. This table does not include any computation overhead figures associated with the pitch detector. The rationale behind this omission is that the pitch detector system will be run in parallel with the rest of the coder, so that its particular design will not affect the computational requirements of the rest of the system.

From Tables 3.2 and 2.2, one can see that the addition of pitch prediction loops to the proposed 16 kb/s sub-band coder increases the total number of multiplies per second by about 17%. Thus, the proposed 16 kb/s sub-band coder incorporating pitch prediction still requires fewer multiplies than the old 16 kb/s sub-band coder (without pitch prediction) proposed in Reference [3].

Finally, it is interesting to note that the bulk of the additional

Table 3.2

Multiplies Required to Implement Pitch Prediction Loops in the Proposed 16 kb/s Sub-band Coder

Sampling Rate: 6.4 kHz

Frame Length: 160 samples (25 ms)

Band No.	Phase Shifter Filter Length	Decimation Rate	Multiplies/Predictor Output Point	Multiplies/ Frame
1	111	32	12	60
2	83	16	16	160
3	55	8	18	360
4	27	4	18	720
5	27	2	32	2560
				3860

Total Multiplies/sec: 1.54×10^5

computation required to implement the pitch prediction loops is spent in the highest sub-band, where, due to the presence of devoicing, the prediction system should be the least effective. Given this fact, it might be worthwhile to leave out the pitch prediction loop in the highest sub-band. This modification might prove to be an advantageous tradeoff between computation costs and performance.

CHAPTER 4

QUANTIZATION OF SUB-BAND SIGNALS

4.1 Introduction

As stated in the introductory chapter, the use of quantizers whose step-sizes are adapted to be proportional to the current short-time signal energy level will assure that the noise level in each sub-band is as low as possible. Note that although the long-term average speech spectrum falls off with increasing frequency, the sub-band signal spectra are essentially flat, with low average sample to sample correlations, due to the relatively narrow sub-band width. Thus, differential coding techniques are not very effective, and the discussion will be restricted to the use of PCM quantizers with various step-size adaptation schemes. In particular, two different step-size adaptation techniques will be discussed, as well as some minor modifications to the scheme which was simulated.

The number of bits used to quantize each sub-band signal will determine the spectral characteristics of the noise. If a single, fixed, bit allocation is used, one may be guided in the bit allocation choice by the long-time properties of speech. If some sort of dynamic bit allocation scheme is used, the allocation scheme may be designed to result in a perceptually desirable noise spectral shape. These bit allocation issues will be discussed later in this chapter.

4.2 Adaptive Quantization

One approach to adaptively coding the sub-band signals is to use the Block Companded PCM (BCPCM) coding scheme proposed by Croisier [10]. In BCPCM, signals are encoded on a block basis, i.e. for each M sample block, the smallest possible step-size is chosen that

will still guarantee that the largest sample in the block does not overload the coder. The M samples are encoded using this step-size, and both the encoded samples and the step-size are transmitted. The block length is chosen large enough to minimize the bit overhead associated with the transmission of the step-sizes, yet small enough to provide useful adaptation to the evolving short-time signal level. Block lengths between 8 and 32 ms have been found [4, 5, 10] to be a good compromise. Figure 4.1 (after Esteban and Galand [4]) shows the step-size adaptation which occurs when encoding three consecutive blocks using a 3-bit quantizer.

The advantages to BCPCM are that transient clipping never occurs, and that transmission errors never propagate past one block. A disadvantage of BCPCM is the bit rate overhead to transmit the step-sizes. In a full-band coder, the bit-rate overhead might be fairly small, but in a sub-band coder, where a separate step-size for each sub-band must be sent, this overhead can become rather significant. For example, in the eight band, 16 kb/s sub-band coder of Reference [4], one-eighth of the transmitted bits are used for the step-sizes. When error correcting codes are used to protect the step-sizes from transmission errors, this bit overhead will increase even further.

Self-adapting step-size techniques eliminate the need for separate transmission of step-sizes. One such scheme for adaptive PCM (APCM) that has been used in sub-band coder systems is based on the one-word step-size memory approach proposed by Jayant, Flanagan and Cummiskey [8]. In this scheme, the input to each sub-band's encoder is quantized to one of 2^B levels according to the quantizer characteristics shown in Fig. 4.2, where B is the number of bits used for quantization.

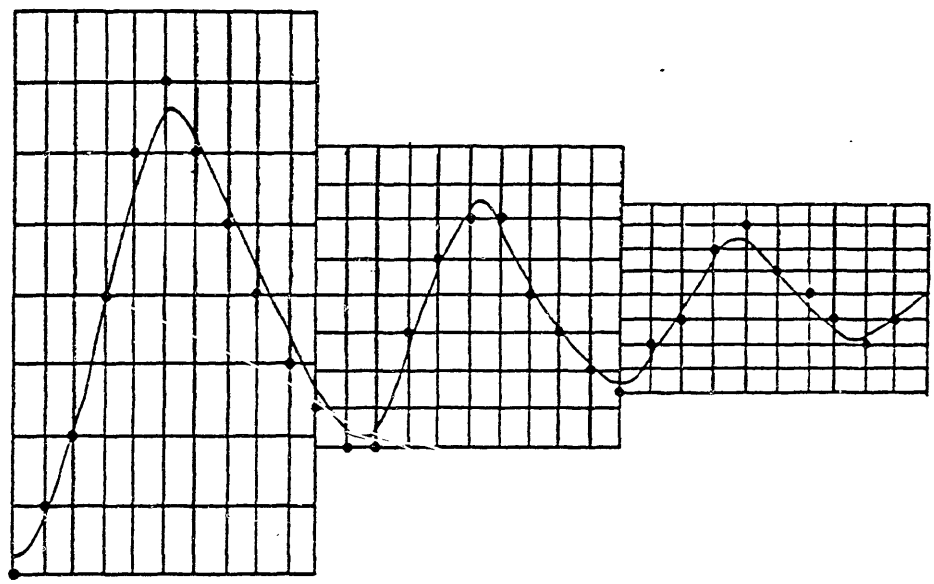

Fig. 4.1 Block companded PCM (BCPCM) principle (after Esteban and Galand [4]).

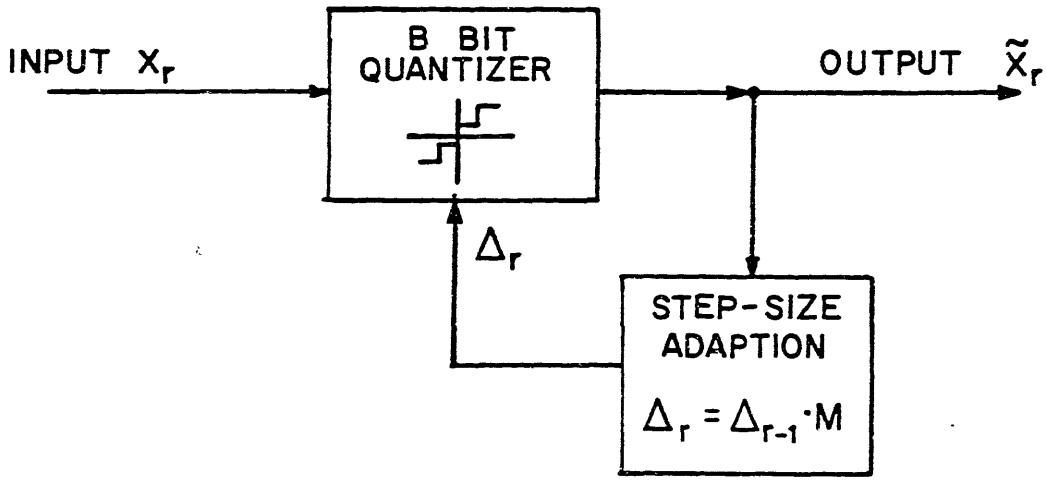

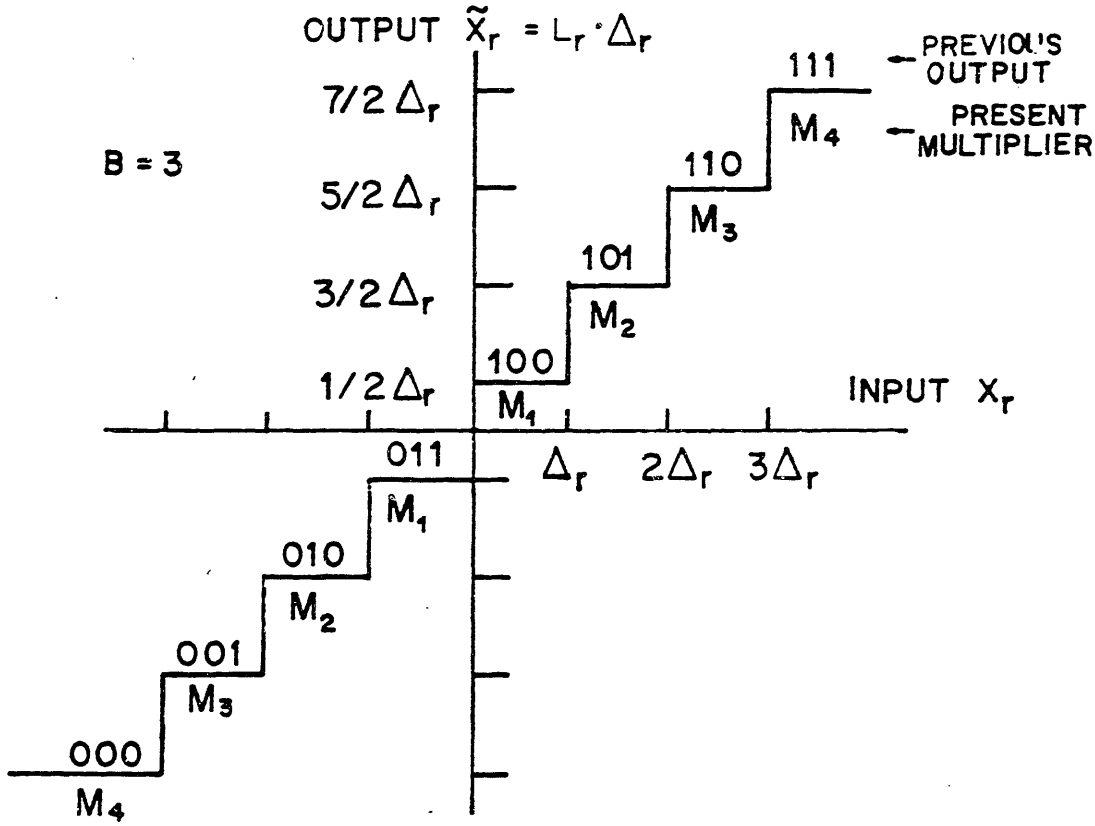

Fig. 4.2 Step-size adaptation algorithm and quantizer characteristics of the APCM coders (after Crochiere [3]).

The characteristic is called mid-rise and is desirable because of its symmetry. The step-size, Δ_r, depends on the previous quantizer magnitude level, $|L_{r-1}|$, and the previous step-size, Δ_{r-1}. Specifically:

$$\Delta_r = \Delta_{r-1} \cdot M(|L_{r-1}|) \tag{4.1}$$

where

$$\Delta_{min} \leq \Delta_r \leq \Delta_{max} \tag{4.2}$$

If a lower magnitude quantizer level is used at time r-1, then the multiplier M will be less than one, decreasing the next step-size. Conversely, if a higher magnitude level is used at time r-1, then M will be greater than one, increasing the next step-size. Thus, the APCM quantizer will continuously adapt its step-size in an attempt to track the short-time signal energy level. In general, the multipliers are selected in a way which will allow the adaptation mechanism to make step-size increases more rapidly than step-size decreases, because overload errors are potentially more harmful to the subjective and objective performance of the quantizing system than granular errors, which are limited in magnitude. Figure 4.3 (after Jayant [9]) indicates the general shape of an optimal multiplier function for use in speech quantization.

Various adaptive quantization techniques, incorporating either backward (as in APCM) or forward (as in BCPCM) estimation of the signal level have been studied by Noll [11]. In this study, the various adaptation strategies yielded essentially equivalent performance when used in conjunction with 3-bit uniform quantizers. Given this fact, APCM seems preferable over BCPCM due to its elimination of the transmission of step-sizes. Thus, APCM was chosen as the quantization

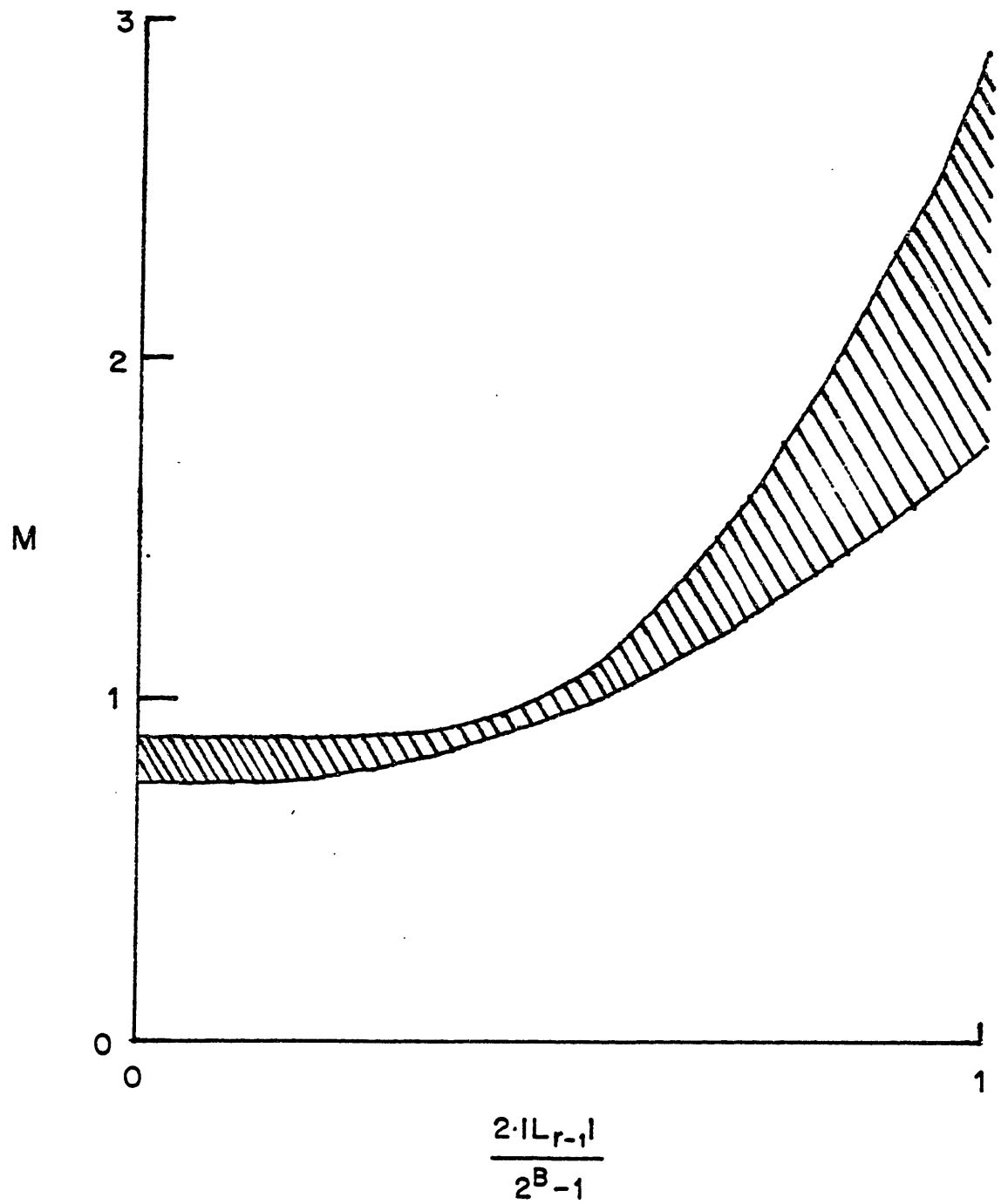

Fig. 4.3 General shape of optimal multiplier function for APCM coders in speech quantization; B > 2 (after Jayant [9]).

algorithm to be used in the new 9.6 kb/s and 16 kb/s sub-band coders.

Table 4.1 lists the actual multipliers used for the 2, 3, and 4 bit APCM quantizers which were simulated in the 9.6 kb/s and 16 kb/s sub-band coders. These values were derived experimentally, and were found to agree reasonably well with the values reported by Jayant [9] and Noll [11] for quantizing full-band signals and the values reported by Crochiere [3] for quantizing sub-band signals. As noted by Jayant [9], Noll [11], and Crochiere [3], small changes in the multiplier values have only a minor effect on the performance of the APCM quantizers.

4.3 Modifications to the APCM Algorithm

A useful modification to this algorithm, proposed by Goodman to Crochiere [3], for use in lower bit rate coders, enables coding at average bit rates of $1 + 1/K$ bits/sample. In this scheme, the sign of the input is encoded for every sample, and every K sample an additional bit is used to also encode the magnitude. The same one-word-step-size adaptation scheme is used as before, except that the adaptation occurs only when magnitude information has been sent, i.e. every K samples. With this reduced bit algorithm, "zero crossing", i.e. phase information is conveyed by the sign bit at the sub-band sampling rate, and amplitude information is conveyed by the magnitude bit at a reduced rate. Table 4.1 also lists the multipliers used for the 1 1/3 bit APCM quantizer which was simulated in the highest sub-band of the 9.6 kb/s coder.

In a similar vein, one could quantize signals at average bit rates of $M + J/K$ bits/sample. In this scheme, for every group of K consecutive samples, one would use an $M + 1$ bit APCM quantizer to encode the first J samples, and then use an M bit APCM quantizer to encode the next K-J samples. If $M > 1$, then step-size adaptation would occur for

Table 4.1

Step-Size Multipliers for the APCM Quantizers of the 9.6 kb/s and 16 kb/s Sub-Band Coders Simulated

B =	4	3	2	1 1/3
M_1	0.9	0.85	0.90	0.90
M_2	0.9	0.95	1.40	1.2
M_3	0.9	1.05		
M_4	0.95	1.65		
M_5	1.05			
M_6	1.45			
M_7	1.90			
M_8	2.40			

all K samples in the group. If M = 1, then step-size adaptation would only occur for the first J samples in each K sample block, since the next K-J samples would only be conveying sign information. In implementing this scheme, it is necessary to adjust the step-size when switching quantizers, in order to take into account the different peak-to-peak ranges of the M-bit and M+1 bit quantizers.

In the coding techniques described above, the quantities Δ_{max} and Δ_{min} represent practical constraints in the adaptation logic. The ratio $2^{B-1} \cdot \Delta_{max}/\Delta_{min}$ determines the dynamic range of the coder, while the actual values of Δ_{max} and Δ_{min} determine the center of this dynamic range. The selection of these parameters may be guided by the long-term properties of speech and the size and location of the sub-bands.

A drawback which all the previously described APCM quantizers share is that the mid-rise quantizer characteristic used does not provide for the representation of a zero output level. During silent regions of speech, when the input signal level is extremely low, or zero, the quantizer output must be $\pm \frac{1}{2}\Delta_{min}$. Although Δ_{min} is chosen to be quite small, in many quantizer implementations, the sign of the output signal varies systematically when the quantizer input is zero, resulting in tones which are perceptually annoying. Even if the quantizer was fixed at $+\frac{1}{2}\Delta_{min}$ or $-\frac{1}{2}\Delta_{min}$, the frequency translation that occurs during the resampling of the sub-bands as part of the full-band regeneration process would result in the dc sub-band signals being modulated into tones at the middle of the full speech band.

Using a mid-tread quantizer characteristic, such as the one shown in Fig. 4.4a, would alleviate these problems, but it does not use the 2^B possible levels of a B-bit quantizer efficiently due to its asymmetry.

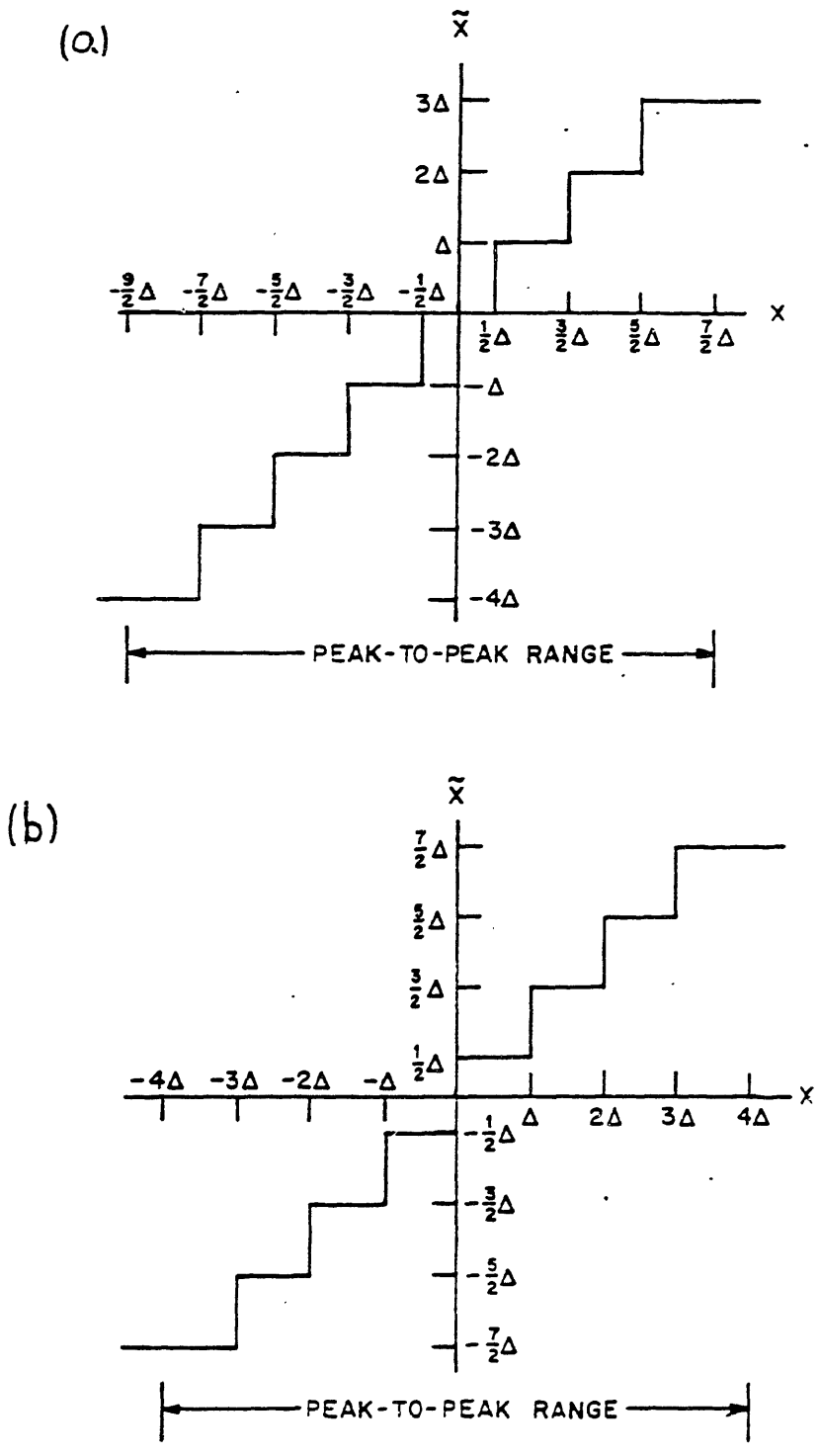

Fig. 4.4 Two common uniform quantizer characteristics; (a) mid-tread (b) mid-rise (after Rabiner and Schafer [18]).

Hence, the mid-tread characteristic of Fig. 4.4a is not as well suited for the quantization of most signals as the mid-rise characteristic of Fig. 4.4b.

Crochiere [28] has proposed a simple but effective solution to the dilemma outlined above, which takes advantage of the signal level information provided by the step-size Δ_r. In particular, the more efficient mid-rise quantizer characteristic is used for most signals, but the lowest magnitude output levels are switched to zero when the step-size Δ_r drops below some predetermined threshold level, typically $1.5\,\Delta_{min}$ to $3\,\Delta_{min}$. When the quantizer is in this low signal level mode, the equivalent of a modified mid-tread characteristic is obtained, as shown in Fig. 4.5. This modified mid-tread characteristic introduces some center-clipping at low input levels, but this has been found to be preferable to the low-level tones and idle channel noise that are perceived when the mid-rise characteristic is always used [28].

4.4 Bit Allocation

As mentioned at the beginning of this chapter, the distribution of the bits available for signal quantization among the different sub-bands will determine the SNR for each sub-band, and hence influence the shape of the overall noise spectrum.

If a single, fixed bit allocation is used to encode every frame of speech data, the use of adaptive quantizers will yield a fairly constant SNR (from one frame to the next) in each sub-band. Thus, the bit allocation should be chosen so as to take into account the long-time properties of speech. In the higher frequency sub-bands, where fricatives and noise-like sounds are often being encoded, the listener is more tolerant of a lower SNR, since quantizing noise is masked by

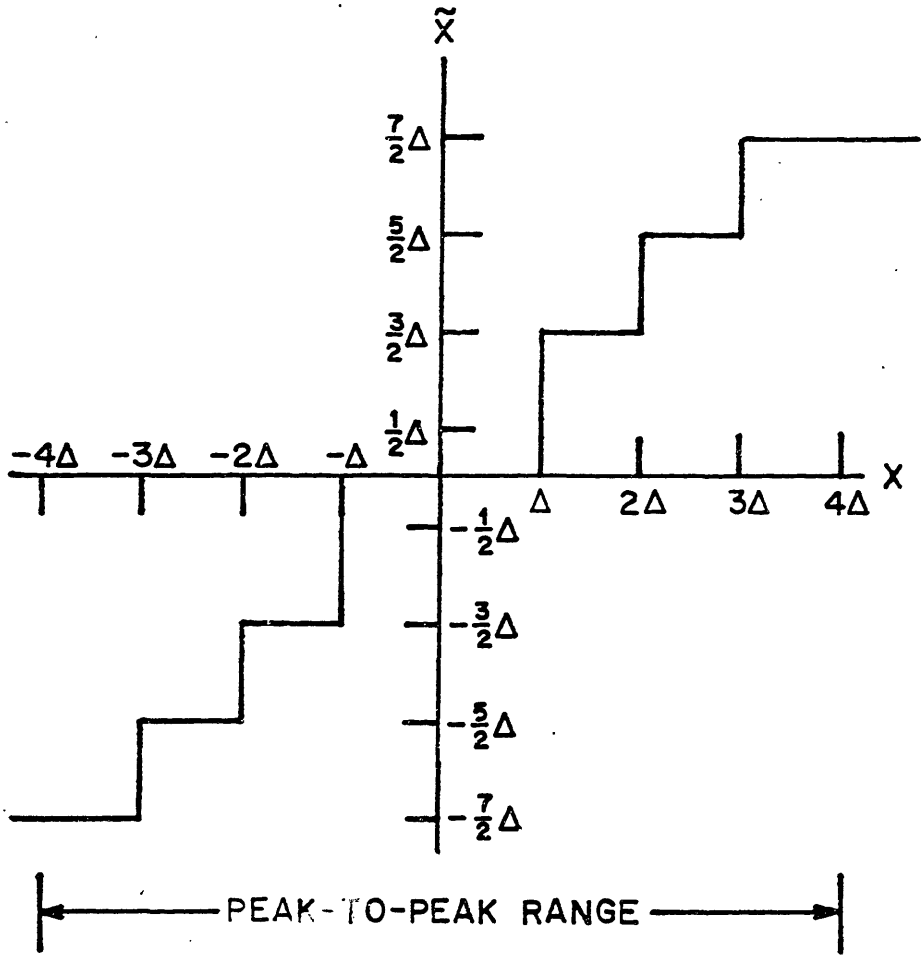

Fig. 4.5 The modified mid-tread quantizer characteristic obtained when the lowest magnitude output levels of the characteristic of Fig. 4.4(b) are switched to zero.

these sounds. In the lower frequency sub-bands, a higher SNR is required to adequately represent the detailed formant and pitch structure. Hence more bits/sample should be used to quantize the lower frequency sub-band signals than the higher frequency sub-band signals. The bit assignments, and the resulting SNR's in each sub-band are shown in Fig. 4.6 for sub-band coders "A" (a 9.6 kb/s coder) and "D" (a 16 kb/s coder) of Reference [3], and the 9.6 kb/s and 16 kb/s sub-band coders simulated as part of this thesis work. In this figure, a warped frequency scale is used to indicate each sub-band's contribution to the intelligibility of the coder, as measured by the articulation index (AI) [13,14] discussed in Chapter 2.

If the bit allocation is allowed to vary from one frame to the next, then the evolving short-time spectral characteristics of the speech signal being encoded can be utilized. One way to incorporate this information is to allocate bits according to the energy in each sub-band, as indicated by the most recent step-sizes used. The sub-band coders of Reference [5] allocated the available bits in a manner which yielded the flattest possible short-time noise spectrum, thus maximizing the overall SNR for each frame [5]. However, research on the use of adaptive predictive coding (APC) [1,21] and adaptive transform coding (ATC) [1,22] for speech coding has indicated that maximizing the overall SNR for each frame by the appropriate bit allocation will not necessarily maximize the subjective performance of the coder. In fact, bit allocations which take better advantage of auditory masking phenomena, and hence provide a more perceptually desirable noise spectrum, allocate the available bits more uniformly among the sub-bands than SNR maximizing schemes. In addition, still greater improvements in the subjective

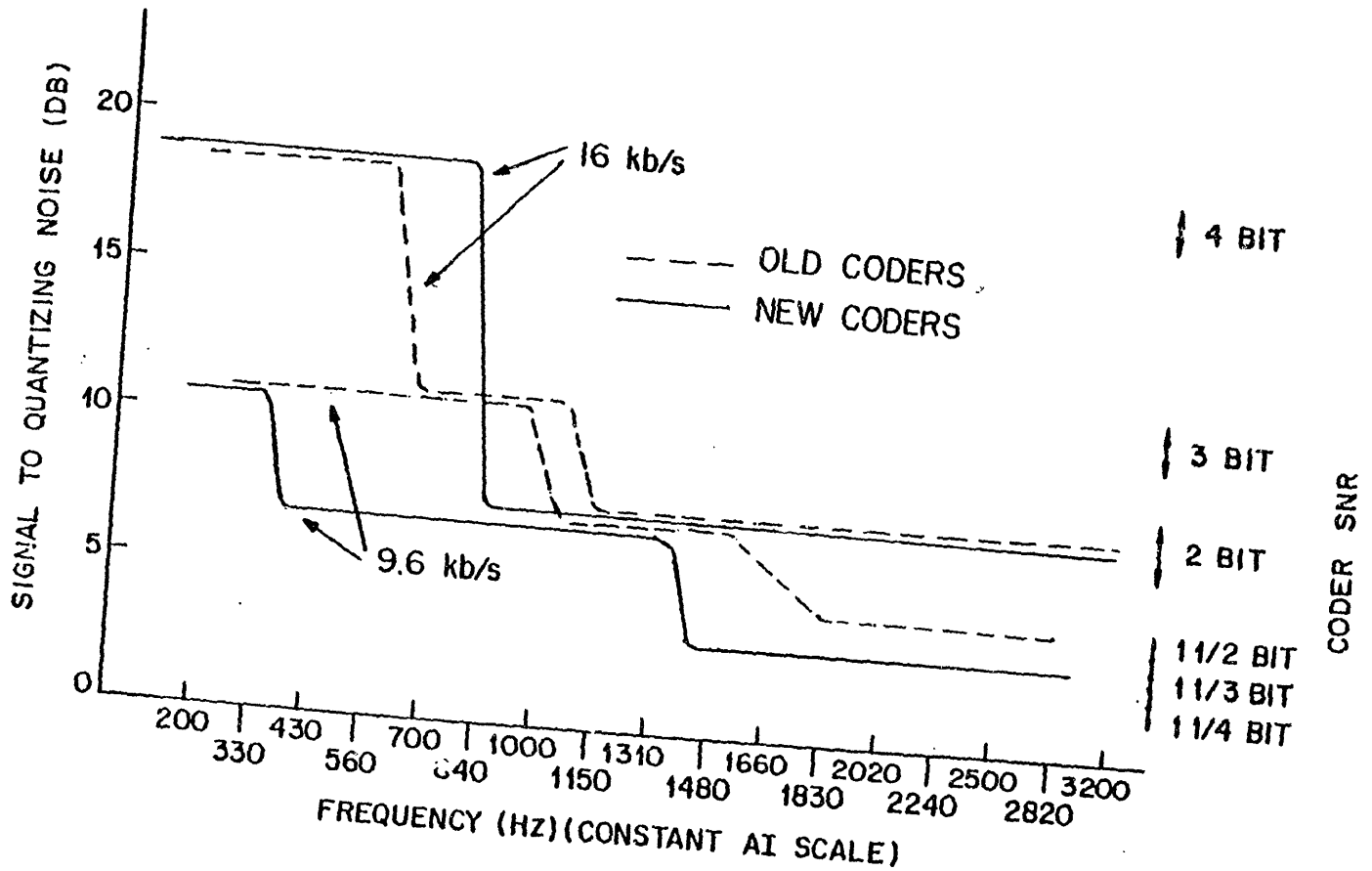

Fig. 4.6 Comparison of bit allocations and resulting sub-band SNR's for new sub-band coders and old sub-band coders of Reference [3].

performance of the coder might be obtainable if one was also to take into account the different masking properties of voiced and unvoiced speech.

The above discussions strongly suggest that the implementation of a fully dynamic bit allocation algorithm could significantly increase the complexity of a given sub-band coding scheme. Not only will the complexity of the coder increase due to the addition of the bit allocation scheme itself, but it will also increase due to the change to a more sophisticated framing and multiplexing algorithm which will be needed to handle the myriad framing alternatives. These systems will become even more complicated for coders which have unequal sub-band widths, as the different sampling rates of each sub-band will also have to be taken into account. In practice, the increase in coder performance might not be great enough to justify the increase in coder complexity associated with full dynamic bit allocation.

A simpler alternative, which might provide for a noticeable increase in coder performance over the use of a single, fixed bit allocation, would be to select one out of a few, say 2-4, alternative bit allocations each time a new frame of speech data is to be encoded. This selection could be based on the same sort of criteria that a fully dynamic bit allocation algorithm would use, but the greatly reduced number of possible bit allocations should make this limited alternative scheme far easier to implement.

CHAPTER 6

SUMMARY AND SUGGESTIONS FOR IMPROVING SUB-BAND CODER PERFORMANCE

6.1 Summary

In this thesis, a fairly comprehensive treatment of the various techniques used in the design and implementation of sub-band coders has been presented. Particular attention has been paid to the many aspects of the use of pitch predictive encoding in sub-band systems. An efficient scheme for implementing pitch predictive encoding in sub-band coders, due to Crochiere [7], has been presented, as well as a discussion on the design and analysis of such systems. The limitations on the effectiveness of such systems due to the occurrence of devoicing phenomena has also been discussed.

New designs for 9.6 kb/s and 16 kb/s sub-band systems incorporating some of the techniques discussed have been presented. These new systems are the first sub-band coders to incorporate pitch predictive coding techniques. Preliminary results of simulations indicate that the new 16 kb/s sub-band coder offers improved performance over the old 16 kb/s sub-band coder of Reference [3], and speech processed by this system is close to toll quality. The choice between the old and new 9.6 kb/s sub-band coders is made somewhat difficult by the different characteristics of the systems, and might be affected by the listening environment.

6.2 Suggestions for Improving Sub-band Coder Performance

In the discussion on preliminary simulation results, we saw that devoicing phenomena limited the effectiveness of pitch predictive encoding in the higher frequency sub-bands. Given that only fixed sub-band pitch

gain weighting factors were used to compensate for the rather transitory devoicing phenomena, these results should have been expected. In the past, researchers have used more sophisticated means for compensating for the fleeting nature of devoicing phenomena. One successful approach in adaptive predictive coding (APC) systems is the implementation of a more sophisticated pitch predictor which uses one additional sample on either side of the pitch delay to provide a frequency-dependent pitch gain factor [1]. Since the three amplitude coefficients associated with the third-order predictor are computed and transmitted every time frame, the devoicing phenomenon can be compensated for without degrading prediction performance when a speech segment is free of devoicing phenomena. In a somewhat different approach, Makhoul et al. [31] used a frequency selective mixed source to drive a linear predictive vocoding (LPC) system. Instead of using just a pulse train to drive the vocal tract model during voiced speech segments, as is usually done in most LPC systems, a mixed source consisting of a low-passed pulse train combined with high-passed white noise was used. The cutoff frequency of these filters was controlled by the presence of devoicing patches, as indicated by a modified frequency domain pitch detector based on the real time harmonic pitch detector proposed by Seneff [24].

By employing a frequency domain pitch detector similar to the one used by Makhoul et al. [31], one could improve the performance of pitch predictive coding in sub-band systems. In such a system, the fixed pitch gain weighting factors could be replaced by switches for each of the higher frequency sub-bands which would turn off the prediction system in a sub-band whenever the pitch detector determined that the signal in the band was too devoiced. A main attraction for this scheme is that the

only additional side information to be transmitted is a voiced/devoiced bit for each of the higher frequency sub-bands.

One way to improve the performance of pitch predictive coding in the narrowest sub-bands would be to use a switch to shut off the prediction system when the pitch harmonics are straddling the band. Since this switch only needs knowledge of the pitch, no extra side information is transmitted.

Another way to possibly improve the performance of the new sub-band coders presented in this thesis is to split the widest sub-band in two, so as to take better advantage of signal level adaptation provided by the adaptive quantizers. This modification should also enhance the performance of the pitch prediction scheme incorporating voiced/devoiced decisions in each sub-band proposed above.

The performance of the 9.6 kb/s system might be enhanced if a smaller total bandwidth was encoded, in order to increase the number of bits per sample available for signal quantization. Pitch predictive encoding performance for this system might be improved by quantizing the pitch gain values in a nonuniform manner, providing finer steps to quantize pitch gain values which are close to one, where the prediction system is most sensitive to errors in pitch gain.

Finally, another area for further exploration is the use of dynamic bit allocation in sub-band coders which have unequal sub-band widths. Some of the issues involved in implementing such schemes were discussed in Chapter 4, but none has been simulated yet. It is even unclear how much subjective performance improvement, if any, would be offered by such schemes if more sophisticated versions of pitch predictive coding were implemented, since a frequency selective pitch prediction scheme

could provide the extra SNR needed to properly encode the more information-laden voiced sub-band signals.

REFERENCES

1. Flanagan, J. L., Schroeder, M. R., Atal, B. S., Crochiere, R. E., Jayant, N. S., and Tribolet, J. M., "Speech Coding", IEEE Trans. Commun., Vol. COM-27, pp. 710-737, April 1979.

2. Crochiere, R. E., Webber, S. A., and Flanagan, J. L., "Digital Coding of Speech in Sub-bands", Bell Syst. Tech. J., Vol. 55, pp. 1069-1085, October 1976.

3. Crochiere, R. E., "On the Design of Sub-band Coders for Low-Bit-Rate Speech Communication", Bell Syst. Tech. J., Vol. 56, pp. 747-770, May-June 1977.

4. Esteban, D. and Galand, C., "Application of Quadrature Mirror Filters to Split Band Voice Coding Schemes", Proc. of the 1977 Int. Conf. on Acoustics, Speech and Signal Processing, Hartford, Conn., pp. 191-195, May 1977.

5. Esteban, D. and Galand, C., "32 KBPS CCITT Compatible Split Band Coding Scheme", Proc. of the 1978 Int. Conf. on Acoustics, Speech, and Signal Processing, Tulsa, OK, pp. 320-325, April 1979.

6. Tribolet, J. M., Noll, P., McDermott, B. J., and Crochiere, R. E., "A Study of Complexity and Quality of Speech Waveform Coders", Proc. of the 1978 Int. Conf. on Acoustics, Speech, and Signal Processing, Tulsa, OK, pp. 1586-1590.

7. Crochiere, R. E., "A Novel Approach for Implementing Pitch Prediction in Sub-band Coding", Proc. of the 1979 Int. Conf. on Acoustics, Speech, and Signal Processing, Washington, D.C., pp. 526-529, April 1979.

8. Cummiskey, P., Jayant, N. S., and Flanagan, J. L., "Adaptive Quantization in Differential PCM Coding of Speech", Bell Syst. Tech. J., Vol. 52, pp. 1105-1118, September 1973.

9. Jayant, N. S., "Digital Coding of Speech Waveforms: PCM, DPCM, and DM Quantizers", Proc. IEEE, Vol. 62, pp. 611-632, May 1974.

10. Crosier, A., "Progress in PCM and Delta Modulation: Block-Companded Coding of Speech Signals", Proc. 1974 Int. Zurich Seminar on Digital Communications, March 1974.

11. Noll, P., "Adaptive Quantizing in Speech Coding Systems", Proc. 1974 Zurich Seminar on Digital Communications, Zurich, March 1974, pp. B3(1)-(6).

12. Crosier, A., Esteban, D., and Galand, C., "Perfect Channel

Splitting by Use of Interpolation/Decimation/Tree Decomposition Techniques", Proc. First Int. Conf. on Info. Sci. and Systems, Patras, Greece, pp. 443-446, 1976.

13. Beranek, L. L., "The Design of Communications Systems", Proc. IRE, Vol. 35, pp. 880-890, September 1947.

14. Flanagan, J. L., Speech Analysis, Synthesis, and Perception, 2nd edition, Springer-Verlag, New York, N.Y., 1972.

15. Crochiere, R. E. and Rabiner, L. R., "Interpolation and Decimation of Digital Signals - A Tutorial Review", Proc. IEEE, Vol. 69, pp. 300-331, March 1981.

16. Oppenheim, A. V. and Schafer, R. W., Digital Signal Processing, Prentice-Hall, Inc., Englewood Cliffs, N.J., 1975.

17. Rabiner, L. R. and Gold, B., Theory and Application of Digital Signal Processing, Prentice-Hall, Inc., Englewood Cliffs, N.J., 1975.

18. Rabiner, L. R. and Schafer, R. W., Digital Processing of Speech Signals, Prentice-Hall, Inc., Englewood Cliffs, N.J., 1978.

19. Johnston, J. D. and Crochiere, R. E., "An All-Digital 'Commentary Grade' Sub-band Coder", Journal of the Audio Engineering Society, Vol. 27, pp. 855-865, November 1979.

20. Simmons, G. F., Introduction to Topology and Modern Analysis, McGraw-Hill Co., New York, N.Y., 1963.

21. Atal, B. S. and Schroeder, M. R., "Adaptive Predictive Coding of Speech Signals", Bell Syst. Tech. J., Vol. 49, pp. 1973-1986, October 1970.

22. Tribolet, J. M. and Crochiere, R. E., "Frequency Domain Coding of Speech", IEEE Trans. Acoustics, Speech, and Signal Processing, Vol. ASSP-27, pp. 512-530, October 1979.

23. Dubnowski, J. J., Schafer, R. W., and Rabiner, L. R., "Real-Time Digital Hardware Pitch Detector", IEEE Trans. Acoustics, Speech, and Signal Processing, Vol. ASSP-24, pp. 2-8, February 1976.

24. Seneff, S., "Real-Time Harmonic Pitch Detector", IEEE Trans. Acoustics, Speech, and Signal Processing, Vol. ASSP-26, pp. 358-365, August 1978.

25. Crochiere, R. E., Rabiner, L. R., and Shively, R. R., "A Novel Implementation of Digital Phase Shifters", Bell Syst. Tech. J., Vol. 54, pp. 1497-1502, October 1975.

26. Schafer, R. W. and Rabiner, L. R., "Digital Representations of

Speech Signals", Proc. IEEE, Vol. 63, pp. 662-677, April 1975.

27. Fujimura, O., "An Approximation to Voice Aperiodicity", IEEE Trans. Audio and Electroacoustics, Vol. AU-16, No. 1, pp. 68-72, March 1968.

28. Crochiere, R. E., "A Mid-Rise/Mid-Tread Quantizer Switch for Improved Idle-Channel Performance in Adaptive Coders", Bell Syst. Tech. J., Vol. 57, pp. 2953-2955, October 1978.

29. Crochiere, R. E., "A General Program to Perform Sampling Rate Conversion of Data by Rational Ratios", in Programs for Digital Signal Processing, ed. Digital Signal Processing Committee IEEE Acoustics, Speech, and Signal Processing Society, IEEE Press, New York, N.Y., 1979.

30. McClellan, J. H., Park, T. W., and Rabiner, L. R., "FIR Linear Phase Filter Design Program", in Programs for Digital Signal Processing, ed. Digital Signal Processing Committee IEEE Acoustics, Speech, and Signal Processing Society, IEEE Press, New York, N.Y., 1979.

31. Makhoul, J., Viswanathan, R., Schwartz, R., and Huggins, A. W. F., "A Mixed-Source Model for Speech Compression and Synthesis", J. Acoust. Soc. Amer., Vol. 64, pp. 1577-1581, December 1978.

THESIS PROCESSING SLIP

FIXED FIELD: ill. _____ name _____

index _____ biblio _____

▸ COPIES: (Archives) Aero Dewey (Eng) Hum

Lindgren Music Rotch Science

TITLE VARIES: ▸☐ _____

_____

NAME VARIES: ▸☐

IMPRINT: (COPYRIGHT) _____

▸ COLLATION: 133 (

(after 126 - mismumbered)

▸ ADD. DEGREE: BS ▸ DEPT.: EE

SUPERVISORS: _____

_____

BIBLIO/INDEX: _____

SUBJECTS/ADDED ENTRIES:

tag

_____ _____ _____

_____ _____ _____

_____ _____ _____

_____ _____ _____

_____ _____ _____

_____ _____ _____

_____ _____ _____

NOTES: 7182603

F6 & F25

cat'r: date: 8

page: ▸ F17

▸ DEPT: EE

▸ YEAR: 1982 ▸ DEGREE: MS

▸ NAME: BARABELL, Arthur Jay